/ PHOTOACOUSTIC ANALYSIS OF WHEAT KERNELS /

by

Arnold J. Eilert

B.Sc., Benedictine College,
Atchison, Kansas, 1984

A MASTER'S THESIS

submitted in partial fulfillment of the

requirements for the degree

MASTER OF SCIENCE

Department of Physics

KANSAS STATE UNIVERSITY
Manhattan, Kansas

1986

Approved by:

_____
Major Professor

TABLE OF CONTENTS

Table of Contents (Continued)

LIST OF FIGURES

List of Figures (Continued)

List of Figures (Continued)

List of Figures (Continued)

List of Figures (Continued)

LIST OF TABLES

ACKNOWLEDGMENTS

I wish to take this opportunity to express my sincere thanks to Dr. Ronald Lee, my major professor, to whom this work is dedicated. His constant support and understanding, and the encouragement and guidance he provided throughout this project, are gratefully appreciated.

In addition, I wish to thank the members of my supervisory committee, Dr. David Wetzel and Dr. Michael O'Shea, for their help and advice. Also, I would like to thank my graduate advisor, Dr. Nathan Folland, for his recommendations, and his encouragement when it was needed.

Finally, I would like to express my thanks to the faculty and staff of the Kansas State University Physics Department, whose assistance has been very much appreciated.

CHAPTER I

INTRODUCTION

The wide diversity and essential nature of the many products
obtained from wheat makes it, perhaps, the most important commod-
ity produced by man. The many uses for wheat byproducts is a
direct result of the complexity of the composition and structure
of each individual wheat kernel. There is currently a large
number of different varieties of wheat grown, some of which have
only recently been developed. It is likely that more such vari-
eties will be developed in the near future. Among these, dis-
tinct classes have been defined within which wheat varieties with
similar physical and compositional properties are placed. In
addition to variety, a number of other factors such as soil and
environment may also influence the composition, quality, and
characteristics of wheat (1). Accurate categorization of wheat,
on the basis of its physical, or structural properties, has
proven to be important in commercial production, where certain
properties are often found to be necessary or desirable for a
given application. Since the demand for a specific type of wheat
by the commercial sector largely dictates its ultimate monetary
value, the category within which a given variety is placed is
also of importance to the farmers who supply the wheat and plant
breeders who develop new wheat varieties for production. It is
therefore important that unambiguous, universally-acceptable
standards be applied to wheat classification and that a suffic-

iently objective method be employed for achieving accurate place-
ment of wheat samples within these classification standards.

1.1 Current Grading Standards

Although distinctions on the basis of the botany of the
wheat plant itself are the most fundamental means of classifica-
tion, such a classification scheme is not practical in commercial
grain trade. Kernel characteristics such as hard or soft, either
red or white, and spring and winter habit are commonly used
throughout the world for wheat classification (2), although spe-
cific market classes using such distinctions have a tendency to
vary somewhat among different countries. In the United States,
commercial wheat is divided into the following seven major cate-
gories: hard red spring, durum, red durum, hard red winter, soft
red winter, white, and mixed wheat (red durum, though still
recognized, has essentially disappeared as a market class) (3).
Defined beneath most of these classes are several subclasses,
into which individual varieties can be placed. Further distinc-
tions are made on the basis of grain quality, with grades of 1-5
and sample grade given on the basis of percent damaged kernels,
amount of foreign material present, etc. Figure 1.1 gives a gen-
eral outline of the standards currently used by the United States
in classifying and grading wheat (4). Traditionally, the grain
classification and grading process has involved few scientific
procedures, and many subjective judgements. The ability to make
such judgements has, however, deteriorated greatly in recent

2
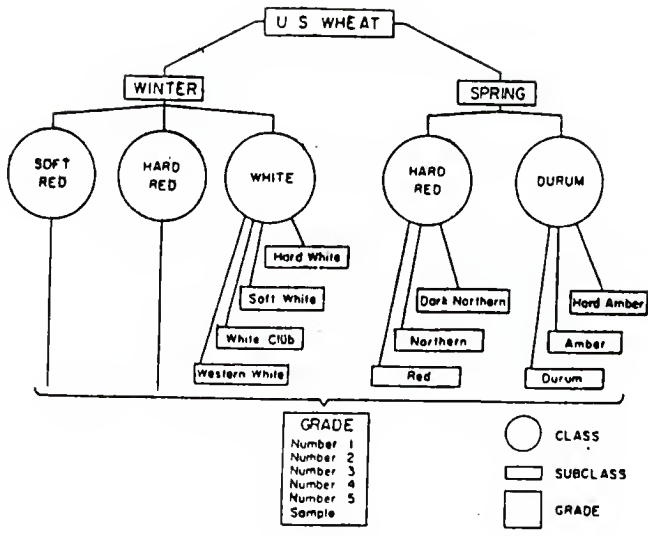
FIGURE 1.1. United States wheat grading system.

3

years due to the introduction by plant breeders of new wheat varieties, crossed between varieties belonging in different market classes.

The criteria needed to effectively determine the suitability of a given sample of wheat for a particular end-use includes more information than is provided by the classification scheme described above. Users of wheat often require further knowledge of variable factors such as moisture and protein content, relative kernel hardness, gluten quality, etc. Much attention is presently being given to more inclusive consideration of such quality factors in the grading process (5). Current grading techniques, which are primarily based on visual inspection, are clearly inadequate for making these types of quality determinations. To facilitate more accurate and comprehensive testing of grain samples, analytical methods must be developed which provide quantitative information about the properties of interest.

1.2 General Structure and Composition of Wheat Kernels

A wheat kernel is most accurately described as dry, one-seeded fruit, known to the botanist as a caryopsis (6). Although the grains of different varieties of wheat may vary considerably in size, form, and color, they all possess a similar fundamental structure. Figures 1.2 and 1.3 provide longitudinal and cross-sectional views of a typical wheat kernel (7). These figures reveal the general shape of the kernel and give an indication of its structural complexity. The kernel structure may be broadly

Hairs of
Brush

Endosperm

Cell filled with
Starch Granules
in Protein
Matrix

Cellulose Walls
of Cells

Aleurone Cell
Layer (part of
endosperm but
separated
with bran)

Nucellar Tissue

Seed Coat
(Testa)

Tube Cells

Cross Cells

Hypodermis

Epidermis

Scutellum

Sheath of Shoot

Rudimentary
Shoot

Rudimentary
Primary Root

Root Sheath

Root Cap
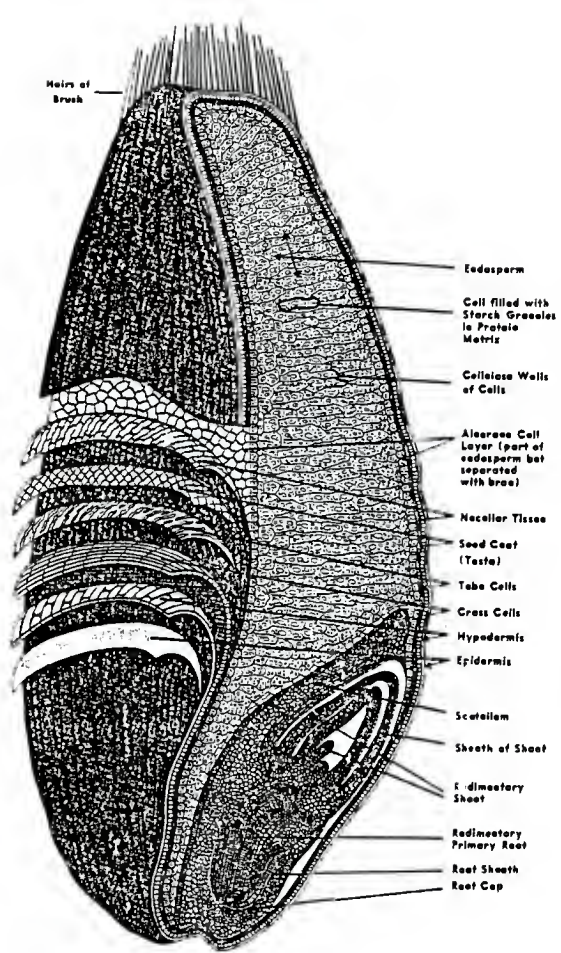
FIGURE 1.2.   Longitudinal section of a wheat kernel.

5

Crease

ENDO-SPERM

Pigment Strand
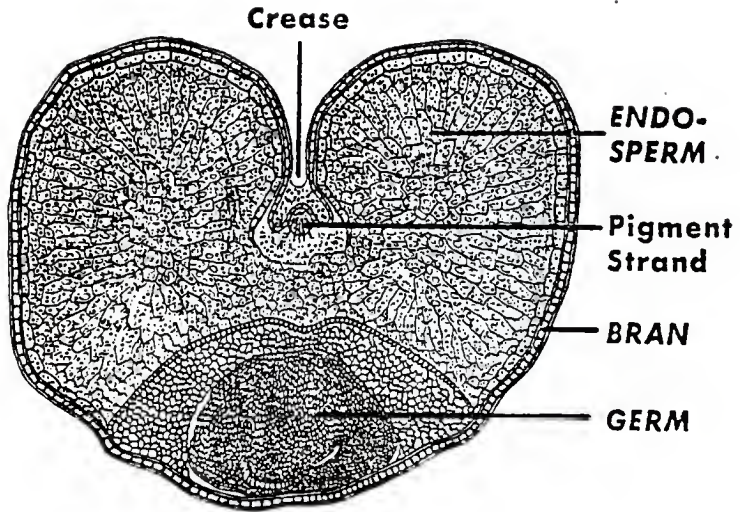
BRAN

GERM

FIGURE 1.3. Cross-sectional view of a wheat kernel.

6

divided into three primary parts, these being the germ and endo-
sperm, which are enclosed in a seed coat (bran). Minor portions
of the kernel not included in these regions are a tuft of fine
hairs located at one end of the kernel and a deeply pigmented
vascular strand located at the bottom of the crease. The rela-
tive location of each of the primary kernel parts is identified
in the cross-sectional diagram. Approximate proportions of the
kernel comprised by these three parts are: endosperm, 83%; germ,
2.5%; and bran, 14.0%. Reported compositional values tend to
vary somewhat, however, depending on methods of separation and
analysis (5). Each of these primary regions of the kernel has a
relatively complex individual structure of its own. Figure 1.4
provides a detailed outline of the major, separately-identifiable
portions of a wheat kernel, and their relation to one another
(8). The longitudinal diagram illustrates the respective loca-
tion of most of these structural regions.

The chemical constituents of wheat are fairly large in
number and are distributed non-homogeneously throughout the ker-
nel. These include carbohydrates, proteins, lipids, vitamins,
water, enzymes, and various minerals. The relative amounts of
these constituents in a given kernel can vary widely, due to
differences in variety and environmental conditions. The major
components, and the percentage of each of the primary regions of
a typical kernel comprised by these components, are outlined in
the following table (9).

7

Parts of the wheat kernel and their relation to each other

Pericarp (fruit coat)

  Outer
    1. Epidermis (epicarp)
    2. Hypodermis
    3. Remnants of thin-walled cells

  Inner
    4. Intermediate cells
    5. Cross cells
    6. Tube cells

Wheat kernel (caryopsis) — Bran

Seed

  Seed coat (testa, spermoderm, tegmen) and pigment strand

  Nucellar epidermis (hyaline layer, perisperm) and nucellar projection

  Endosperm
    1. Aleurone layer
    2. Starchy endosperm

Germ (embryo)

  Scutellum (cotyledon)
    1. Epithelium
    2. Parenchyma
    3. Provascular tissues

  Embryonic axis
    Plumule, including coleoptile
    Primary root, covered by coleorhiza
    Secondary lateral rootlets

  Epiblast

FIGURE 1.4. Outline of the structural components of a wheat kernel.

Table 1.1. Composition of the Endosperm, Germ, and Bran.

Constituent	Endosperm	Germ	Bran
Moisture	14.0%	11.7%	13.2%
Protein	9.6%	28.5%	14.4%
Fat	1.4%	10.4%	4.7%
Mineral	0.7%	4.5%	6.3%
Starch	71.0%	14.0%	8.6%
Hemicellulose	1.8%	6.8%	26.2%
Sugars	1.1%	16.2%	4.6%
Cellulose	0.2%	7.5%	21.4%
Carbohydrate (total)	74.1%	44.5%	60.8%

The endosperm, which comprises most of the wheat kernel, is
of primary commercial interest, since most products produced from
wheat utilize material from this region. The endosperm mainly
consists of starch granules embedded in a matrix which is largely
protein. Starch is by far the most abundant carbohydrate present
in the wheat kernel, constituting approximately 64% of the dry
matter of the entire wheat grain and about 70% of the endosperm
(10). The starch contained in the endosperm is in the form of
lenticular or spherical granules which are tightly packed toge-
ther, with the protein filling the inter-granular spaces. The
structure and composition throughout the endosperm is not com-
pletely uniform, however, with the concentration of protein de-
creasing as the central portion of the endosperm is approached.
The concentration of protein is known to be dependent upon envi-
ronmental factors as well as variety, with hard red winter wheats

9

typically containing a higher protein content than soft red
winter varieties.

Although the germ and bran contain much lower percentages of
starch than does the endosperm, the concentration of protein in
these regions is greater. The concentration of most other con-
stituents of the kernel are also greater in these regions. The
composition of the multi-layered bran varies to a large extent
with increasing depth beneath the kernel surface, as the various
structural portions of this region are encountered. Likewise,
the components of the germ are non-homogeneously distributed,
with their relative concentrations varying with its structural
complexity. A summary of more extensive and detailed information
regarding the structure and composition of a wheat kernel has
been compiled by MacMasters, Hinton, and Bradbury (11).

1.3 Kernel Hardness

Hardness is one of many distinguishing characteristics of
wheat which may vary from sample to sample. As properties of
wheat kernels, hardness and softness relate to the manner with
which the endosperm of the kernel breaks down during the milling
process. In hard wheats, fragmentation of the endosperm tends to
occur along the lines of the of the starch and protein cell
boundaries, whereas in soft wheats the endosperm fractures in a
random way. This seems to suggest a pattern of areas of mechani-
cal strength and weakness in hard wheats and uniform mechanical
weakness in soft wheats. Upon milling, the degree of mechanical

10

damage to the starch granules of the endosperm is greater for
hard wheats than for soft, and hard wheat typically requires a
greater amount of grinding force in the milling process. Hard-
nesa also affects the ease of detachment of the endosperm from
the bran, as the bran is found to separate more cleanly with hard
wheats than with soft. Although it is not completely understood
why some wheats are "harder" than others, one view is that hard-
ness is related to the degree of adhesion between the starch
particles and protein matrix which comprise the endosperm (12).
This hypothesis is supported in research done by Hoseney and Seib
(13), where it was shown that sliced hard wheat kernels typically
dissociate by rupturing of the starch particles, whereas in soft
wheats the dissociation occurs at the starch-protein bonds, leav-
ing the starch particles intact. Another view is that kernel
hardness is dependent upon the continuity of the protein matrix
of the endosperm within which the starch particles are embedded.
Hardness is a characteristic known to be inherited in the Mendel-
ian fashion (14), which implies that hardness should not greatly
vary for kernels of a given variety.

Due to the above-cited differences, the type of flour ob-
tained from hard wheats is different than that obtained from
soft, tending to be more coarse, gritty, and more freely flowing
and easily sifted. Soft wheats yield a very fine flour consist-
ing of irregular-shaped fragments of endosperm cells which adhere
together, sift with difficulty, and tend to clog the apertures of
sieves (12). Flour from hard wheats, due to its granular nature,

11

as well as its relatively high protein content and desirable gluten quality, is well-suited for breadmaking. Soft wheat flour, however, is found to be preferable for production of cake and pastry products (15). Since hard and soft wheats require different processing techniques for optimum utilization, it is important that knowledge of the relative hardness of wheat to be processed be obtained prior to its use.

In the classification of wheat, hardness is usually judged on the basis of visual appearance rather than actual measurement. For research purposes, objective measurements of hardness are often made by determining the wheat's "pearling index", which is defined as percentage of material pearled-off from a sample of wheat of prescribed weight in a laboratory barley pearler operated for a prescribed period of time. The equipment and procedures for this technique have, however, never been standardized. Furthermore, in studying segregates produced from crossing hard and soft wheats, it has been found that the pearling technique produces wide differences in the pearling indexes, and visual classification for such material is frequently faulty (16). In addition to this procedure, a number of other tests have been designed to determine kernel hardness (17), with varying degrees of success. At present, no single one of these techniques is either universally used or accepted. These tests, in general, require samples consisting of a relatively large number of kernels in order to yield meaningful results. A satisfactory method for determining the hardness of a single kernel has not yet been

12

developed.

It is suggested in the above discussion that the hardness of
a wheat kernel is related to structural properties of the endo-
sperm. It is therefore quite possible that the bulk thermal
and/or optical properties of hard wheats differ to some extent
from soft wheats. If the variation between hard and soft wheats
is sufficiently large and is consistent, it might be feasible to
make a determination of the relative hardness of a single kernel
on the basis of these properties. Since hardness is genetically
transmitted, it should also be possible to make a determination
of the hardness of a kernel by positively identifying it as being
of a particular variety, assuming that the relative hardness of
that variety is understood. A method for making distinctions on
the basis of the optical or thermal properties of a kernel might,
therefore, prove successful in determining relative kernel hard-
ness, either by providing information reflecting properties which
are directly related to hardness, or indirectly by identifying
properties which are uniquely common to a given variety.

1.4 Photoacoustic Analysis of Wheat Kernels

A sample analysis technique utilizing a phenomenon commonly
known as the photoacoustic effect was studied and subsequently
used in this research project for the examination of individual
wheat kernels. The photoacoustic effect occurs when a substance
in a closed cell is illuminated by chopped light, or some other
intensity-modulated energy source. The result of the illumina-

13

tion is an acoustic signal with frequency equal to the modulation
or chopping frequency of the incident beam. The effect is more
thoroughly discussed in the following chapter. The photoacoustic
response of a material is known to be dependent upon that mater-
ial's optical and thermal properties. Thus, it should be possi-
ble to differentiate between wheat kernels in which optical or
thermal properties vary by comparing the photoacoustic responses
obtained from them. If thermal or optical properties vary be-
tween varieties, or these properties differ for hard and soft
kernels, the variations should be reflected in their respective
photoacoustic responses, which should vary as well.

As a method for making determinations on the basis of such
factors as kernel hardness, a technique incorporating photoacous-
tic sample analysis would offer several advantages over analysis
techniques currently used. First, the test would provide a non-
destructive examination of a sample, enabling use of the sample
for further testing or continued research. Secondly, photoacous-
tic analysis accommodates small sample sizes, and would thus
permit evaluation on the basis of a sampling as small as a single
kernel. Although small sample size is not imperative in most
instances requiring the grading of wheat, such as milling opera-
tions and international grain trade, it might be advantageous for
certain grain research and plant breeding applications. Also,
photoacoustic sample analysis is capable of providing quantita-
tive comparisons, and would thus allow for objective determina-
tions of kernel properties, relative to other kernels.

14

1.5   Summarization of Thesis Objectives

Although the primary objective of this project was to examine the photoacoustic response of wheat kernels, and attempt to correlate it to kernel hardness, a number of other preliminary procedures and experiments needed to be performed as well.   A general outline of the major objectives of the project is given below:

1. Develop a microcomputer-operated data acquisition system to work with the photoacoustic sampling apparatus.

2. Test the apparatus and acquisition system by checking acquired data with theoretical predictions, and make any necessary equipment modifications.

3. Examine the effect of moisture on the photoacoustic response, and determine a satisfactory method for standardization of moisture content for wheat samples to be studied.

4. Obtain the photoacoustic response throughout a modulation frequency range of 1–1000 Hz for single kernel samples of several different hard and soft wheat varieties, and compare results.

A theoretical discussion of the photoacoustic effect in solids, a description of the apparatus and acquisition system used, and a presentation and discussion of the results obtained are provided in the subsequent chapters of this thesis.

15

CHAPTER II

PHOTOACOUSTIC EFFECT IN SOLIDS; THEORY

2.1 Introduction

In order to understand clearly the significance of the
information provided by photoacoustic examination of various
wheat varieties, it is first necessary to understand the theore-
tical basis for the photoacoustic effect. Since all photoacous-
tic studies done in this thesis work have been on solid samples,
in this discussion we will concentrate on the photoacoustic
effect in solids.

The photoacoustic effect, in general, refers to the produc-
tion of an acoustic signal by a sample, either solid, liquid, or
gaseous, when that sample is illuminated by an intensity modulat-
ed energy beam, usually in the form of electromagnetic radiation.
It was initially observed in the early 1880´s when Alexander
Graham Bell detected an audible sound through a listening tube
connected to a chamber containing a solid sample surrounded by a
gaseous atmosphere, through which the sample could be illuminated
with a periodically interrupted sunlight beam (18). Subsequent
experimentation shortly following this discovery revealed that an
acoustic signal could also be detected when an intensity-modu-
lated sunlight beam was allowed to impinge upon various liquids
and light-absorbing gases. Motivated by these findings, Tyndall
and Roentgen found that the effect could also be created using
chopped artificial light (19). At the time of its discovery, the

16

processes responsible for production of the acoustic signal were not well understood, with a number of qualitative theories being proposed. Interest in the effect was, however, soon diminished as it was generally considered merely a laboratory curiosity of no practical importance. Although approximately fifty years later interest in the photoacoustic effect in gases was renewed, becoming a well-established method for gas analysis, the photoacoustic effect in solids and liquids remained essentially forgotten until the early 1970's, when its potential for analysis of the bulk physical properties of non-gaseous materials began to be realized.

The experimental apparatus used by Bell, Tyndall, and Roentgen in the initial discovery and early investigation of the photoacoustic effect, possessed the crude essentials necessary to observe the effect. This apparatus consisted roughly of an intensity-modulated light source, an airtight enclosure through which the light source could penetrate containing either a gaseous sample or a non-gaseous sample surrounded by a gaseous atmosphere, and an acoustic signal detection device by which the photoacoustic signal could be monitored. Figure 2.1 gives a schematic representation of such a photoacoustic effect detection arrangement as used for monitoring the photoacoustic signal emitted by a solid sample. Although this apparatus alone is insufficient for performing the quantitative studies of solid samples as done in this thesis work, such an illustration is sufficient for demonstrating the effect, and is useful in describing the

17

SUNLIGHT ⟶

SAMPLE

MECHANICAL CHOPPER

SAMPLE CELL

LISTENING TUBE
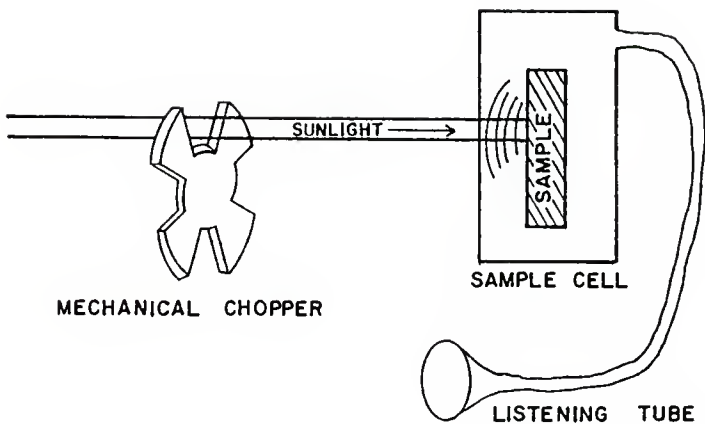
FIGURE 2.1. Simple arrangement for photoacoustic signal detection.

basic mechanisms by which the photoacoustic effect arises.

2.2 Fundamental Description

In attempting to describe the underlying physical processes which give rise to the photoacoustic effect in solids, it is perhaps best to begin by giving a qualitative discussion of these processes, followed by a more rigorous mathematical treatment of the phenomenon.

As earlier stated, the photoacoustic effect occurs when an intensity modulated energy beam is allowed to impinge upon a sample when that sample is confined to an enclosed chamber, generally referred to as the photoacoustic cell. The modulated energy source used is usually, but not always, monochromatic electromagnetic radiation in or near the visible spectrum. Unless specified otherwise, incident monochromatic electromagnetic radiation will be assumed throughout this discussion. The photoacoustic signal, or response, is in the form of an acoustic signal at the same frequency as the energy beam modulation frequency. The photoacoustic signal is monitored by an acoustic signal detection device sufficiently sensitive to measure it, commonly a high sensitivity microphone built into some portion of the chamber. In the case of photoacoustic experimentation with solids, it is necessary that the solid sample be at least partially surrounded by a gaseous atmosphere, preferably using a gas that will absorb a minimal amount of the incident energy.

When a given cycle of the modulated energy beam (e-m radia-

tion) becomes incident upon the sample, the sample will absorb all or part of this energy throughout a depth beneath the illuminated surface characterized by the optical absorption depth of the sample for the wavelength of the e-m radiation used. This energy absorption results in localized excitation of atomic energy levels within the sample medium at the absorption depth. When the subsequent deexcitation of these energy levels occurs, it generally does so by non-radiative heat producing processes, which results in a localized heating of the sample in the vicinity of the initial absorption. This heat then diffuses outward from the point of absorption in all directions as individual atoms and/or molecules are vibrationally excited in a non-cooperative and highly dissipative manner. This heat diffusion within the sample has the characteristics of a highly damped wave, being formally equivalent to wave propagation in a very lossy medium, with a wavelength approximately equal to the thermal diffusion length of the sample in the region through which it propagates. Thus, this heat propagation through the sample is often referred to as a thermal wave.

If the initial energy absorption occurs at a shallow-enough depth beneath the surface so that the thermal wave is able to propagate to the surface of the sample before being entirely dissipated, the heat which reaches the surface will produce an increase in temperature at the sample surface. If the incident e-m radiation is maintained at a constant modulation frequency, this will result in a periodic heating of the surface of the

20

sample, with the heat contribution from a given depth beneath the surface of the sample being essentially the same for each modulation cycle. Because a finite amount of time is required for the heat produced within the sample to propagate to its outer surface, a thermal wave propagating from some depth beneath the surface of the sample will cause a heat contribution at the sample surface which lags, to some extent, in phase with respect to the incident e-m source. Since a gaseous atmosphere surrounds the surface of the sample, this heat is then transferred to a thin layer of gas at the gas-sample interface. The periodic heating of this thin gas layer causes it to expand and contract at a frequency equal to the modulation frequency of the incident e-m radiation, creating periodic pressure fluctuations which occur in the photoacoustic cell at the modulation frequency, and resulting in the acoustic signal which can be detected by a sufficiently sensitive microphone.

From the above discussion, it is easily seen that the photoacoustic response obtained from a solid sample depends on the thermal properties of the sample, which influence the propagation of the thermal wave through the sample to the sample surface. Also, the response is dependent upon the optical properties of the sample, which dictate the distance beneath the surface at which the thermal waves will be generated. Although this adds to the complexity of a quantitative treatment of the problem, both of these dependencies are individually important, for each can be used to obtain information regarding the bulk physical properties

21

of a given sample. For example, if the modulation frequency of
the e-m radiation is held constant and the wavelength of the
incident radiation is allowed to vary through some range, infor-
mation similar to that achieved by conventional optical absorp-
tion spectroscopy can be obtained; as strong absorption by the
sample will lead to thermal waves emerging at the surface before
being greatly dispersed, and radiation not absorbed will not
contribute to the acoustic signal. Furthermore, this technique
can often be applied in instances where the opaqueness of the
sample or problems with scattered light pose serious difficulties
with conventional absorption or reflection studies (20). Another
important application of the photoacoustic effect in solid sample
analysis takes advantage of a functional dependence of the ther-
mal diffusion length, or the wavelength of the thermal waves
which contribute to the measured acoustic signal from deepest
within the sample, on the modulation frequency of the incident
electromagnetic radiation. This technique, commonly referred to
as photoacoustic depth profiling, is unique to photoacoustics,
and essentially permits one to obtain a depth profile of the
thermal characteristics of a sample while the sample itself
remains intact. Both the phase lag of the acoustic response with
respect to the incident radiation and the amplitude of the signal
provide information regarding the thermal properties encountered
in the portion of the solid through which the thermal wave propa-
gates prior to reaching the surface. Variation of the thermal
diffusion length as the modulation frequency is changed allows

information from different sample depths to be acquired. It is
this aspect of photoacoustic sample analysis that was primarily
utilized in the studies done throughout this thesis work.

In the above discussion, only a qualitative description of
the photoacoustic effect in solids has been given. Although
dependencies of the effect on the optical and thermal properties
of the sample were alluded to, the exact nature of these depend-
encies was not stated. If meaningful quantitative sample analy-
sis is to be performed utilizing this effect, a more exact theo-
retical model needs to be employed. Rosencwaig and Gersho, in
1976, published such a theoretical model, presently referred to
as the Rosencwaig-Gersho, or R-G theory (19). Although this
theoretical description is one-dimensional, and assumes a homo-
geneous solid sample, it yields valuable information concerning
many aspects of the photoacoustic effect in solids. Hence, the
main points of this theory, and some of its predictions in spe-
cial cases of interest, are given below.

2.3   Rosencwaig-Gersho Theory

A. Heat Flow Equations

To begin this theoretical treatment of the problem, some
basic assumptions first need to be made. Let us assume a simple,
closed, cylindrical photoacoustic cell with length L and diameter
D, as illustrated in Figure 2.2. This cell contains a disk-
shaped sample of length ℓ which has the same diameter D as the
cell. The sample is positioned in the cell so that its back

23
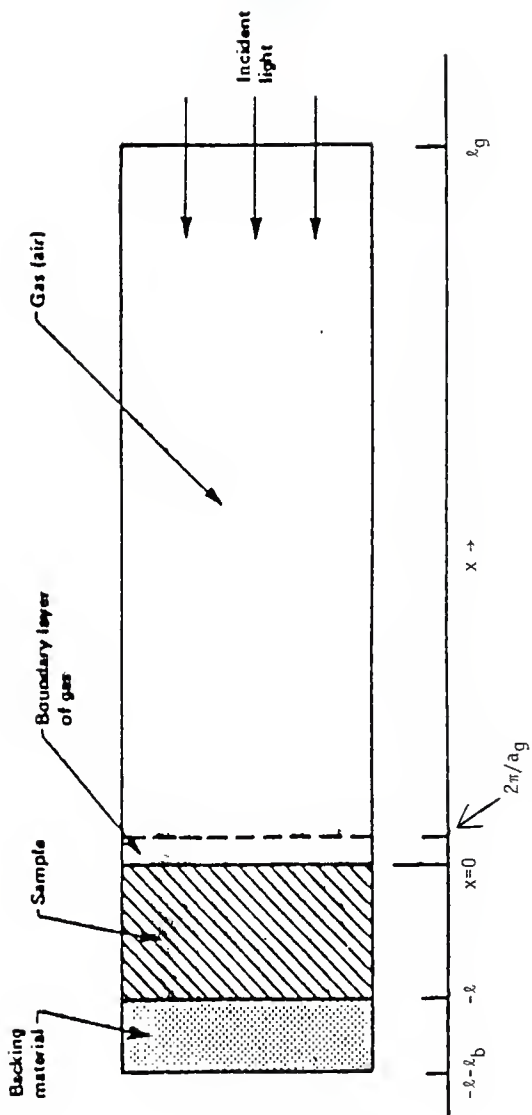
FIGURE 2.2. Cross-sectional view of a simple cylindrical photoacoustic cell.

24

surface is placed directly against a backing material of low thermal conductivity, and its front surface faces the gas filled volume of the cell. The gas and the backing materials are assumed non-absorbing for the wavelength λ of the incident e-m radiation, modulated at frequency ω (rad/sec), impinging upon the sample's front surface. The sample itself is assumed to have an absorption coefficient β (1/cm).

We now define the following parameters for the gas, sample, and backing material; where the subscript i takes on the value g for the gas, s for the solid, and b for the backing material:

k_i: thermal conductivity (cal/cm-sec-deg) of material i

ρ_i: density (g/cm^3) of material i

C_i: specific heat (cal/g-deg) of material i

$\alpha_i = k_i/\rho_i C_i$: thermal diffusivity (cm^2/sec) of material i

$a_i = (\omega/2\alpha_i)^{1/2}$: thermal diffusion coef. (1/cm) of material i

$\mu_i = 1/a_i$: thermal diffusion length of material i

Let the incident e-m radiation be sinusoidally modulated with intensity I, given by:

$$I = \frac{1}{2}I_0(1+\cos\omega t),$$

where I_0 is the incident monochromatic light flux (W/cm^2).

Using these parameters, the heat produced at a given point x within the sample due to the light absorbed at that point is given by:

$$\frac{1}{2}I_0 \exp(\beta x)(1+\cos\omega t),$$

with x taking on negative values from x=0, where the light is incident upon the sample, to x=$-\ell$, at the back end of the sample.

The thermal diffusion equation for the interior of the solid ($-\ell$<x<0), taking into account the distributed heat source, can be written as:

$$\frac{\partial^2 \phi}{\partial x^2} = \frac{1}{\alpha_s} \frac{\partial \phi}{\partial t} - A \ \exp(\beta x) \left[1 + \exp(j\omega t)\right]$$

$$\text{for } -\ell < x < 0, \tag{1}$$

with

$$A = \beta \ I_0 \eta \ / 2k_s,$$

where ϕ is the temperature and η is the efficiency at which the absorbed light is converted to heat by the non-radiative, heat producing deexcitation processes. Here, we will assume that $\eta = 1$, which is reasonable for most solids at room temperature. For the backing material and the gas, the respective heat diffusion equations are simplified, since the optical absorption coefficient for these is zero. They are:

$$\frac{\partial^2 \phi}{\partial x^2} = \frac{1}{\alpha_b} \frac{\partial \phi}{\partial t} \qquad\qquad -\ell - \ell_b < x < -\ell \tag{2}$$

$$\frac{\partial^2 \phi}{\partial x^2} = \frac{1}{\alpha_g} \frac{\partial \phi}{\partial t} \qquad\qquad 0 < x < \ell_g \tag{3}$$

The real part of the complex-valued solutions for the temperature ϕ for the above thermal diffusion equations is the solution of physical interest, representing the temperature in the cell relative to the ambient temperature as a function of posi-

26

tion and time. Therefore, the actual temperature field in the cell is given by:

$$T(x,t) = Re[\phi(x,t)] + \Phi$$

with "Re" denoting the real part of the solution, and Φ being the ambient (room) temperature.

In order to completely specify the solution to the above heat diffusion equations, the appropriate boundary conditions need to be applied. These boundary conditions are obtained from the requirement of temperature and heat-flux continuity at the boundaries of the sample ($x=0$ and $x=-\ell$), and from assuming that the temperature at the cell walls $x=\ell_g$ and $x=-\ell-\ell_b$ is ambient. Finally, it is assumed that the dimensions of the cell are small enough that convective heat flow in the gas can be ignored at steady state conditions.

B. Temperature Distribution in the Cell

The general solution for $\phi(x,t)$ in the cell, neglecting transients, can be written as:

$$
\begin{aligned}
\phi(x,t) &= (1/\ell_b)(x+\ell+\ell_b)W_0 + W\exp[\sigma_b(x+\ell)+j\omega t], \\
&\qquad\qquad\qquad\qquad\qquad -\ell-\ell_b < x < -\ell \\
&= e_1 + e_2 x + d\exp(\beta x) + [U\exp(\sigma_s x) + V\exp(-\sigma_s x) \\
&\quad - E\exp(\beta x)]\exp(j\omega t), \qquad -\ell < x < 0 \\
&= (1-x/\ell_g)\theta_0 + \theta\exp(-\sigma_g x + j\omega t), \\
&\qquad\qquad\qquad\qquad\qquad 0 < x < \ell_g,
\end{aligned}
\qquad (4)
$$

where W, U, V, E, and θ are complex-valued constants; e_1, e_2, d, W_o, and θ_o are real valued constants, and $\sigma_i = (1+j)a_i$, with $a_i = (\omega/2\alpha_i)^{1/2}$.

It should be noted that θ and W represent the complex amplitudes of the periodic temperature at the sample-gas interface (x=0) and the sample-backing material boundary (x=-ℓ), respectively. The quantities θ_o and W_o represent the real, dc component of the temperature, relative to ambient, at these boundaries (x=0 and x=-ℓ), respectively. The dc solution in the backing material and gas already make use of the assumption that the temperature, relative to ambient, is zero at the ends of the cell. The quantities E and d, which are determined by the forcing function in Equation (1), are given by:

$$d = -A/\beta^2 \tag{5a}$$

and

$$E = \frac{A}{(\beta^2 - \sigma^2)} = \frac{\beta I_o}{2k_s(\beta^2 - \sigma^2)} \tag{5b}$$

In the general solution, Equation (4), the growing exponential component of the solutions to the gas and the backing material has been omitted, since for all frequencies ω of interest, the thermal diffusion length is small compared to the length of both the gas and backing materials. Thus the sinusoidal components of these solutions are sufficiently damped so as to be essentially zero at the cell walls, hence the growing exponential components of the solutions must have coefficients essentially

28

equal to zero in order to satisfy the temperature constraint at
the cell walls.

The temperature and flux continuity conditions at the sam-
ple's front and back surfaces are explicitly given by:

$$\phi_g(0,t) = \phi_s(0,t), \tag{6a}$$

$$\phi_b(-\ell,t) = \phi_s(-\ell,t), \tag{6b}$$

$$k_g \frac{\partial \phi_g}{\partial x}(0,t) = k_s \frac{\partial \phi_s}{\partial x}(0,t) \tag{6c}$$

and

$$k_b \frac{\partial \phi_b}{\partial x}(-\ell,t) = k_s \frac{\partial \phi_s}{\partial x}(-\ell,t) \tag{6d}$$

where the subscripts s, b, and g identify the solution to equa-
tion (4) for the solid, backing, and gas. The above-stated
constraints apply separately to the dc component and the sinusoi-
dal component of the solution. From Equation (6), we obtain for
the dc component of the solution:

$$\theta_o = e_1 + d, \tag{7a}$$

$$W_o = e_1 - e_2 \ell + d \exp(-\beta\ell), \tag{7b}$$

$$-(k_g/\ell_g)\theta_o = k_s e_2 + k_s \beta d \tag{7c}$$

$$(k_b/\ell_b)W = k_s e_2 + k_s \beta d \exp(-\beta\ell). \tag{7d}$$

Equations (7) determine the coefficients e_1, e_2, W_o, and θ_o for
the time-independent (dc) component of the solution. Applying

Equations (6) to the sinusoidal component of the solution yields:

$$\theta = U+V-E, \tag{8a}$$

$$W=U\exp(-\sigma_s\ell)+V\exp(\sigma_s\ell)-E\exp(-\beta\ell), \tag{8b}$$

$$-k_g\sigma_g\theta=k_s\sigma_sU-k_s\sigma_sV-k_s\beta E, \tag{8c}$$

and

$$k_b\sigma_bW=U\exp(-\sigma_s\ell)-k_s\sigma_sV\exp(\sigma_s\ell)-k_s\beta E\exp(-\beta\ell). \tag{8d}$$

These equations together with the expression for E in Equation (5b) determine the coefficients U, V, W, and θ. Hence the solutions to Equations (7) and (8) allow for evaluation of the temperature distribution, Equation (4), in the cell in terms of the optical, thermal, and geometric parameters of the system. The explicit solution of the complex amplitude of the periodic temperature at the solid-gas boundary (x=0) is given by:

$$\theta = \frac{\beta I_0}{2ks(\beta^2-\sigma^2)}\frac{(r-1)(b+1)\exp(\sigma_s\ell)-(r+1)(b-1)\exp(-\sigma_s\ell)+2(b-r)\exp(-\beta\ell)}{(g+1)(b+1)\exp(\sigma_s\ell)-(g-1)(b-1)\exp(-\sigma_s\ell)} \tag{9}$$

where

$$b=\frac{k_ba_b}{k_sa_s} \tag{10}$$

$$g=\frac{k_ga_g}{k_sa_s} \tag{11}$$

$$r=(1-j)\frac{\beta}{2a_s}, \tag{12}$$

and

$$\sigma_s=(1-j)a_s$$

Thus, Equation (9) can be evaluated for specific parameter values yielding a complex number whose real and imaginary parts θ_1 and θ_2 respectively, give the in-phase and quadrature components of the periodic temperature variation at the sample's front surface. Specifically, the actual temperature at the sample surface $(x=0)$ is given by:

$$T(0,t)=\Phi+\theta_0+\theta_1\cos\omega t-\theta_2\sin\omega t,$$

where Φ is the ambient temperature (room temperature) at the cell walls and θ_0 is the increase in temperature from the steady state component of the absorbed heat.

C. Production of the Acoustic Signal

As previously stated, the acoustic signal detected in the photoacoustic cell arises from the periodic heat flow from the sample to a layer of the gas at the gas-sample interface. This periodic heat diffusion causes a periodic temperature variation in the gas given by the sinusoidal (ac) component of Equation (4), which is:

$$\phi_{ac}(x,t)=\theta\exp(-\sigma_g x+j\omega t). \tag{13}$$

Taking the real part of Equation (13), it can be seen that the actual temperature variation in the gas is:

$$T_{ac}(x,t)=\exp(-a_g x)[\theta_1\cos(\omega t-a_g x)-\theta_2\sin(\omega t-a_g x)], \tag{14}$$

where θ_1 and θ_2 are the real and imaginary parts of θ, as given

31

by Equation (9). The time-dependent component of the temperature in the gas attenuates rapidly to zero with increasing distance from the surface of the solid sample, and, at a distance of only $2\pi\mu_g$ from the surface, is effectively fully damped out. We can therefore define a boundary layer of thickness $2\pi\mu_g$, and make the approximation that only this gas layer is capable of responding thermally to the periodic temperature at the sample surface.

The spatially averaged temperature within this gas boundary layer can be determined, as a function of time, by evaluating:

$$\overline{\phi}(t) = (\frac{1}{2\pi\mu_g})\int_0^{2\pi\mu_g}\phi_{ac}(x,t)dx$$

From Equation (13) this gives:

$$\overline{\phi}(t) \approx (\frac{1}{2\sqrt{2}\,\pi})\theta\exp\left[j(\omega t - \tfrac{1}{4}\pi)\right]$$

(15)

using the approximation that $\exp(-2\pi) \ll 1$.

Since the gas boundary layer expands and contracts periodically due to the periodic diffusion of heat into this layer from the sample surface, it can be treated as an acoustic piston acting on the rest of the gas column, producing an acoustic pressure signal that is transmitted through the entire column. The displacement of the gas piston due to its periodic heating can be estimated by using the ideal gas law,

$$\delta x(t) = 2\pi\mu_g\frac{\overline{\phi}(t)}{T_0} = \frac{\theta\mu_g}{\sqrt{2}\,T_0}\exp\left[j(\omega t - \tfrac{1}{4}\pi)\right]$$

(16)

where we have set the average dc temperature of this gas boundary layer equal to the dc temperature at the sample surface ($T_o = \phi + \theta_o$). Equation (16) is a reasonable approximation to the actual displacement of the layer since $2\pi\mu_g$ is only approximately 0.1 cm for $\omega/2\pi = 100$ Hz and even smaller for higher frequencies.

If we assume that the rest of the gas responds to the action of this piston adiabatically, then the acoustic pressure in the cell due to the displacement of the gas piston is derived from the adiabatic gas law:

$$PV^\gamma = \text{constant},$$

where P is the pressure, V is the gas volume, and γ is the ratio of the specific heats. Thus the incremental pressure is:

$$\delta P(t) = \frac{\gamma P_o}{V_o} \delta V = \frac{\gamma P_o}{\ell_g} \delta x(t)$$

where P_o and V_o are the ambient pressure and volume, and $-\delta V$ is the incremental volume. Then from Equation (16) we have:

$$\delta P(t) = Q \exp[j(\omega t - \tfrac{1}{4}\pi)], \tag{17}$$

where

$$Q = \frac{\gamma P_o \theta}{\sqrt{2} \, \ell_g a_g T_o} \tag{18}$$

Therefore, the actual physical pressure variation, $\Delta P(t)$, is given by the real part of $\delta P(t)$, and is:

$$\Delta P(t) = Q_1 \cos(\omega t - \tfrac{1}{4}\pi) - Q_2 \sin(\omega t - \tfrac{1}{4}\pi), \tag{19}$$

or,

33

$$\Delta P(t) = q\cos(\omega t - \psi - \tfrac{1}{4}\pi),\tag{20}$$

where Q_1 and Q_2 are, respectively, the real and imaginary parts of Q, and q and $-\psi$ are the magnitude and phase of Q, thus,

$$Q = Q_1 + jQ_2 = q\exp(-j\psi).$$

The value Q specifies the complex envelope of the sinusoidal pressure variation. Combining Equations (9) and (18) we get the explicit formula:

$$Q = \frac{\beta I_0}{2\sqrt{2}k_s\ell_g a_g T_0} \frac{\gamma P_0}{(\beta^2 - \sigma_s^2)} \cdot \frac{(r-1)(b+1)\exp(\sigma_s\ell) - (r+1)(b-1)\exp(-\sigma_s\ell) + 2(b-r)\exp(-\beta\ell)}{(g+1)(b+1)\exp(\sigma_s\ell) - (g-1)(b-1)\exp(-\sigma_s\ell)}$$

$$\tag{21}$$

where $b = k_b a_b / k_s a_s$, $g = k_g a_g / k_s a_s$, $r = (1-j)\beta / 2a_s$, and $\sigma_s = (1+j)a_s$ as previously defined. At ordinary temperatures T_0 is essentially equal to Φ, thus the dc components of the temperature distribution need not be evaluated. Hence, Equation (21) may be evaluated for the magnitude and phase of the photoacoustic response, represented by the acoustic pressure wave produced in the cell.

D. Special Cases

Although the full expression for $\delta P(t)$ is somewhat difficult to interpret due to the complicated expression for Q as given by Equation (21), physical insight may be gained by examining special cases of interest, where the expression for Q can be simplified. Some such special cases for optically opaque and optically transparent samples are considered here, with opaqueness being

34

determined by the relation of the optical absorption length,

$$\mu_\beta = 1/\beta$$

to the thickness ℓ of the solid. For each category of optical opaqueness, three cases are considered according to the relative magnitude of the thermal diffusion length μ_s, as compared to the physical length ℓ and the optical absorption length μ_β. For all of these cases, we make the reasonable assumptions that g<b and b is approximately one. Also, it is convenient to define

$$Y = \frac{\gamma P_0 I_0}{2\sqrt{2} \, \ell_g T_0} \tag{22}$$

which appears in the expression for Q in each case. The six cases are illustrated in Figure 2.3 (19) and are individually considered in the following discussion.

Case 1: Optically Transparent Solids $(\mu_\beta > \ell)$

In these cases, absorption of light occurs throughout the entire length of the sample.

Case 1(a): Thermally thin solids $(\mu_s >> \ell; \ \mu_s > \mu_\beta)$

Here we set $\exp(-\beta\ell) \overset{\sim}{=} 1 - \beta\ell$, $\exp(\pm\sigma_s\ell) \overset{\sim}{=} 1$, and $|r| > 1$ in Equation (21). We then obtain:

$$Q = \frac{\ell Y}{2a_g a_b k_b}(\beta - 2a_s b - j\beta) \simeq \frac{(1-j)\beta\ell}{2a_g}(\mu_b/k_b)Y \tag{23}$$

The acoustic signal is thus proportional to $\beta\ell$ and, since μ_b/a_g is proportional to $1/\omega$, the acoustic signal has a ω^{-1} dependence.

35
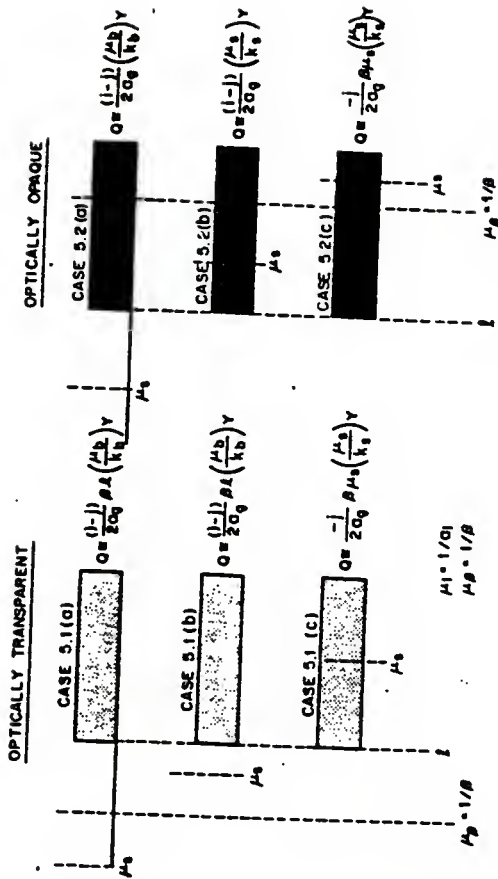
FIGURE 2.3. Schematic illustration of special cases considered in Rosencwaig-Gersho theory.

36

Since the thermal diffusion length of the sample is greater then the sample length, the thermal properties of the backing material affect the photoacoustic response, and the expression for Q is thus a function of these properties.

Case 1(b): Thermally thin solids ($\mu_s > \ell$; $\mu_s < \mu_\beta$)

Here we set $\exp(-\beta\ell) = 1-\beta\ell$, $\exp(\pm\sigma_s\ell) = (1\pm\sigma_s\ell)$, and $|r| < 1$ in Equation (21). We then obtain:

$$Q = \frac{\beta\ell Y}{4k_s a_g a_s^3 b}\left[(\beta^2+2a_s^2)+j(\beta^2-2a_s^2)\right]$$

$$\approx \frac{(1-j)\beta\ell}{2a_g}(\mu_b/k_b)Y \qquad\qquad (24)$$

Here, the acoustic signal is again proportional to $\beta\ell$, varies as ω^{-1}, and depends on the thermal properties of the backing material as well. The expression for the acoustic signal in this case is identical to Equation (23).

Case 1(c): Thermally thick solids ($\mu_s < \ell$; $\mu_s \ll \mu_\beta$)

Here, the approximations that are made are $\exp(-\beta\ell) = 1-\beta\ell$, $\exp(-\sigma_s\ell) \overset{\sim}{=} 0$, and $|r| \ll 1$. The acoustic signal then becomes:

$$Q = -j\frac{\beta\mu_s}{2a_g}(\mu_s/k_s)Y \qquad\qquad (25)$$

The acoustic signal here is now proportional to $\beta\mu_s$ rather than $\beta\ell$. That is, only the light absorbed within the first thermal diffusion length of the sample contributes to the signal. Also, since $\mu_s < \ell$, the thermal properties of the backing material pres-

37

ent in Equation (24) are replaced by those of the solid. In this expression, the dependence of Q on the modulation frequency varies as $\omega^{-3/2}$.

Case 2: Optically Opaque Solids ($\mu_\beta << \ell$)

In these cases, most of the light being absorbed by the sample is within a distance small compared to the length ℓ of the sample.

Case 2(a): Thermally thin solids ($\mu_s >> \ell$; $\mu_s >> \mu_\beta$)

In Equation (21), we set $\exp(-\beta\ell) \overset{\sim}{=} 0$, $\exp(\pm\sigma_s\ell) \overset{\sim}{=} 1$, and $|r| >> 1$. We then obtain:

$$Q = \frac{(1-j)}{2a_g}(\mu_b/k_b)Y$$

(26)

In this case, we have photoacoustic "opaqueness" as well as optical opaqueness, in that the acoustic signal is independent of β, This would be the case of a very black absorber such as carbon black. The acoustic signal is quite strong, and depends on the thermal properties of the backing material. For this case, the dependence of the signal on frequency is given as a function of ω^{-1}.

Case 2(b): Thermally thick solids ($\mu_s < \ell$; $\mu_s > \mu_\beta$)

In Equation (21), we set $\exp(-\beta\ell) \overset{\sim}{=} 0$, $\exp(-\sigma_s\ell) \overset{\sim}{=} 0$, and $|r| > 1$. We obtain:

$$Q = \frac{-j\beta Y}{4a_g a_s^3 k_s}(2a_s-\beta+j\beta) \overset{\sim}{=} \frac{j\beta\mu_s}{2a_g}(\mu_s/k_s)Y$$

(27)

38

Equation (27) is analogous to Equation (26), but the thermal parameters of the backing are now replaced by those of the solid. Again, the acoustic signal is independent of the optical absorption coefficient and varies as ω^{-1}.

Case 2(c): Thermally thick solids ($\mu_s \ll \ell$; $\mu_s < \mu_\beta$)

Here, again, we set $\exp(-\beta\ell) = 0$, $\exp(-\sigma_s\ell) \cong 0$, and let $|r| < 1$ in Equation (21). We obtain:

$$Q = \frac{-j\beta Y}{4a_g a_s^3 k_s}(2a_s - \beta + j\beta) = \frac{j\beta\mu_s}{2a_g}(\mu_s/k_s)Y$$

(28)

In this case, although the solid is optically opaque, it is not photoacoustically opaque, since only the light absorbed within the first thermal diffusion length will contribute to the acoustic signal. Even though the solid is opaque, the photoacoustic signal will be proportional to the optical absorption coefficient. As in case 1(c), the signal varies as $\omega^{-3/2}$.

2.4 Summary

The Rosencwaig-Gersho theory presented above provides a derivation of the exact solutions for the acoustic pressure produced in an enclosed cell by the photoacoustic effect. These equations are then evaluated to give specific solutions for special cases of physical significance. Three characteristic lengths are important in determining which of the specific solutions are applicable for a given sample, these being the thermal diffusion length, optical absorption length, and the physical

39

thickness of the sample. Since our experiments primarily in-
volved wheat kernels, which are optically opaque, only the theo-
retical cases for which the optical absorption length of the
sample is less than the length of the sample itself are relevant
with respect to our results. It should be noted that the theory
assumes one-dimensional photoacoustic apparatus, no reflection
from the sample surface, 100% non-radiative deexcitation within
the sample, a non-absorbing gas, and a gas thermal diffusion
length less than the length of the column of gas contained in the
cell. These assumptions will generally not all be completely
valid in practice, and may affect the agreement of experimental
results with theoretical predictions. The following chapter
gives a detailed description and discussion of the actual photoa-
coustic apparatus which we used in the experiments performed
throughout this thesis work.

EXPERIMENTAL APPARATUS FOR PHOTOACOUSTIC ANALYSIS

All sample analysis studies utilizing the photoacoustic effect are similar in that they require the basic components needed to produce the effect; these being an enclosed sample cell, some intensity modulated energy source made incident upon the enclosed sample, a suitable acoustic signal detection device, and a method by which this signal can be recorded and analyzed. Even so, the particular components used and the methods by which they are employed will vary widely with respect to the material being studied and the information sought regarding this material. In this section, the actual experimental apparatus and analysis techniques used in these studies will be described and discussed.

Shown in Figure 3.1 is a schematic diagram of the photoacoustic sampling apparatus used in these studies. The primary components of this setup include: 1, a photoacoustic cell with built in LED, light sensitive PIN diode, and microphone; 2, a Hewlett-Packard model 3311A function generator; 3, a current amplifier; 4, an Ithaco model 393 lock-in amplifier; and 5, a Zenith Z-150 personal computer with installed Qua-Tech D-A and A-D converters, connected to a Qua-Tech input/output terminal connector board. Additional supporting components include two dc power supplies needed to power the current amplifier and the microphone, and a Keithley Instruments model 155 microvoltmeter used to monitor the light intensity in the photoacoustic cell as

41
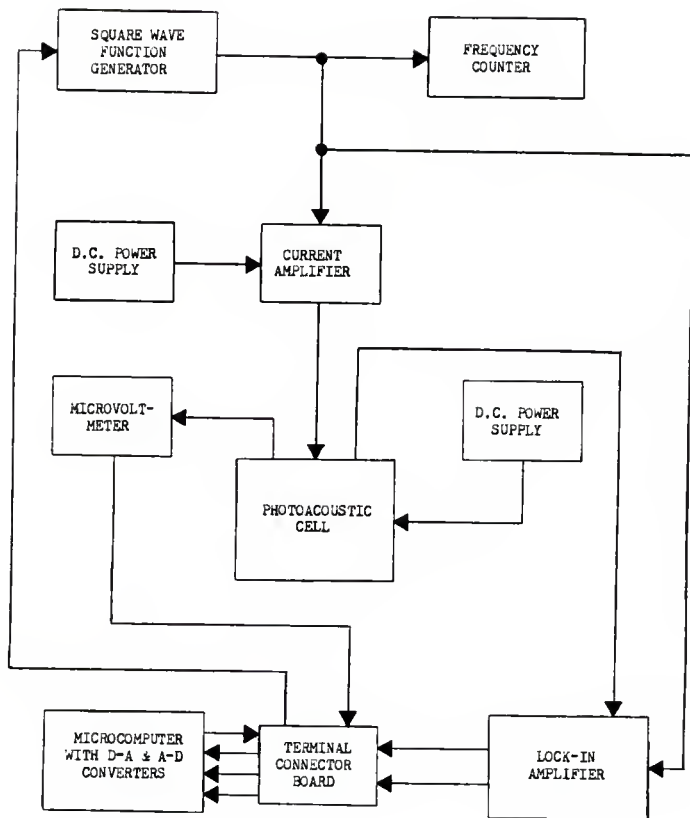
FIGURE 3.1. Schematic diagram of the photoacoustic sampling apparatus.

42

detected by the PIN diode. A more detailed discussion of these components, and how they are incorporated into the actual arrangement used in these photoacoustic sample analysis studies, is given below.

3.1 The Photoacoustic Cell

There is probably no single photoacoustic cell design which is best for all types of photoacoustic sample analysis. The cell must be able to accommodate the sample being analyzed, the modulated energy beam used, the acoustic signal detector, and any other experimental requirements. Designs, therefore, will vary according to these constraints. There are, however, certain criteria that must be considered in the design in order to maximize the acoustic signal obtained from the sample and minimize all extraneous signals and noise. These include the size of the sample chamber, the acoustic isolation of the cell, the material of which the cell is constructed, and the relative placement of the microphone in the cell.

A. Description of Photoacoustic Cell

A diagram of the cell used in these studies is given in Figure 3.2. The main structure of the cell was constructed from a rectangular block of aluminum, having a height of 7.6 cm a length of 10.2 cm and a width of 6.4 cm. Each of the two 6.4x7.6 cm sides of the cell had rectangular-shaped cavities machined into the main cell structure. Installed into the cavity on the left side was a Hewlett-Packard 5082-4200 light-sensitive PIN

43

PIN DIODE OUTPUT

INPUT POWER FOR
LED OPERATION

PAS OUTPUT TO
LOCK-IN AMPLIFIER

PIN DIODE

WINDOW

LED

TO D.C. POWER
SUPPLY

M

MICROPHONE

WHEAT GRAIN SAMPLE
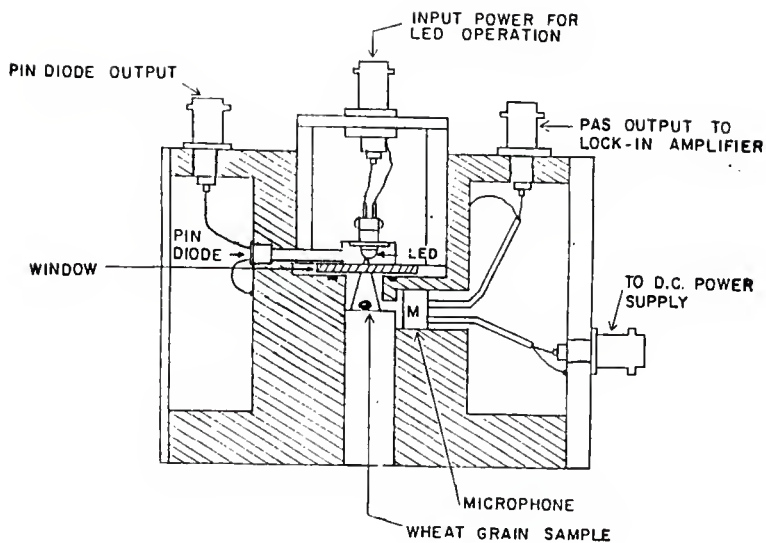
FIGURE 3.2.   Cross-sectional diagram of the photo-
acoustic cell.

diode, and installed into the right-side cavity was a Radio Shack
Archer electret microphone element. The volume in these cavities
not occupied by the diode and microphone was packed with an
insulating filler material. The cavities were sealed by 1.25-cm-
thick lead plates, which were fastened to each side by two tight-
ening screws. A thin sheet of compressible plastic foam was
positioned between each lead plate and the main structure of the
cell to improve the seal at the aluminum-lead interface.

Centered at the top of the main structure of the cell was a
cylindrical cavity having a 3.8 cm diameter, which extended from
the top surface to a depth of 3.0 cm. Centered at the base of
this cavity was a smaller cylindrical cavity with 1.0 cm diameter
and adjustable depth. This portion of the cell was the actual
sample chamber. The base of this chamber consisted of a separate
cylinder held in place by a pair of O-rings which were installed
in two separate circular depressions formed about the circumfer-
ence of the cylinder, permitting a tight fit between the sample
chamber cavity and the chamber base. By applying sufficient
pressure, the cylindrical base could be forced to slide up or
down within the chamber cavity, thus giving the sample chamber an
adjustable depth and variable volume, with a maximum chamber
depth of approximately 1.7 cm. Surrounding the circumference of
this chamber, in the base of the larger cylindrical cavity, was a
circular notch into which was placed a rubber O-ring. On the top
of this O-ring, which protruded slightly above the surface of the
cavity base, was centered a square, 1.57 millimeter thick, Supra-

45

sil fused quartz window. Gas ports were drilled in the front and
rear sides of the photoacoustic cell, extending from the sample
chamber to the outside of the cell. These ports could be opened
or closed using needle valves installed into these openings on
the outside of the cell's main structure. Also, a port extended
from the sample chamber to the right side cavity of the main
structure, where it met with the microphone installed into this
cavity.

Into the larger cylindrical cavity extending downward from
the top of the cell was fitted a removable light source contained
in a cylindrical plug. The plug was constructed of aluminum,
with a diameter equal to that of the cavity and length slightly
greater then the cavity depth. Once inserted completely into the
cavity, this cylindrical plug could be fastened in place by
tightening a plastic set screw installed into the front side of
the cell's main structure. The bottom end of the plug (the end
placed into the cavity) had a shallow, disk-shaped recess. The
light source built into this plug, which protruded slightly from
a small hole at the center of this recess, was a Texas Instru-
ments TIL-31 high-intensity, infrared-emitting LED, positioned so
that it irradiated downward, through the quartz window and into
the sample chamber. The recess in the base of the plug was small
enough in diameter so that when the plug was inserted into the
cavity, the corners of the quartz window encountered the outer,
non-recessed portion of the plug base, thus allowing the quartz
window to be pressed up against the rubber O-ring, with pressure

46

applied to the inserted plug being transmitted to the O-ring seal. In the side of the plug, near its base, extending through to the recess in the plug base, was a small hole allowing for a small amount of the scattered radiation emitted by the LED to escape. Also, in the left side of the main structure of the photoacoustic cell was a hole which extended to the left side cavity in the main structure, into which was installed the PIN diode. The relative position of these two holes was such that, when the cylindrical plug was properly aligned the cavity, the holes would be aligned as well, and an opening would completely extend from the recess in the plug to the light sensitive PIN diode, allowing for a measure of the relative intensity of e-m radiation produced by the LED.

In order to monitor the output of the microphone and PIN diode, BNC connectors were installed on the left and right sides of the top surface of photoacoustic cell's main structure with electrical connections extending to the PIN diode and the micro-phone respectively. Also, toward the left side of the rear of the main structure, a BNC connector also was installed, extending to the microphone, so as to provide it with a power input. A BNC connector was also positioned on the top surface of the cylindri-cal plug, with electrical connections extending to the LED, in order to provide the LED with a power source.

B. Discussion of the Photoacoustic Cell Design

The photoacoustic cell used in these experiments was con-structed of aluminum so as to minimize the photoacoustic response

47

produced by the walls of the sample chamber. Although it is not
feasible to completely eliminate the chamber response, use of a
material, such as aluminum, with relatively low absorption (high
reflectivity), high density, and high thermal conductivity,
should give rise to a chamber response small in comparison with
that of the sample being studied, assuming that the sample does
not possess similar characteristics. The microphone in the cell
was sufficiently remote from the illuminated portion of the
chamber so that any scattered light incident upon it should be
insignificant in comparison to the direct illumination of the
sample; thus any contribution to the photoacoustic signal arising
from the microphone's interaction with this stray light should be
minimal. The fused quartz window used in the cell has a high
degree of transparency, allowing the sample to receive as much of
the emitted radiation as possible from the LED, and absorbing
very little so as to minimize the response of the window itself.

In photoacoustic examination of solids, the purpose of the
gas in the cell is to undergo pressure fluctuations in response
to temperature increases at the surface of the solid sample, and
to transmit these pressure increases to the microphone. Thus, it
is important that the gas used in the cell be as non-absorbing as
possible, as e-m radiation absorbed in the gas will lead to a
strong undesirable photoacoustic response from the gas itself.
The gas used in the sample chamber was helium, which was intro-
duced through the needle-valve-controlled openings in the front
and rear sides of the cell. Since helium is a non-absorbing gas,

problems with absorption and subsequent photoacoustic responses from the gas were minimized. Furthermore, the Rosencwaig-Gersho theory states that the amplitude of the photoacoustic response for a given sample increases as the thermal conductivity of the gas used in the chamber is increased, varying as $k^{1/2}$. Since it is desirable to obtain as high of a signal amplitude as possible, it is beneficial to use a gas, such as helium, with a relatively high thermal conductivity.

Another concern in photoacoustic cell design is minimization of the effects of noise from the outside environment. Since a lock-in amplifier was used to amplify the photoacoustic signal, locking-in-on and amplifying only signals having the same frequency and a constant phase relationship as compared to the modulation frequency of the incident e-m radiation, a certain amount of noise could be tolerated, as long as the noise was not periodic with the same frequency as the modulation frequency being used. For the most part, external noise did not present any serious problem, which is at least partially due to the design of our photoacoustic cell. Although the cell was primarily constructed of aluminum, a material of fairly low density, the walls of the cell were sufficiently thick for adequate acoustic isolation of the sample chamber from outside noise, as reflected in the dimensions of the cell previously given. Also, the lead plates used to enclose the ends of the cell helped to provide better acoustic isolation for the chamber, and the entire photoacoustic cell was placed on a thick lead block throughout

49

all the experiments to help reduce the effects of external vibrations.

The physical size of the sample chamber is also an important consideration in the design of a photoacoustic cell. As previously stated, the design of the sample chamber was such that the volume of the chamber in the photoacoustic cell could be varied by changing the the chamber depth. The volume of the chamber is important, since the acoustic signal is inversely proportional to the length of the gas column occupying the cell, as stated previously in the theoretical section. This dependency suggests using as small a volume as possible in order to maximize the amplitude of the response. However, according to the Rosencwaig-Gersho theory, it is also important that the dimensions of the sample chamber be greater than one thermal diffusion length of the gas occupying the cell, since the gas layer of one diffusion length thickness at the gas-sample interface expands to create the pressure fluctuation in the cell, or acoustic signal, which is ultimately transmitted to the microphone. In addition, the chamber size should be large enough so that dissipation of the signal to the walls and window of the cell prior to the detection of the signal by the microphone is not excessive.

The Rosencwaig-Gersho theory is strictly valid only for cases where the length of the gas column is substantially greater than the thermal diffusion length of the gas used in the chamber. For helium, the density, specific heat, and thermal conductivity are 0.180 kg/cm^3, 5232 $J/kg-deg$ C, and 0.142 $J/m-s-deg$ C respec-

50

tively (21). The values of these parameters result in a thermal diffusion length for helium of 1.73 cm, at a modulation frequency of 1 Hz, which corresponds approximately to the maximum chamber depth obtainable for the photoacoustic cell used. Of course, as the modulation frequency is increased, the thermal diffusion length, which varies as $\omega^{-1/2}$, will decrease, becoming 0.055 cm at a modulation frequency of 1000 Hz. It is therefore to be expected that the Rosencwaig-Gersho theory will not be completely applicable to the results obtained at low modulation frequencies, and becoming even less so as the chamber depth is decreased.

The size effects of a photoacoustic chamber having dimensions comparable to or less than the thermal diffusion length of the gas used in the sample chamber have been investigated, both theoretically and experimentally, by Aamodt, Murphy, and Parker (22). In a theoretical derivation, they obtain a relationship giving the photoacoustic signal amplitude as a product of two separately defined parameters A and g; with A being dependent upon the optical absorption coefficient, thermal properties, and length of the sample, as well as the thermal properties of the backing material for optically and thermally thin samples; and g being essentially a sensitivity factor, determined by such parameters as the cell length and gas thermal properties, being relatively insensitive to the sample's thermal properties when the cell is long compared to the thermal diffusion length of the gas. In the case where the the length of the gas column is much greater than the gas thermal diffusion length, their results

51

parallel the conclusions of the Rosencwaig-Gersho theory, with the amplitude of the photoacoustic response varying inversely as the length of the sample chamber. As the length, L, of the sample chamber is decreased and approaches the thermal diffusion length, μ_g, of the gas, the amplitude vs chamber length curve levels off and reaches a maximum at a chamber length value of approximately $\ell = \mu_g$. For $\ell < \mu_g$, the amplitude vs chamber length curve generally takes on a positive slope, with signal amplitude decreasing as chamber length is decreased. In this region the exponential dependence of the amplitude of the signal on the sample chamber length is dependent on the thermal properties of both the sample and chamber window. Figure 3.3 shows some of their published experimental data, for both the amplitude and the phase of the signal, illustrating this effect. The sample used in their experiment was carbon black and the gas used was helium. The maximum amplitude for a given modulation frequency occurs at approximately the point at which the chamber length is equal to the thermal diffusion length for helium.

3.2 The Modulated Electromagnetic Radiation Source

The source of e-m radiation used throughout all experiments done in this thesis work was a Texas Instruments TIL-31 light (infrared) emitting diode. This LED was built into the photoacoustic cell, as previously described, and was oriented so that e-m radiation emitted from the diode was directed downward, illuminating the sample located directly below it. The diode had

52
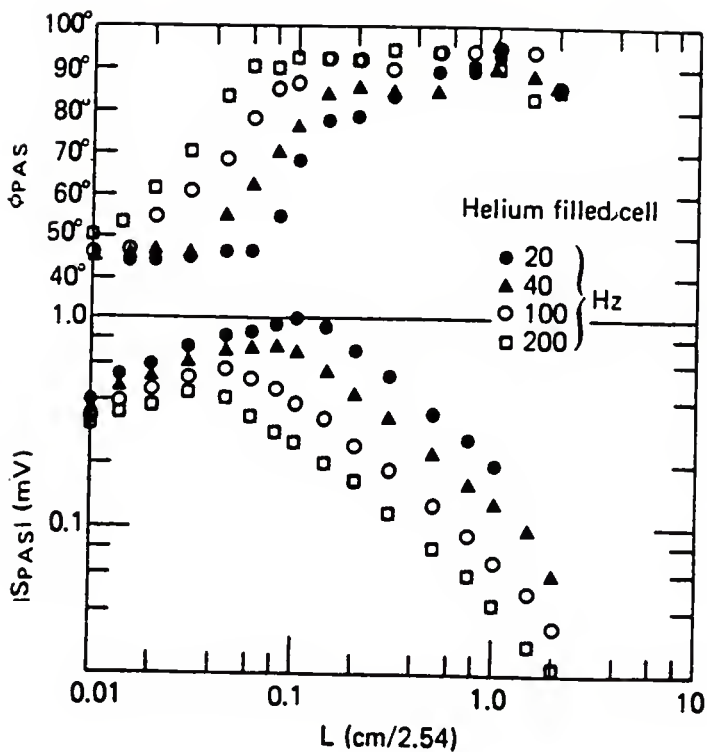
FIGURE 3.3. A plot of the variation in the photoacoustic
response of carbon black with cell length at
several different modulation frequencies.

53

a fixed lens positioned on its surface to help focus the beam. The half-intensity beam angle of the diode was only 10 degrees, thus a minimal amount of beam spreading was experienced, enabling the majority of the e-m radiation output of the diode to be directed to the sample surface. The output radiation of the LED was essentially monochromatic, having a peak emission wavelength of 9400 angstroms with a typical total bandwidth of 500 angstroms. The on-off and off-on switching times of the LED were 350 ns and 600 ns respectively, which were more than adequate for the modulation frequencies used in these experiments.

Intensity modulation of the LED´s output radiation was achieved by modulation of its power supply. The modulation was in the form of an on/off square wave, with the signal being supplied by a Hewlett-Packard model 3311A variable frequency function generator. This function generator allowed the user to select a frequency range via a front panel selector switch and then vary the output frequency of the generator throughout this range either by adjusting a frequency calibrated front panel potentiometer, or by sending a 0 to -15 volt dc signal into a voltage-controlled-oscillator (VCO) input located in the back of the instrument (0 volts correspond-ing to lowest frequency of selected range). The frequency output of the instrument with respect to a given voltage input was designed to be linear throughout the selected frequency range. A factor of 10 frequency increase from the lowest frequency of a given range was per-mitted, using either of these two methods, before an increase in

the frequency range of the instrument needed to be made. A current amplifier was used to amplify the signal supplied to the LED by the frequency generator, drawing power from a Lambda model LP 410 FM dc power supply.

A measure of the relative LED intensity as detected by the PIN diode installed in the photoacoustic cell was provided by connection of the PIN diode output to a Keithley Instruments model 155 microvoltmeter. A front panel meter with variable range selector was provided by the instrument for monitoring of the input voltage. In addition, the microvoltmeter also provided a voltage output, ranging from 0 to 1 volt, directly proportional to the input voltage, with a proportionality constant equal to the selected range setting. Since at low modulation frequencies, a stable voltage reading initially could not be obtained due to the periodicity of the light source being detected, a resistor-capacitor circuit was connected in parallel with the microvoltmeter to rectify the output voltage from the diode.

3.3 The Acoustic Signal Detection Apparatus

In photoacoustic sample analyses which utilize a gas transfer medium for the acoustic signal, the most commonly used device to monitor the acoustic signal is a sensitive microphone, either flat or cylindrical-surfaced. Although cylindrical microphones are generally more sensitive then flat microphones due to their larger surface area, the acoustic response of a cylindrical microphone typically varies with the frequency of the signal that

55

it monitors, while a flat microphone typically maintains a flat response over a wide frequency range. A flat frequency response is more desirable for depth profiling studies where the modulation frequency is varied over a wide frequency range. Consequently, since a frequency-independent response was desired in these experiments, a flat-surfaced microphone was used.

The microphone incorporated into the photoacoustic cell was a Radio Shack Archer electret microphone element with a built-in preamplifier. It had a flat frequency response throughout a 20-3000 Hz frequency range, with the frequency response dropping off somewhat at frequencies lower than 20 Hz. Throughout this experimentation, the microphone proved to be sufficiently sensitive to detect the acoustic signals. The microphone preamplifier was powered by a Lambda model LL-903 variable voltage power supply, maintained at a constant voltage of 8 volts. The preamplifier output was sent directly to an Ithaco model 393 lock-in amplifier.

This lock-in amplifier was capable of accepting a periodic external reference signal within a limited frequency range, and amplifying from an input signal only the ac components with frequencies identical to the reference. Modification of the range of reference frequencies which could be accepted by the lock-in amplifier was possible, being achieved by replacement of several removable internal component boards. In these experiments, two sets of these component boards were used; one set enabling amplification of input signals within a frequency range of 1-100 Hz,

56

and the other within a 10-1000 Hz frequency range. For a given
set of installed boards, amplification of signals at frequencies
higher than a factor of ten increment above their lowest accepta-
ble frequency required changing the setting of a toggle switch
located on the front panel of the lock-in amplifier. Also lo-
cated on the front panel was a sensitivity selector, which needed
to be positioned to an appropriate sensitivity setting, with
respect to the signal being monitored. The amplitude, in-phase
component, and out-of-phase component of the amplified signal
could be monitored either by viewing a selectable front panel
meter built into the instrument, or by measuring voltages sup-
plied by three BNC outputs located in the back of the instrument.
These voltage outputs were proportional to the amplified signal,
with the proportionality constant being essentially equivalent to
the sensitivity setting of the amplifier.

In order to achieve amplification of the true photoacoustic
response, the signal used to modulate the LED was also used as a
reference input for the lock-in amplifier. Since the photoacous-
tic signal is of the same frequency as that of the modulated
light source, this allowed the lock-in amplifier to amplify only
the photoacoustic signal, and and essentially disregard all am-
bient noise in the chamber detected by the microphone. One
source of noise with distinct periodicity which needed to be
minimized was inductive pickup from the 60 Hz ac line voltage and
ripple in the power supply for the microphone preamplifier.

Modulation frequencies close to 60 Hz, and multiples thereof,
were therefore avoided.

3.4   The Data Acquisition System

In acquiring the data with the above-described apparatus, a
software driven data acquisition system was used.   The components
of the acquisition system consisted of a Zenith Z-150 microcompu-
ter, used in conjunction with a Qua Tech PXB-721 parallel expan-
sion board, with added ADM8-10 analog-to-digital (A-D) and DM8-10
digital-to-analog (D-A) converter modules.   The expansion board,
with converter modules, was installed into one of the computer's
expansion slots, with ribbon cables extending from these to the
exterior of the computer.   The ribbon cables were attached to a
Qua Tech UIO-10 universal I/O board which permitted connecting of
the installed expansion board and converter modules to the ex-
perimental apparatus.   A capacity for eight inputs to the A-D
converter and eight outputs from the D-A converter were provided.
The analog voltage output from the D-A converter could be varied
from -5 to 5 volts in increments of 0.03922 volts.   The analog to
digital converter was configured to accept analog voltage inputs
from 0 to 0.5 volts, with a resolution of 8 bits, or 1.953
millivolts.

The software used to control the operation of the A-D and D-
A converters was written in Microsoft BASICA, and used in con-
junction with a software package provided by Qua Tech, enabling
acceas to the converter modules within the context of a BASIC

program. This software package, entitled LABSTAR, defined a series of BASIC commands, allowing various modes of access to the D-A and A-D modules via a machine language program, LABSTAR.EXE; which needed to be separately loaded into computer memory prior to loading the Microsoft BASIC interpreter. The actual BASIC application program utilizing these specialized commands required initial execution of a small BASIC program segment, provided by Qua-Tech under the filename LABSTAR.BAS, designed to compose the first 99 lines of the application program. The purpose of this segment of the application program was to define commands to be used within the program to invoke the machine language subroutines. Prior to execution of one of these specialized commands, a CALL statement specifying memory address information regarding the appropriate machine language subroutine first needed to be executed, and any user-assigned variables associated with the command needed to be properly defined. Some programming capabilities for A-D conversion provided by these commands included the ability to rapidly acquire blocks of data, at a maximum sampling rate of one data point every 33 microseconds, either from a single channel or from a specified range of channels. Also possible was the acquiring of either a single point or block of data upon the request of an external trigger signal or an external clock. Similar commands associated with the D-A converter were capable of specifying either output of single-valued voltages from a given channel, maintained until a different voltage at that channel is specified, or block voltage outputs specified

59

within an array. For block voltage outputs, voltages could be rapidly varied from a single channel, or sequentially from a range of channels, at a maximum output rate of 42 microseconds. Also single point or block data output could be initiated by way of request from an external trigger. A more detailed listing and description of allowed commands is provided in a user's manual supplied by Qua-Tech.

The primary tasks of the data acquisition program were to scan through a range of modulation frequencies, achieved by incrementing the frequency output of the waveform generator, and obtain and record the photoacoustic response from the lock-in amplifier for each of the modulation frequencies produced.   Incrementation of the modulation frequency was achieved by incrementally varying a dc voltage sent to the VCO inputs of the waveform generator, provided by a channel from the D-A converter. Since the D-A converter was capable of providing negative voltage outputs within a range of only 0 to -5 volts, the waveform generator was modified so that the entire frequency range for a given front panel range setting of the instrument could be scanned within this voltage range, instead of its normal 0 to -15 volt range.   This modification affected somewhat the linearity of the output frequency vs input voltage curve, therefore, a best-fit polynomial function was found to relate the modulation frequency to a given input voltage.   The frequency values provided by this function were accurate to approximately +/- 1%, with the deviation being consistent from run to run.   The amplitude and the in-

60

phase component of the photoacoustic response, aa provided by the
lock-in amplifier, were accessed by the computer via two separate
channels of the installed A-D converter. A default number of
fifty consecutive samplings were taken from the lock-in amplifier
at evenly spaced intervals, over a length of time equal to the
time constant setting of the lock in amplifier, for both of these
parameters at a given modulation frequency. The fifty values for
each parameter were subsequently averaged to give the value of
that parameter corresponding to the current modulation frequency.
Since the A-D converter was configured only to accept input
voltages from 0 to 0.5 volts, the lock-in amplifier was used so
as to provide output voltages below this 0.5 volt constraint.

Since the amplitude of the acoustic signal decreases as the
modulation frequency of the incident radiation increases, manual
changes in the sensitivity setting of the lock-in amplifier
needed to be made periodically in the course of analysis of a
given sample. When the amplitude of the photoacoustic response
became low enough that an increase in the sensitivity setting of
the lock-in amplifier could be achieved without producing an
output signal to the A-D converter exceeding 0.5 volts, the
execution of the program was temporarily stopped to allow for
such a sensitivity increase. Once the setting change was made,
the program could be allowed to continue. Another point in the
sampling procedure that required manual setting changes was the
reaching of the upper end of the frequency range for a given
range setting of the waveform generator. At this point the

61

execution of the program needed to be temporarily terminated to allow for increasing this frequency range. Since the upper end of the input frequency range for the lock-in amplifier was reached at this point as well, a manual setting adjustment to increase the acceptable frequency range needed to be made on the lock-in amplifier at this point also. Due to the power law dependence of the signal amplitude on the modulation frequency, fewer data points were needed at the higher modulation frequencies. Therefore, periodically (at multiples of 250 Hz), the size of the modulation frequency increment was allowed to increase to help increase the speed of the sampling process.

Another experimental parameter monitored by the A-D converter was the PIN diode voltage, as detected by the microvoltmeter to which it was connected. In this instance, the 0 to 1 volt voltage output range of the instrument was reduced to a 0 to 0.5 voltage range using a 2-1 voltage divider. The output voltage from the microvoltmeter within this range was sent to a channel of the A-D converter from which a series of fifty readings were taken over a one second interval, and subsequently averaged, for each modulation frequency. Due to the fact that the intensity of the LED did not vary greatly throughout the entire range of modulation frequencies experimentally used, modification of the range selection of the microvoltmeter was not required in the course of a given run, provided that a sufficiently low range selection had initially been chosen.

When scanning through the desired range of modulation fre-
quencies was completed for a given sample (1-50 Hz for the low
frequency, and 10-1000 Hz for the high frequency lock-in ampli-
fier component boards), sampling was terminated and the acquired
data was filed on 5.25 inch floppy disks for future analysis. A
hard copy of the data was also printed as acquired during the
actual experimental run. Given below is a general outline sum-
marizing the major objectives used in programming the Zenith Z-
150 microcomputer for the task of data acquisition. Two slightly
different versions of the program were created, one for data
acquisition in the 1-50 Hz frequency range, and one for the 10-
1000 Hz frequency range, since both ranges could not be scanned
at once due to the frequency range limitations of the lock-in
amplifier. However, both programs followed this general outline
(with the exception of step 10 and part of step 5 being omitted
in the lower frequency range acquisition program). A generalized
flowchart of the data acquisition routine utilized in these
programs (steps 5 through 14) is provided in Appendix I.

Data Acquisition Programming Objectives

1. Initially define Labstar commands to be used with the D-
A and A-D converters (this portion of the program, lines 1-99,
provided by Qua-Tech).

2. Initialize 0 volts to VCO input of waveform generator.

3. Calibrate waveform generator frequency output with fre-
quency counter using front panel potentiometer so that 0 volts

63

input results in lowest frequency output for selected frequency range.

4. Request and/or initialize required parameters for data acquisition process (increment size, sampling rate, etc.).

5. Compute modulation frequency from input voltage to waveform generator, and check to see if it is a multiple of 60 Hz; if so, then increase modulation frequency by appropriate increment and continue execution of program, otherwise, increase data counter by one and store value in data matrix.

6. Execute a delay loop of length approximately equal to 4 times the time constant setting on the lock-in amplifier, to allow lock-in amplifier to reach equilibrium.

7. Acquire fifty samplings of the relative LED signal intensity as provided from the microvoltmeter's measurement of the PIN diode voltage, average these values, and store the average value in the data matrix.

8. Acquire from the lock-in amplifier numerous samplings of the photoacoustic signal amplitude and the in-phase component of the amplitude via the A-D converter, average these values, and store the averaged values in the data matrix.

9. Compute the phase angle from the amplitude and in-phase component of the photoacoustic response, and store this value in the data matrix.

10. Check to see if the size of the frequency increment should be increased; if so, increase it by the prescribed amount.

11. Check to see if the sensitivity setting of the lock-in

64

amplifier should be increased; if so, temporarily halt execution of the program to allow for the setting adjustment.

12. Check to see if the maximum frequency has been reached for the current range setting of the waveform generator; if it has not, then increase the modulation frequency via the D-A converter and continue execution of program at step 4.

13. Check to see if the current modulation frequency has reached the desired termination point; if it has not, then temporarily halt execution of the program to allow for increasing the frequency range setting of the waveform generator, reinitialize appropriate parameters for continued program execution at this new setting, and continue program execution at step 4.

14. Print out the important parameter values used in acquiring the data, provide the option for saving the data matrix as a data file on floppy disk for future analysis, and terminate program execution.

Complete listings of the two acquisition programs actually used in these experiments, both for the low modulation frequency (1-50 Hz) and high modulation frequency (10-1000 Hz) ranges, are provided in Appendices II and III.

Once the data were acquired for a given run and saved as a data file on floppy disk, the Lotus 1-2-3 (23) spreadsheet and graphics software was used manipulate the data and display the results. Data files saved by the acquisition software were organized so that they could be easily read into Lotus 1-2-3 by

65

using its FILE IMPORT command. Once the data were read into a Lotus spreadsheet file, procedures such as normalization and data averaging could be experimented with and performed, and graphic displays of the data could be easily generated for comparisons between kernels.

CHAPTER IV

RESULTS AND DISCUSSION

The results of the various experiments performed throughout this thesis work will be presented and discussed in this chapter. Although the ultimate goal of these experiments was to study the photoacoustic response of various varieties of wheat kernels, a number of other studies were also done to determine the validity and reproducibility of the results and to examine the nature of the photoacoustic response for the empty sample chamber and for various chamber sizes.

At a given modulation frequency, theory states that the photoacoustic response of a sample is dependent upon the sample's thermal and optical properties. However, it also predicts a dependence upon such parameters as the incident e-m radiation intensity, the ambient pressure, thermal diffusivity, and length of the gas column contained in the cell, and the ambient temperature of the sample and its surroundings. In order to attribute variations observed in the photoacoustic response to actual variations in the samples tested, it is imperative that parameters not associated with the sample itself, whose alteration could affect the response, be maintained at constant values between runs for a given experiment. The variable parameters capable of influencing the photoacoustic response in these experiments, and the values used and/or procedures required to initialize them, are as follows:

67

1. The waveform generator was operated at maximum ampli-
tude, with 0 volts dc offset throughout all experiments, and was
checked for proper frequency calibration with 0 volt VCO input
prior to each run.

2. Settings on the current amplifier and power supply
powering the amplifier were maintained so that at a modulation
frequency of 10 Hz the voltage output of the power supply was 3.1
volts and the average current output was 0.19 amps.

3. The microphone voltage input was maintained at a con-
stant value of approximately 8 volts.

4. The lock-in amplifier was operated with zero suppress in
off position, signal mode in maximum noise rejection position,
and phase adjust set at 0 degrees. Also, the ground/isolate
toggle was set for isolated signal input and an external refer-
ence input was provided for all experiments.

5. The sample chamber was provided with a helium gas atmos-
phere at a pressure approximately equal to atmospheric pressure.
In order to achieve this, the following procedure was followed.
For each run, the input and output needle valves were opened
approximately two full turns, and a mild flow of helium gas was
allowed to pass through the chamber for five minutes. After five
minutes had elapsed, both valves were closed nearly simultaneous-
ly, with the output valve being closed approximately one second
after the input valve to allow for pressure equalization with the
outside environment.

6. The ambient temperature of the chamber and the samples

tested was room temperature, which was essentially constant.

7. For each run, the sample being examined was centered as closely as possible in the chamber to allow for direct illumination by the LED.

8. For experiments concerned with detection of variations between wheat varieties, the cell volume was left unaltered between runs.

9. The sample chamber was kept closed between runs, and was periodically cleaned with ethyl alcohol, as was the cell window, to prevent accumulation of contaminants within the cell.

The experiments were performed using the apparatus described in the previous chapter, with the data acquisition process being driven by the BASIC programs listed in the appendix. The quantities measured were the amplitude and in-phase component of the amplitude, from which the phase lag of the photoacoustic response was also derived. Also measured for many of the experiments was the relative intensity of the LED. These quantities were all monitored as a function of the modulation frequency of the LED, throughout overlapping frequency ranges of 1-50 Hz and 10-1000 Hz, with separate runs required to scan each of these frequency ranges for a given sample, due to the earlier-mentioned input frequency limitations of the lock-in amplifier.

4.1 Sample Chamber Studies

A. Black Cloth Study

As a test of the photoacoustic cell and supporting appara-

69

tus, the photoacoustic response of a black cloth sample was measured as a function of modulation frequency, throughout a frequency range of 1-1000 Hz. The cloth sample was cut in the shape of a circular disk, and sized so as to completely cover the bottom of the sample chamber. The depth of the sample chamber for this experiment was 4.8 mm. The log of the amplitude and the phase lag of the response were then plotted as a function of the log of the modulation frequency, and are shown in Figures 4.1 and 4.2 respectively. The slight vertical shift observed in the data, which is most evident in the overlapping 10-50 Hz frequency range, is a result of a variation in the signal processing electronics of the lock-in amplifier caused by replacing its set of removable internal component boards.

The black cloth sample used in this experiment was optically opaque, and it would be reasonable to expect that its optical absorption coefficient was relatively large, resulting in a relatively short optical absorption length. If the optical absorption length is much less then the thermal diffusion length of the sample for the range of modulation frequencies used in this experiment, which would be quite likely in this instance, the Rosencwaig-Gersho theory predicts that the amplitude of the photoacoustic response should vary as ω^{-1}. Upon evaluating the data for this experiment, such a dependence is clearly observed, with the exception of the response at frequencies below approximately 15 Hz, where the slope of the log-log plot becomes less negative. At a modulation frequency of approximately 13 Hz, the thermal

70

Figure 4.1. A log-log plot of the amplitude of the

photoacoustic response vs modulation frequency

for the black cloth sample. Sample chamber
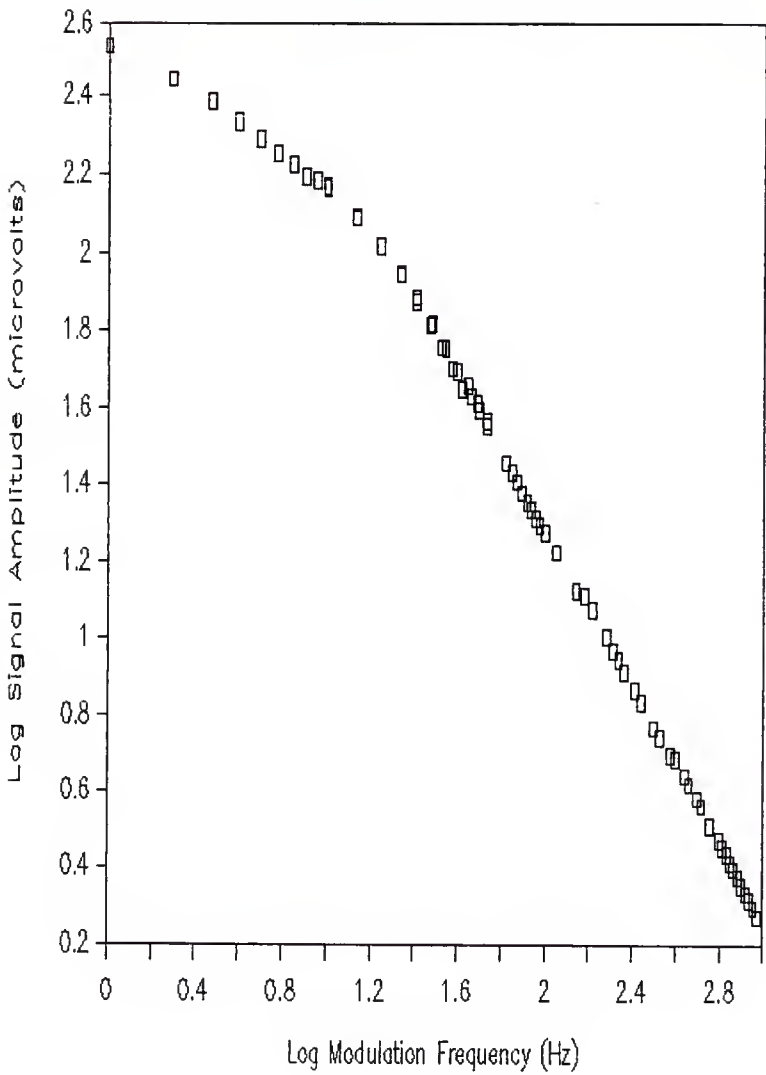
depth = 4.8 mm.

Fig 4.2. A plot of the phase of the photoacoustic

response vs log modulation frequency for the

black cloth sample. Sample chamber depth = 4.8 mm.

73
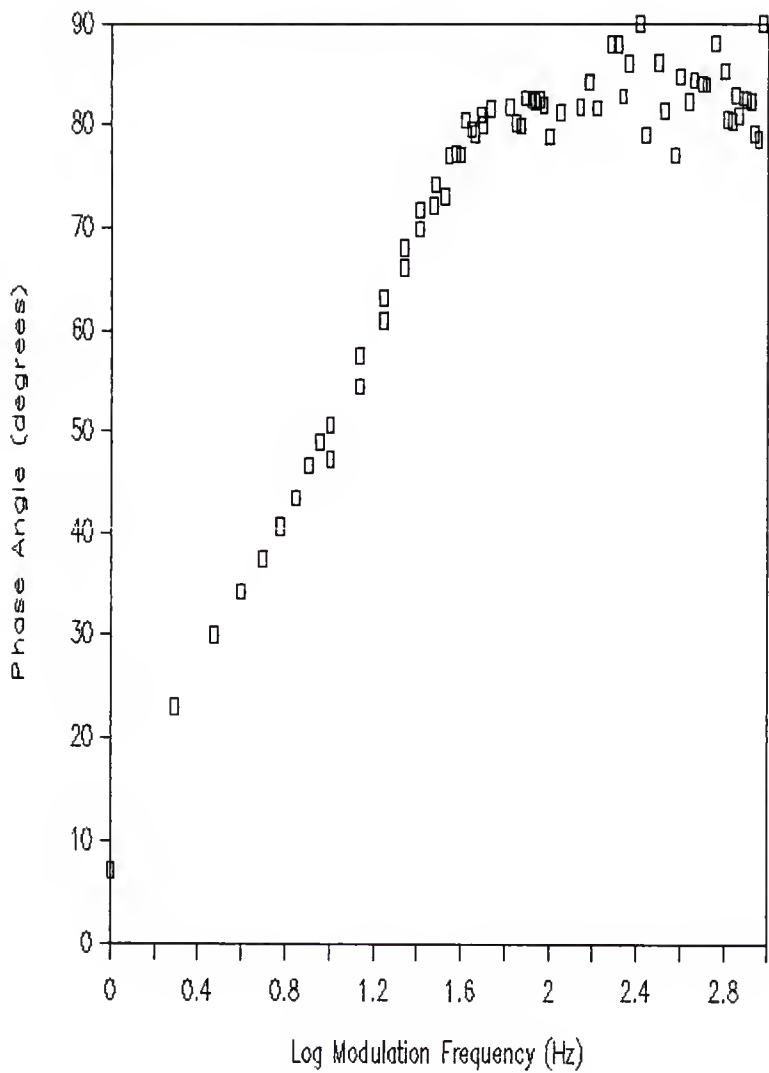
diffusion length for helium, which is frequency dependent, be-
comes equivalent to the sample chamber length used for this
experiment. A plausible explanation for this behavior is that at
these low modulation frequencies, the Rosencwaig-Gersho theory
becomes invalid, as it assumes a gas column of length much great-
er than the thermal diffusion length of the gas. The behavior
is, however, in agreement with the previously discussed findings
of Aamodt, Murphy, and Parker (22), who predict a decrease in the
amplitude of the photoacoustic signal for cases where the size of
the sample chamber becomes comparable to, or less than, the
thermal diffusion length of the gas. Although, in our case, the
relative amplitude of the signal still increases as the thermal
diffusion length of the gas is increased at low modulation fre-
quencies, the amplitude of the signal at a given modulation
frequency is decreased from what it would potentially be if a
larger chamber volume were used.

B. Empty Chamber Studies

Although the sample chamber was designed to minimize its own
empty chamber signal, it is reasonable to expect that the chamber
walls will exhibit a measurable photoacoustic response, as a
relatively large surface area of solid material is being illumi-
nated. Even with a wheat kernel sample present in the chamber,
the cell walls may contribute significantly to the resultant
photoacoustic response, due to the limited size of the kernel and
scattered radiation reflected from its surface. Thus, it is
important to have a knowledge of the photoacoustic response from

75

the empty chamber itself.

Figures 4.3 and 4.4 show the amplitude and phase of the empty chamber response as compared to the signals measured with the black cloth sample present. These results show that the amplitude of the empty chamber signal, although certainly measurable, is more than one order of magnitude lower then the black cloth signal, and that the phase lag vs modulation frequency curves are distinctly different for the empty chamber and black cloth sample. This result is not surprising in that the black cloth, being a very strong absorber and having a fairly large surface area, should be expected to produce a relatively strong photoacoustic response; whereas the empty chamber, whose design was aimed at minimizing its own response, should produce a signal small in comparison. It is also seen that the phase of the black cloth signal is very much different empty chamber response at frequencies greater than approximately 5 Hz. In the empty chamber phase angle vs frequency curve, there is seen a fairly large difference between values obtained for the low-frequency and high-frequency runs. It is our contention that this discrepancy was due to a variation in the manner with which the complex wave forms detected by the microphone were interpreted by the lock-in amplifier, caused by the exchanging of the internal component boards of the amplifier between these runs.

To make a determination of the empty chamber response as compared to the response obtained from wheat kernel samples, a series of tests were performed in which the photoacoustic re-

Figure 4.3. A log-log comparison of the amplitude of
the photoacoustic response vs modulation frequency
obtained with the black cloth sample present to
that obtained from the empty chamber. Sample cham-
ber depth = 4.8 mm.

Legend:

square - black cloth sample present

plus - no sample present (empty chamber)

77

Figure 4.4. A comparison of the phase of the photo-
       acoustic response vs log modulation frequency ob-
       tained with the black cloth sample present to that
       obtained from the empty chamber. Sample chamber
       depth = 4.8 mm.

       Legend:

            square - black cloth sample present
            plus - no sample present (empty chamber)
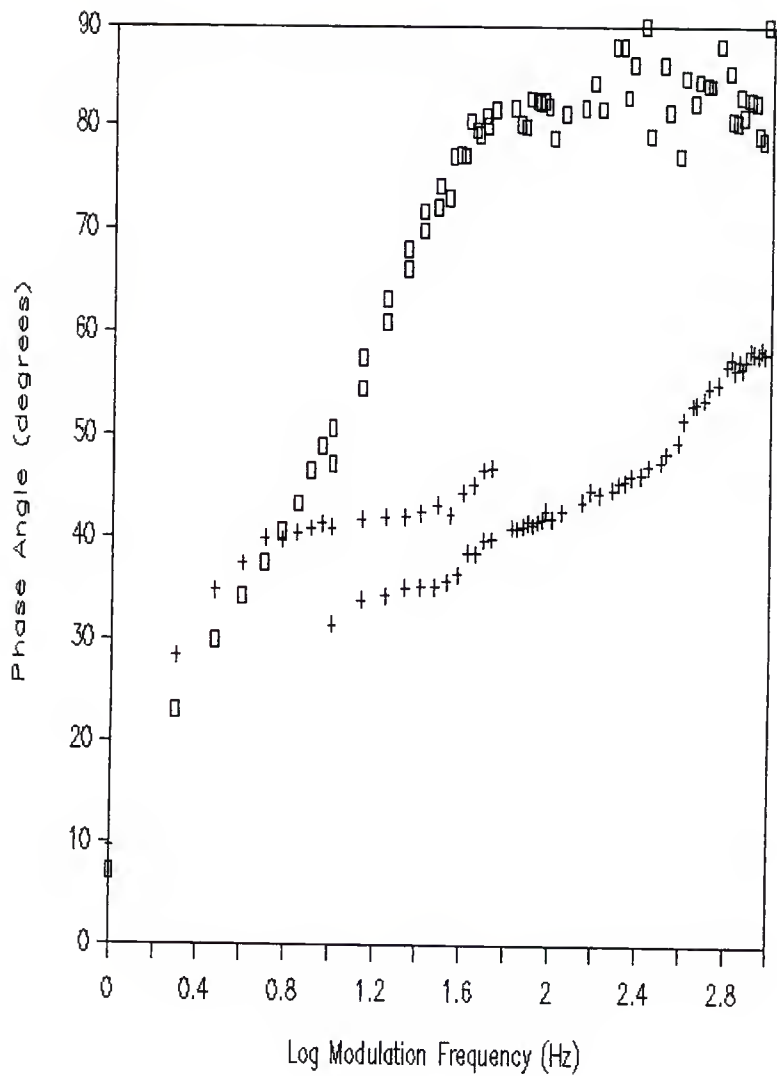
sponse was monitored as a function of modulation frequency for the empty chamber, a single kernel, and five kernels (five being the maximum number of normal-sized kernels which could be placed on the floor of the chamber). In the case of the single kernel, the kernel was placed crease-up at the center of the floor of the sample chamber. For five kernels, one kernel was centered in the chamber with the other four kernels placed around it. The results of these studies, for both the amplitude and phase of the photoacoustic response, are shown in Figures 4.5 and 4.6 respectively. It can be seen from these results that the measured amplitude of the photoacoustic response when a sample was present in the chamber was slightly greater then the empty chamber response throughout most of the frequency range, with the response being greatest for five kernels. The phase angle measurements for these runs reflect a similar trend, with the phase lag being smaller for the empty chamber, except for within approximately the 100-500 Hz frequency range.

Upon inspection of the sample chamber, we decided that the protruding portion of the O-ring sealing the window to the sample chamber was possibly receiving a sufficient amount of e-m radiation to cause it to contribute significantly to the measured photoacoustic response of the chamber. To reduce this problem, and to increase the percentage of the incident radiation striking the sample, we reduced the O-ring thickness so that it barely protruded above the plug cavity base, and installed a 3 mm diameter aperture at the base of the cylindrical plug containing the

81

Figure 4.5. A log-log comparison of the amplitude of

the photoacoustic response vs modulation frequency

obtained with a single kernel and five kernels of

wheat present to that obtained from the empty cham-

ber. Sample chamber depth = 4.8 mm.

Legend:

square - no sample present (empty chamber)

plus - one kernel present

diamond - five kernels present

Figure with y-axis labeled "Log Signal Amplitude (microvolts)" ranging from -0.2 to 1.5, and x-axis labeled "Log Modulation Frequency (Hz)" ranging from 0 to 2.8. Legend: □ E. CHAM. + 1 KERNEL ◇ 5 KERNELS

83
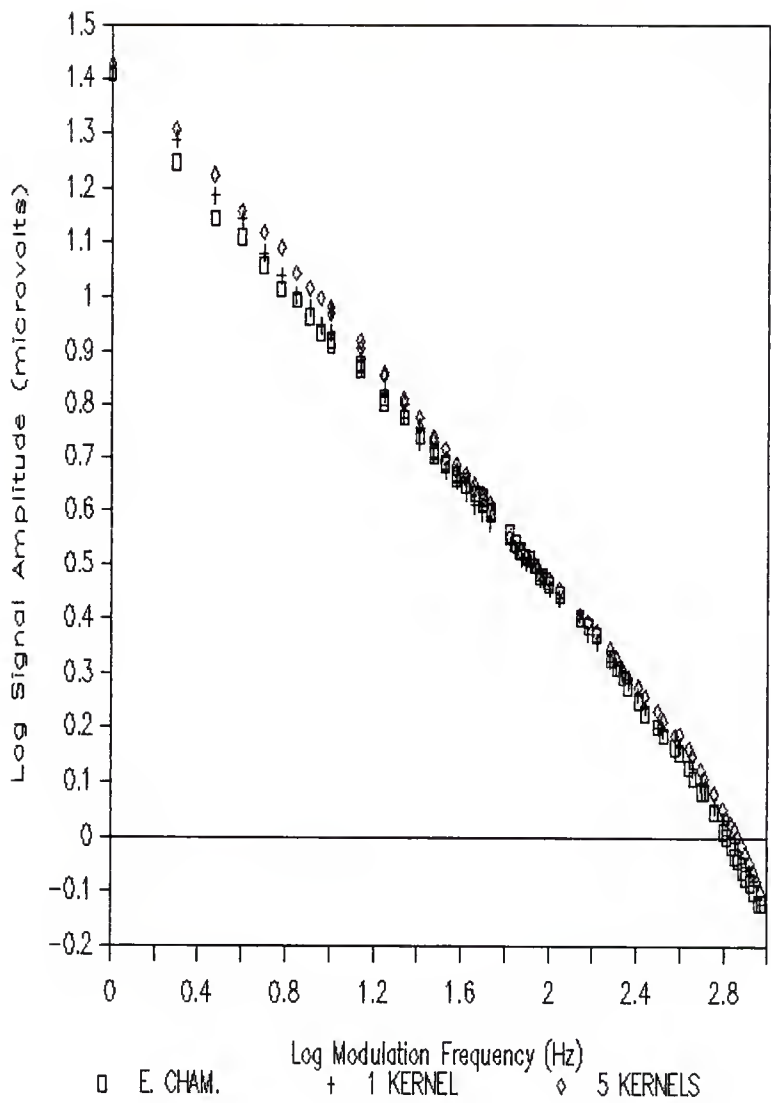
Figure 4.6. A comparison of the phase of the photo-
    acoustic response vs log modulation frequency ob-
    tained with a single kernel and five kernels of
    wheat present to that obtained from the empty cham-
    ber. Sample chamber depth = 4.8 mm.

    Legend:

        square - no sample present (empty chamber)
        plus - one kernel present
        diamond - five kernels present

84

Phase Angle (degrees) vs Log Modulation Frequency (Hz)

E. CHAM.   +   1 KERNEL   ◊   5 KERNELS
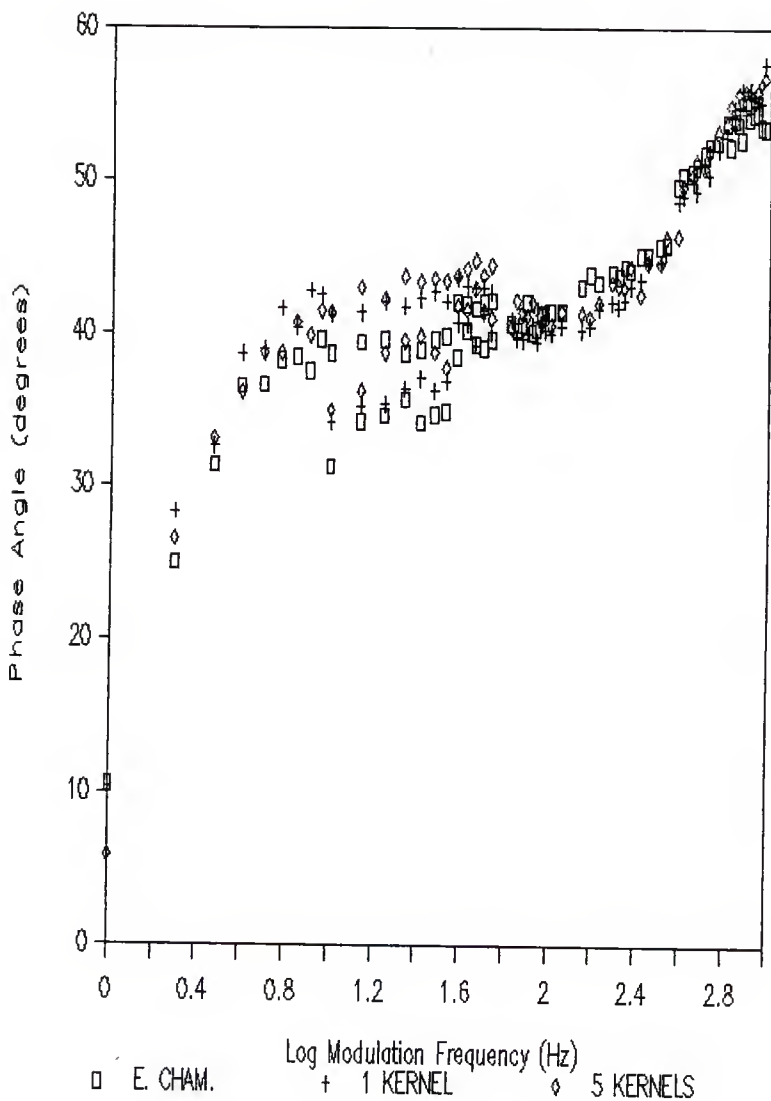
LED. Assuming the LED to be a point light source, this aperture
provided an absolute restriction of approximately 13 degrees on
the half-angle divergence of the cone of e-m radiation entering
the sample chamber, and prevented the O-ring from being directly
illuminated.

After making these modifications, we repeated the measure-
ments for the empty chamber, a single kernel, and five kernels.
Figures 4.7 and 4.8 show the results of these studies. Since the
total amount of e-m radiation entering the chamber was reduced by
the installed aperture, the amplitude of the photoacoustic re-
sponse is reduced in all cases, as is theoretically expected.
However, the separation between the amplitude of the empty cham-
ber response and the response obtained with a wheat sample pre-
sent was improved substantially, except for at frequencies above
approximately 200 Hz, where the curves are found to converge.
Also, at frequencies above approximately 15 Hz, the phase of the
single kernel response become distinctly different from the empty
chamber response, although converging once again at frequencies
approaching 1000 Hz. There are also some significant differences
which occur in both the amplitude and phase angle vs modulation
frequency curves for a single kernel and five kernels. Because
of the increased separation from the empty chamber response
achieved, the modifications were considered an improvement, and
were maintained in all experiments subsequently performed with
the cell.

Given the appropriate parameters for the thermal properties

86

Figure 4.7. A log-log comparison of the amplitude of

the photoacoustic response vs modulation frequency

obtained with a single kernel and five kernels of

wheat present to that obtained from the empty cham-

ber. An aperture (diameter = 3 mm) was installed

to restrict spot size. Sample chamber depth = 4.7 mm.

Legend:

square - no sample present (empty chamber)
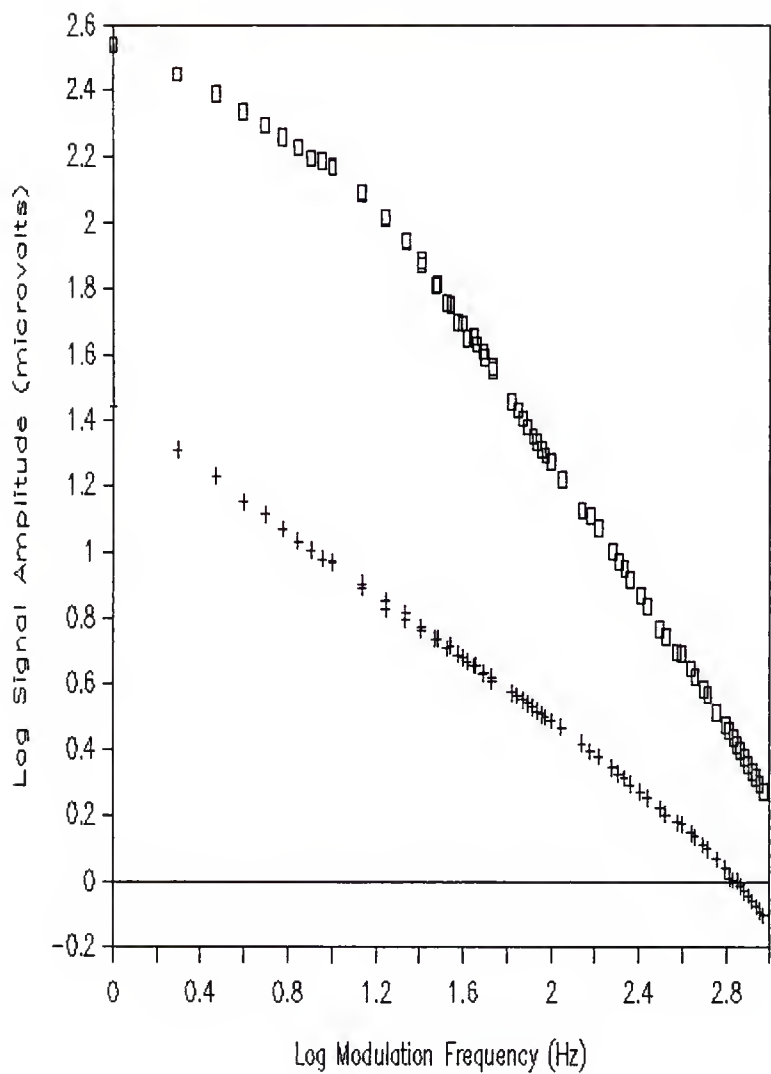
plus - one kernel present

diamond - five kernels present

.

87
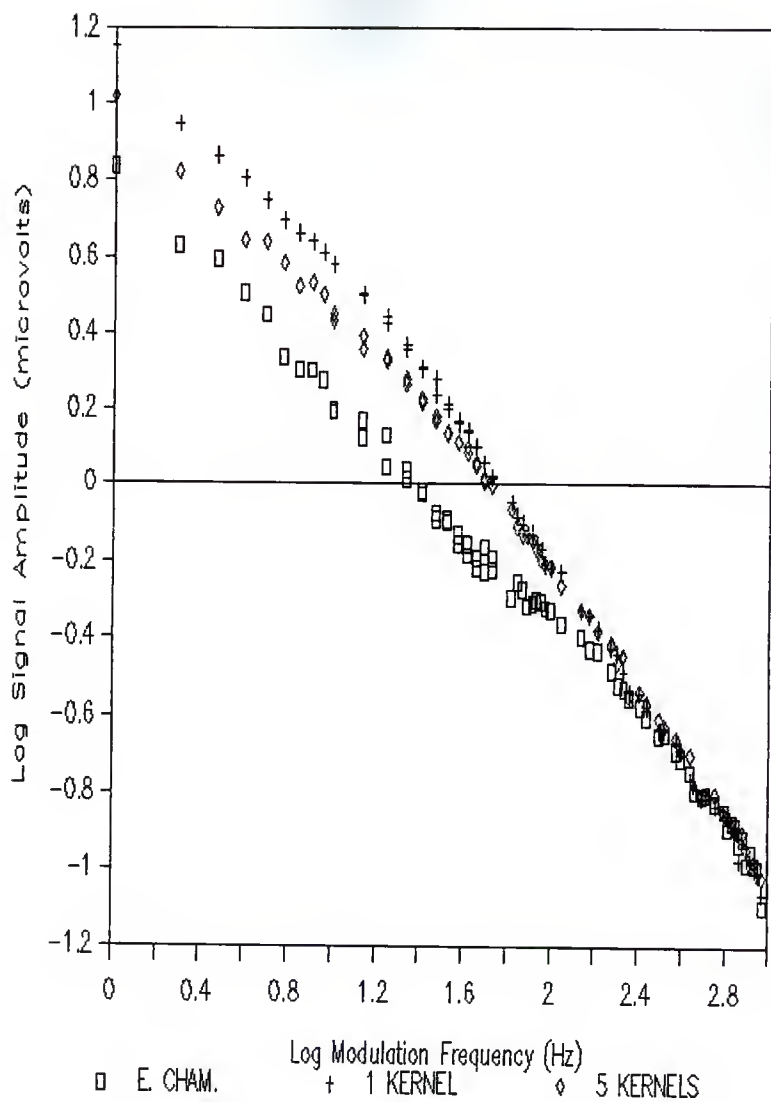
Figure 4.8. A comparison of the phase of the photo-
acoustic response vs log modulation frequency ob-
tained with a single kernel and five kernels of
wheat present to that obtained from the empty cham-
ber. An aperture (diameter = 3 mm) was installed
to restrict spot size. Sample chamber depth = 4.7 mm.

Legend:

square - no sample present (empty chamber)
plus - one kernel present
diamond - five kernels present

89
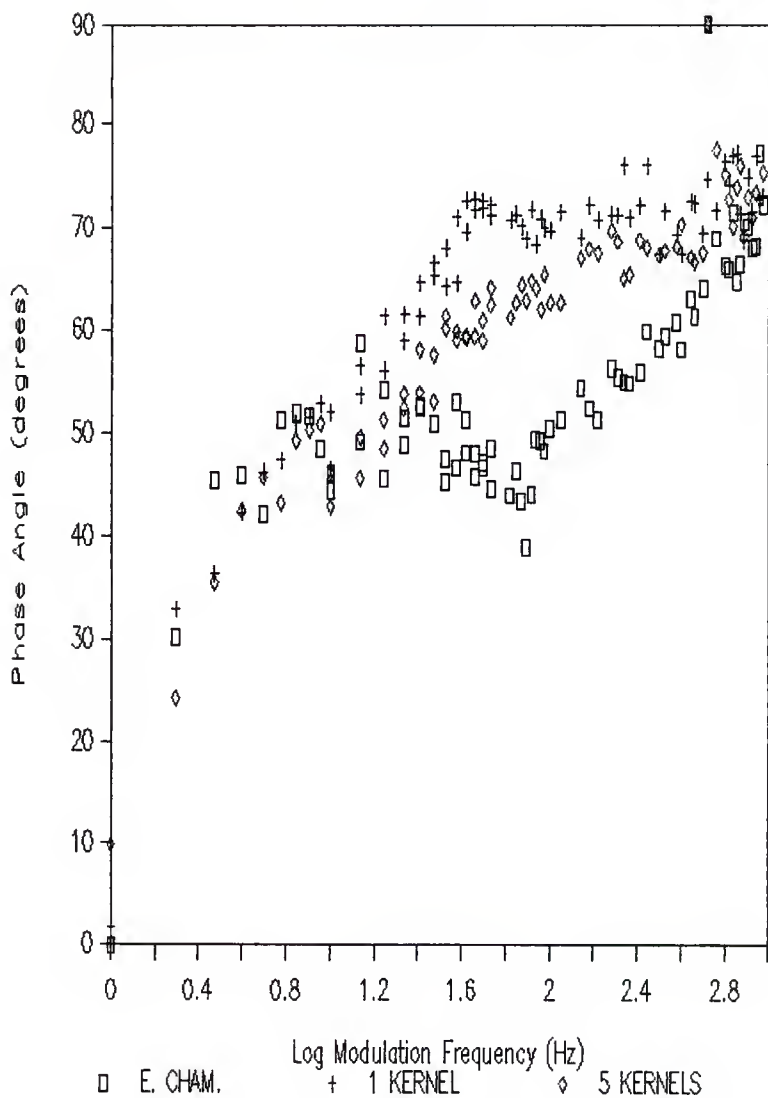
of helium, aluminum, and wheat, the Rosencwaig-Gersho theory
should permit a theoretical determination of the relative magni-
tudes of the amplitude of the photoacoustic response for these
two substances, as well as the manner with which the amplitude
will change with variation of the modulation frequency. Known
values for the density, thermal conductivity, and specific heat
for the materials associated with these studies are tabulated
below (21, 24). In addition, a plot showing the thermal diffu-
sion length for these materials as a function of modulation
frequency, as derived from these parameters, is given in Figure
4.9.

TABLE 4.1. Thermal Parameters.

Material	Density Kg/m^3	Therm. Conduct. $J/m-sec-K$	Specific Heat $J/Kg-K$
Helium (1 atm)	0.180	0.1423	5232
Aluminum	2699	237	899
Wheat (hard)	1300	0.140	1548
Wheat (soft)	1320	0.117	1397
Wheat (avg)	1310	0.128	1473

Special case 2(b) of the Rosencwaig-Gersho theory should be
most applicable in the case of the empty chamber response, since
the thermal diffusion length of aluminum, which is at a maximum
of 1.4 cm at 1 Hz, is less than the thickness of the chamber
walls, and never becomes less than the optical absorption length
throughout the frequency range used. Theory thus predicts that

Figure 4.9. A plot of the thermal diffusion length
     as a function of modulation frequency for various
     materials of interest in these experiments.

     Legend:

          square - helium
          plus - aluminum
          diamond - wheat (hard)
          triangle - wheat (soft)
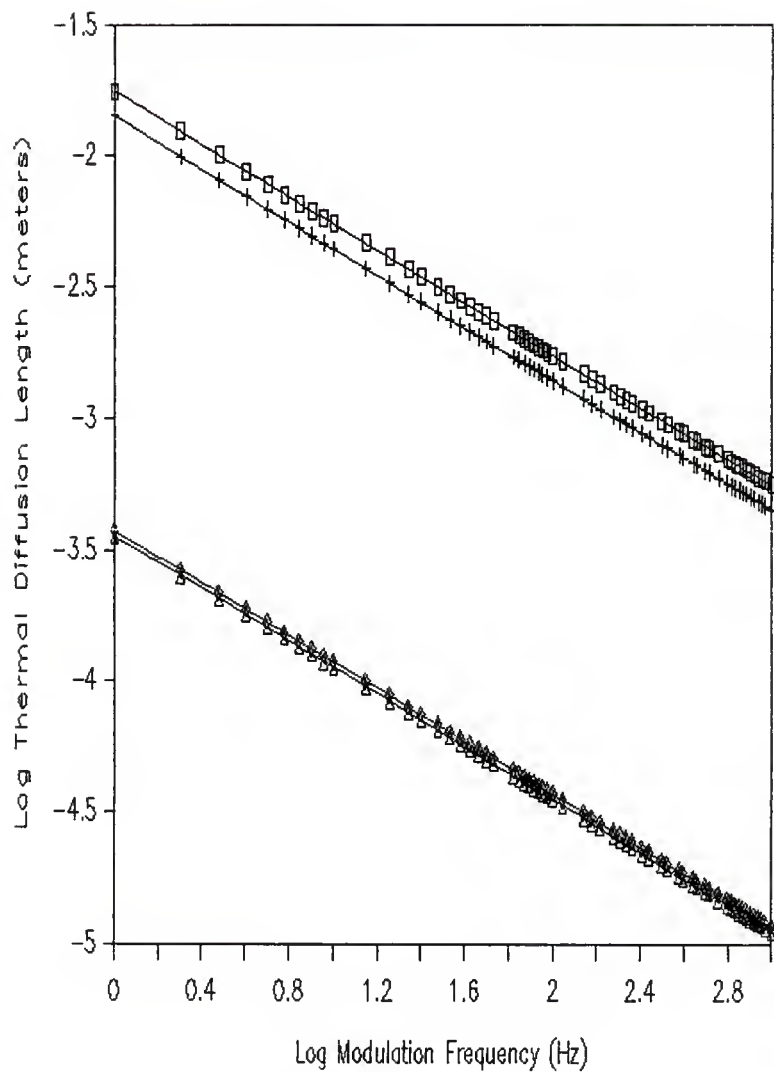
the signal amplitude should vary as ω^{-1}, which is experimentally

observed at frequencies above approximately 300 Hz. At lower

frequencies, however, the log amplitude vs log modulation fre-

quency curve is found to deviate from this dependence, with the

signal amplitude not increasing as much as predicted with de-

creasing frequency. The reason for this behavior is most likely

that, at low modulation frequencies, the thermal diffusion length

becomes significantly large with respect to the spot size being

illuminated, making a one-dimensional theory no longer applica-

ble, as three-dimensional diffusion occurs from the illuminated

portion of the chamber.

In the case of a wheat kernel, which is optically opaque as

well, the thermal diffusion length, which is approximately 0.37

mm at a modulation frequency of 1 Hz, is also less than the

sample thickness throughout the entire frequency range used. If

it is assumed that the optical absorption length is less than the

thermal diffusion length of the sample, then in this instance, as

was the case with aluminum, special case 2(b) of the Rosencwaig-

Gersho theory should most accurately describe the experimental

observations. However, when the ratio of the amplitude for a

wheat kernel to the amplitude for the empty chamber is computed

making this assumption, theoretically a signal with amplitude

approximately 50 times greater should be observed with a wheat

kernel sample present, throughout the entire frequency range.

Such a large separation is clearly not seen in the experimental

data, where the greatest separation is no more than approximately

a factor of two. It is, however, quite possible that the optical absorption length is greater than the thermal diffusion length, as the thermal diffusion length for wheat is fairly small, even for low modulation frequencies. If this is correct, then, the amplitude of the signal would be dependent upon the optical absorption coefficient of wheat, and would theoretically vary as $\omega^{-3/2}$. The fact that the slope of the log amplitude vs log modulation frequency curve experimentally obtained is more negative with both one and five wheat samples present in the chamber substantiates this hypothesis. Although the slope of this curve deviates from the expected -3/2 slope, except for at modulation frequencies approaching 1000 Hz, where the slope appears to converge to this value, the degree to which it deviates from theory is similar to the deviation of the empty chamber curve from its expected slope of -1. This suggests that these observed deviations may be due to the same causes, namely, that the three-dimensional nature of the sample becomes significant as the thermal diffusion length becomes sufficiently large. Assuming that the Rosencwaig-Gersho theory is valid at 1000 Hz, and that the optical absorption length is greater than the thermal diffusion length for wheat at this frequency; in order for the response of a wheat kernel sample to have an amplitude equal to the amplitude obtained for the empty chamber, as is experimentally observed, the optical absorption length for a wheat kernel would have to be approximately 0.56 mm. This number seems to be reasonable, and implies that the optical absorption length is great-

95

er than the thermal diffusion length, even at modulation frequencies as low as 1 Hz, where the thermal diffusion length was calculated to be approximately 0.36 mm.

Another result obtained from this experiment was that, at the lower modulation frequencies (less than and approximately equal to 40 Hz), the amplitude of the photoacoustic signal obtained for a single kernel was greater than that obtained for five kernels. However, at higher frequencies, there was essentially no difference between the signals. This variation is most likely due to a decrease in the volume of gas occupying the cell, as more volume was occupied by the sample with five kernels present, causing the thermal diffusion length of helium to become comparable to the effective chamber length at a higher modulation frequency than in the case of a single kernel. For this experiment (with the aperture installed), the chamber was maintained at a depth of 4.7 mm. If an average kernel thickness of 2.4 mm is subtracted from this depth with 5 kernels present, the resultant effective length of the gas column becomes approximately 2.3 mm. The modulation frequency at which the thermal diffusion length for helium is 2.3 mm is approximately 50 Hz, which closely corresponds to the 40 Hz modulation frequency at which the variation between the single kernel and five kernel response becomes apparent. The fact that the entire chamber floor was not completely covered when five kernels were present, due to gaps between the kernels, is possibly responsible for the fact that the above approximation gives a theoretical frequency at which separation

96

between the curves should begin slightly higher than that actual-
ly observed, as a larger gas volume than that allowed for in the
above approximation was present.

C. Chamber Volume Studies

The effects of the size of the sample chamber in relation to
the thermal diffusion length of the gas used, in this case he-
lium, have been treated in the discussion above. However, all of
the experiments previously discussed were performed at essential-
ly the same chamber depth. The purpose of the following experi-
ment was to study specifically how an actual variation in the
depth of the sample chamber will affect the photoacoustic re-
sponse, throughout the entire modulation frequency range of 1-
1000 Hz.

For this experiment, the photoacoustic cell was adjusted so
that its chamber depth was 1.66 cm, which was, by design, the
maximum chamber depth possible. At this chamber depth, runs were
made for the empty chamber, a single kernel, five kernels, and
the black cloth sample. Figures 4.10 and 4.11 show the amplitude
and phase variation with modulation frequency of the black cloth
photoacoustic response at this new chamber depth, as compared to
the response obtained at a chamber depth of 0.47 cm. It is clear-
ly seen that the amplitude of the response is decreased with the
increased chamber depth, as is theoretically predicted. However,
since the volume of the chamber was increased by more than a
factor of three, theory predicts that the amplitude of the signal
at this new chamber depth should be approximately one-third as

97

Figure 4.10. A log-log comparison of the amplitude of
        the photoacoustic response vs modulation frequency
        obtained for the black cloth sample at two different
        chamber depths.

        Legend:
            square - chamber depth = 4.7 mm
            plus - chamber depth = 17 mm

Log Signal Amplitude (microvolts) vs Log Modulation Frequency (Hz)

□ 0.47 cm   + 1.7 cm
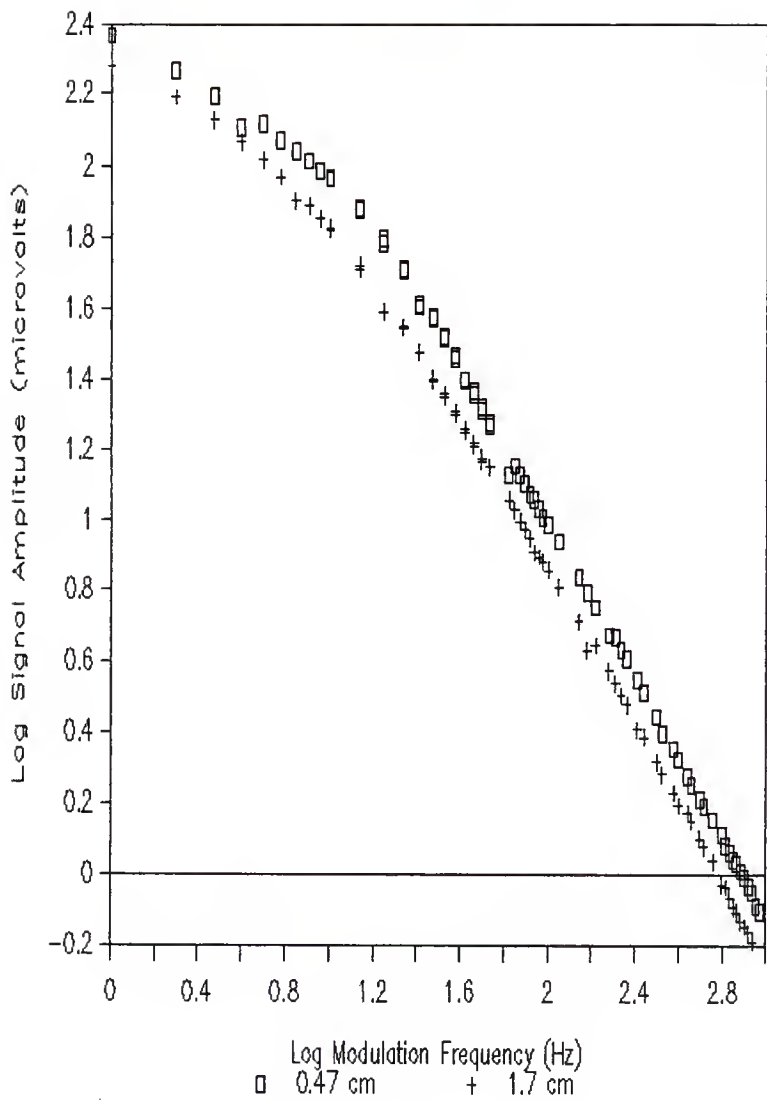
Figure 4.11. A comparison of the phase of the photo-
    acoustic response vs log modulation frequency ob-
    tained for the black cloth sample at two different
    chamber depths.

    Legend:

        square - chamber depth = 4.7 mm
        plus - chamber depth = 17 mm

Phase Angle (degrees) vs Log Modulation Frequency (Hz)

□ 0.47 cm   + 1.7 cm

101
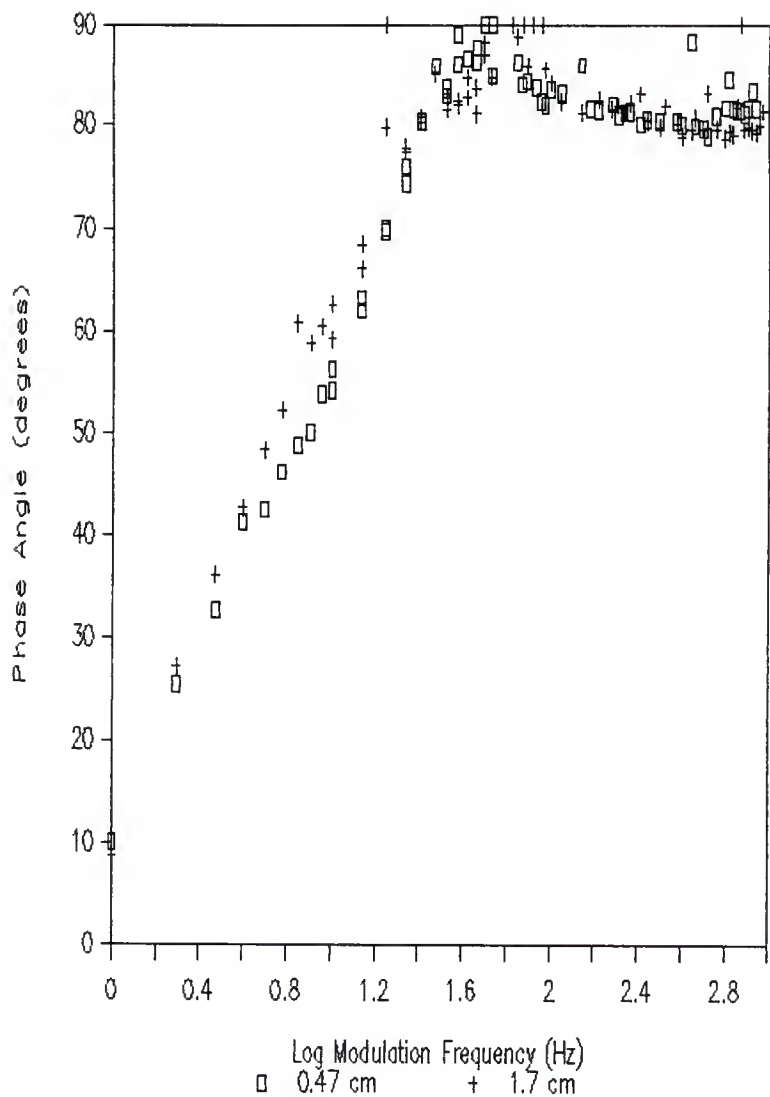
great as the amplitude at the more shallow depth. Experimentally, we see an amplitude approximately 0.7 times as great. A
possible reason for this deviation from theory is that, at the
larger chamber depth, a greater amount of the black cloth surface
is being illuminated due to the increased beam spreading of the
incident e-m radiation. This would cause an increase in the
volume of gas actually being heated in the case of the larger
chamber depth, and may result in complicating a strictly theoretical comparison of the two cases. Another factor which may be
responsible for the deviation of our experimental results from
theoretical predictions is the assumption of one-dimensional heat
propagation in the Rosencwaig-Gersho theory, whereas, in reality,
propagation of heat parallel to the surface occurs within the
sample as well. Since as the chamber depth is made larger, the
amount of material illuminated increases, it is reasonable to
expect that the effect of three-dimensional propagation of heat
at larger chamber depths is less significant than at shallow
depths. Thus, in our experiment, it is possible that at the
larger chamber depth a one-dimensional approximation is valid,
whereas at the shallower depth, the three-dimensional nature of
the heat propagation process becomes significant, leading to a
higher percentage of heat being dissipated within the sample.

Since the thermal diffusion length for helium at 1 Hz is
approximately equal to the length of the sample chamber at this
new chamber depth, as the modulation frequency approaches 1 Hz,
the point where the thermal diffusion length of the gas becomes

102

equal to the length of the gas column is approached. It is seen that at these low modulation frequencies, the slope of the log amplitude vs log frequency curve becomes less negative for the 1.66 cm chamber depth, although more gradually than at the 0.47 cm depth. This behavior is reasonable since for the deeper chamber depth, the thermal diffusion length of helium only becomes comparable to the gas column length; whereas for the shallower chamber depth, the thermal diffusion length of helium actually becomes significantly greater than the gas column depth, at low modulation frequencies.

Figures 4.12 and 4.13 show the amplitude and phase of the photoacoustic response at a chamber depth of 1.66 cm for the empty chamber, a single kernel, and 5 kernels. The change in the slope of the amplitude curves at low modulation frequencies is much more gradual than that seen in Figure 4.7 for the smaller chamber depth, as is expected. The relative amplitude of the photoacoustic response for five kernels as compared to a single kernel at this depth seems to be shifted up somewhat with respect to the results obtained at the lower chamber depth throughout the entire frequency range. Here we find that at the lower modulation frequencies, the single kernel and five kernel amplitudes are nearly identical, whereas, at the higher modulation frequencies, the amplitude for five kernels becomes greater than that obtained for a single kernel. This is possibly due to an increased contribution from those kernels surrounding the central kernel, as these kernels receive a greater amount of incident

103

Figure 4.12   A log-log plot of the amplitude of the

photoacoustic response vs modulation frequency for

the empty chamber, a single kernel, and five ker-

nels.   Sample chamber depth = 17 mm.

Legend:

square — no sample present (empty chamber)

plus — one kernel present

diamond — five kernels present

Log Signal Amplitude (microvolts) vs Log Modulation Frequency (Hz)

□ E. CHAM.   + 1 KERNEL   ◇ 5 KERNELS
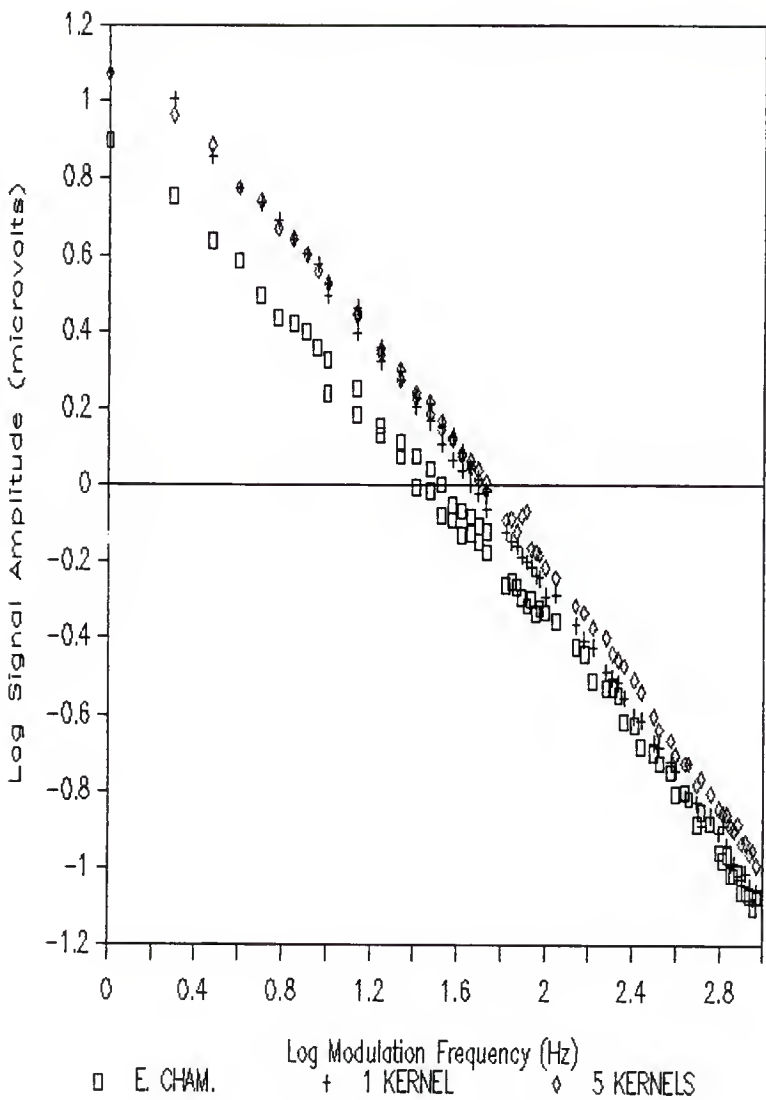
Figure 4.13. A plot of the phase of the photoacoustic
response vs log modulation frequency for the empty
chamber, a single kernel, and five kernels. Sam-
ple chamber depth = 17 mm.

Legend:

square - no sample present (empty chamber)
plus - one kernel present
diamond - five kernels present

Phase Angle (degrees) vs Log Modulation Frequency (Hz)

□ E. CHAM.   + 1 KERNEL   ◇ 5 KERNELS
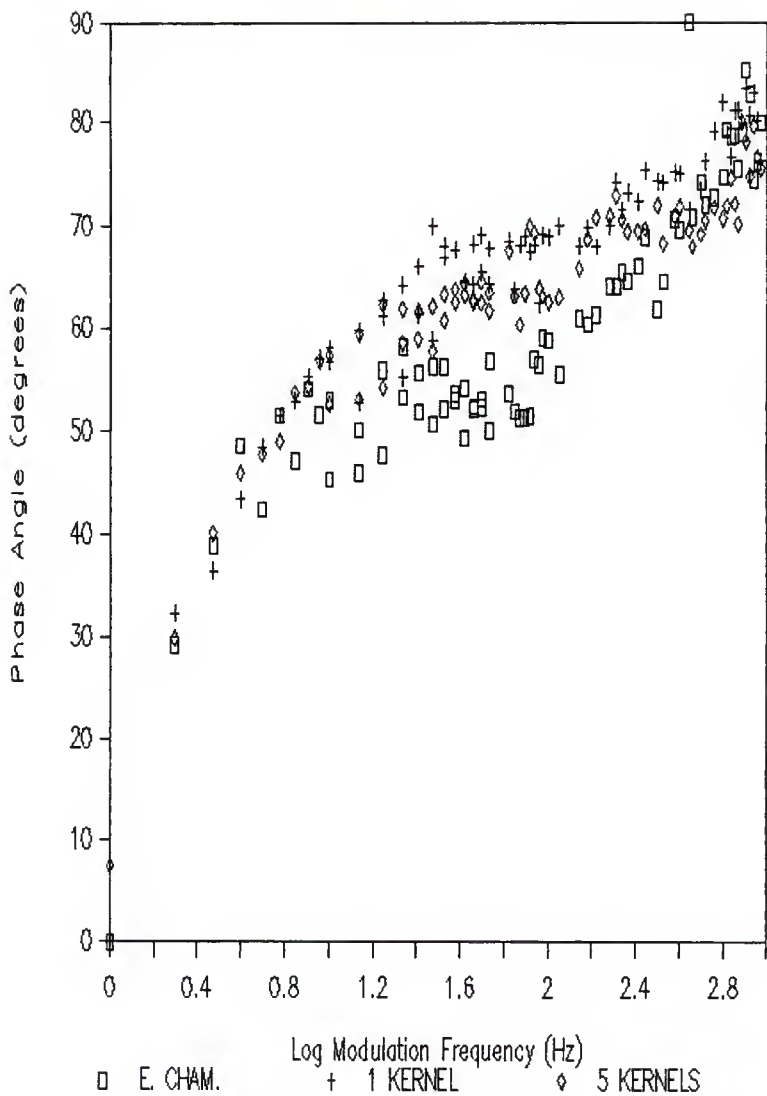
radiation due to the increased spot size at this chamber depth. This reasoning parallels that used above, in the case of the black cloth signal comparisons, to help explain the discrepancy between the theoretical and experimental drop in the signal amplitude. From these results, it seems that increasing the surface area, while keeping the total radiation flux entering the sample chamber constant, results in an increase in the amplitude of the response. Similar reasoning can be used to explain the fact that the separation between the empty chamber and single kernel amplitudes seems to decrease at this larger chamber depth. Since the empty chamber has a much larger surface area than a single kernel, an increase in the spot size, assuming that it becomes greater than the size of the kernel, will result in a larger increase in the amount of the empty chamber illuminated as compared to the increased amount of wheat illuminated. The phase relationship of the single kernel photoacoustic response with modulation frequency appears to become less distinctly separate from the empty chamber response as the chamber depth is increased. This may be due to the increased contribution of illuminated portions of the empty chamber when the single kernel run was performed because of the increased spot size. The phase relationship with five kernels present appears to be essentially the same for both chamber depths, which is reasonable since as the spot size increases, kernels surrounding the central kernel are illuminated instead of the chamber itself, causing the type of material being illuminated to be essentially unchanged.

108

4.2   Reproducibility Studies

A series of runs were made to find out the extent to which
reproducible data could be obtained. Although these studies were
done using an aperture of somewhat larger diameter than that
previously described, they still should give a reasonably valid
representation of the variability in our results due to uncer-
tainties in the signal measurement by the electronics systems,
along with variations in the percentage of helium and presence of
contaminants in the chamber between runs.

Figures 4.14 and 4.15 show the amplitude and phase results
of five runs for which the empty chamber response was monitored
as a function of modulation frequency, throughout the entire 1-
1000 Hz frequency range. The runs 1-5 were sequentially per-
formed, without reflushing of the sample chamber between runs. A
single reflushing of the chamber was performed only when the
internal component cards of the lock-in amplifier were changed,
and the higher-frequency range portion of the runs were begun.
These results should represent the limit to which variations
between samples can be detected with the apparatus used in these
experiments. In the case of the amplitude, it is seen that the
scatter between runs is not large. The percentage of uncertainty
represented by the standard deviation of the values obtained at a
given frequency, averaged over all frequencies at which measure-
ments were made, gives an experimental uncertainty of 1.70% for
the amplitude and 1.78% for the phase measurement.

Some of the most probable sources of uncertainty in these

109

Figure 4.14. A log-log plot of the amplitude of the

photoacoustic response vs modulation frequency

for the empty chamber. The results of five separ-

ate runs which were sequentially performed without

reflushing the sample chamber are plotted.

Legend:

square - run #1

plus - run #2

diamond - run #3

triangle - run #4

cross - run #5

Log Modulation Frequency (Hz)

□ Run #1,   + #2,   ◊ #3,   △ #4,   X #5.
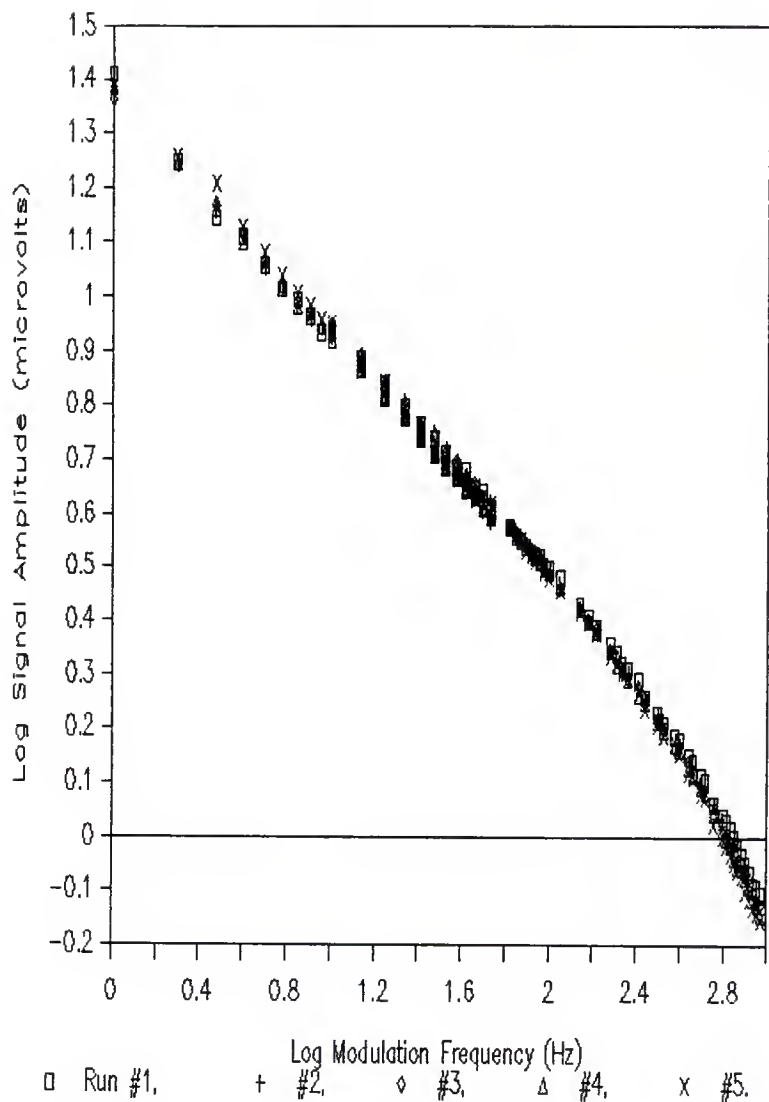
Figure 4.15. A plot of the phase of the photoacoustic
    response vs log modulation frequency for the empty
    chamber. The results of five separate runs which
    were sequentially performed without reflushing the
    sample chamber are plotted.

    Legend:

        square - run #1
        plus - run #2
        diamond - run #3
        triangle - run #4
        cross - run #5

Phase Angle (degrees) vs Log Modulation Frequency (Hz)

□ Run #1,   + #2,   ◊ #3,   △ #4,   x #5.
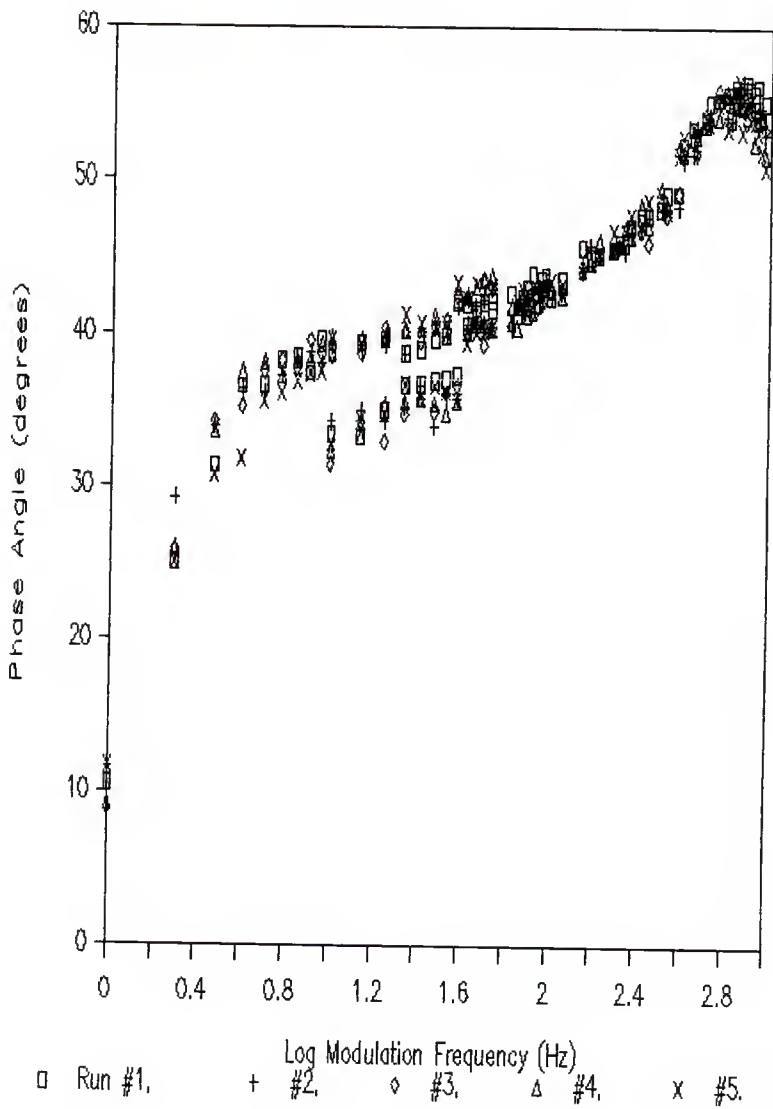
measurements include variations in the intensity of the e-m
radiation intensity and a decrease with time in the percentage of
helium actually present in the chamber due to leakage, as well as
possible fluctuations in ambient temperature, variations in out-
side noise levels, and drift or uncertainty in the microphone's
signal detection capability. Studies in which the LED intensity,
as detected by the PIN diode, was monitored over a period of time
show that the intensity of the incident radiation does decrease
very slightly over a period of continuous usage, with a decrease
of no more than one percent over several hours. Looking closely
at the amplitude data, it is seen that the slope of the log
amplitude vs log frequency curve becomes slightly more negative
with successive runs. It is likely that this change in the
frequency dependence of the amplitude is due to a gradual diffu-
sion of air into, and helium out of, the sample chamber. This
hypothesis is backed by the fact that the empty chamber amplitude
without helium flushing is greater than with helium flushing at
low modulation frequencies, and less than the helium flushed
chamber signal at higher modulation frequencies. This implies
that it is advantageous to perform the run soon after the chamber
is flushed. Another source of uncertainty, which ultimately dic-
tates the minimum accuracy of the acquired data, is the limited
resolution of the A-D converter used in the data acquisition
process. Although the consistency of the analog to digital
conversion process was made was very good, as tested by inputting
constant voltages and monitoring the resultant digital values,

114

the accuracy to which the converter could detect changes in voltage was limited to 1/255 of its 0.5 volt working range, or approximately 1.5% at half scale output from the lock-in amplifier.

Figures 4.16 and 4.17 show the results of an experiment similar to that described above, in which five runs were made monitoring the photoacoustic response of a single wheat kernel as a function of modulation frequency. For each run in this experiment, however, the sample was removed, and then centered once again in the sample chamber, and the chamber was reflushed. Despite the potential increased uncertainties associated with the repositioning of the kernel, presence of unwanted contaminants, and the percentage of helium successfully introduced into the chamber for each run, the scatter in this data is even slightly less than the scatter observed in the empty chamber runs described above, with an average percent standard deviation from average of 1.25% for the amplitude and 0.96% for the phase. The decrease in scatter in this case is probably due to the fact that the chamber was reflushed prior to each run, and an additive reduction in the percentage of helium in the chamber does not occur with successive runs. The scatter that is observed is likely caused by other factors cited in the above discussion for the empty chamber experiment, which are relevant to this case. The experimental procedures used in this particular study closely corresponded to those used in the single kernel comparisons later discussed. These results therefore demonstrate that a satisfac-

115

Figure 4.16. A log-log plot of the amplitude of the
photoacoustic response vs modulation frequency
for a single wheat kernel (variety: Scout-66).
For each of the five runs plotted, the kernel was
removed and placed in the sample chamber again,
and the chamber was reflushed with helium.

Legend:

square - run #1
plus - run #2
diamond - run #3
triangle - run #4
cross - run #5
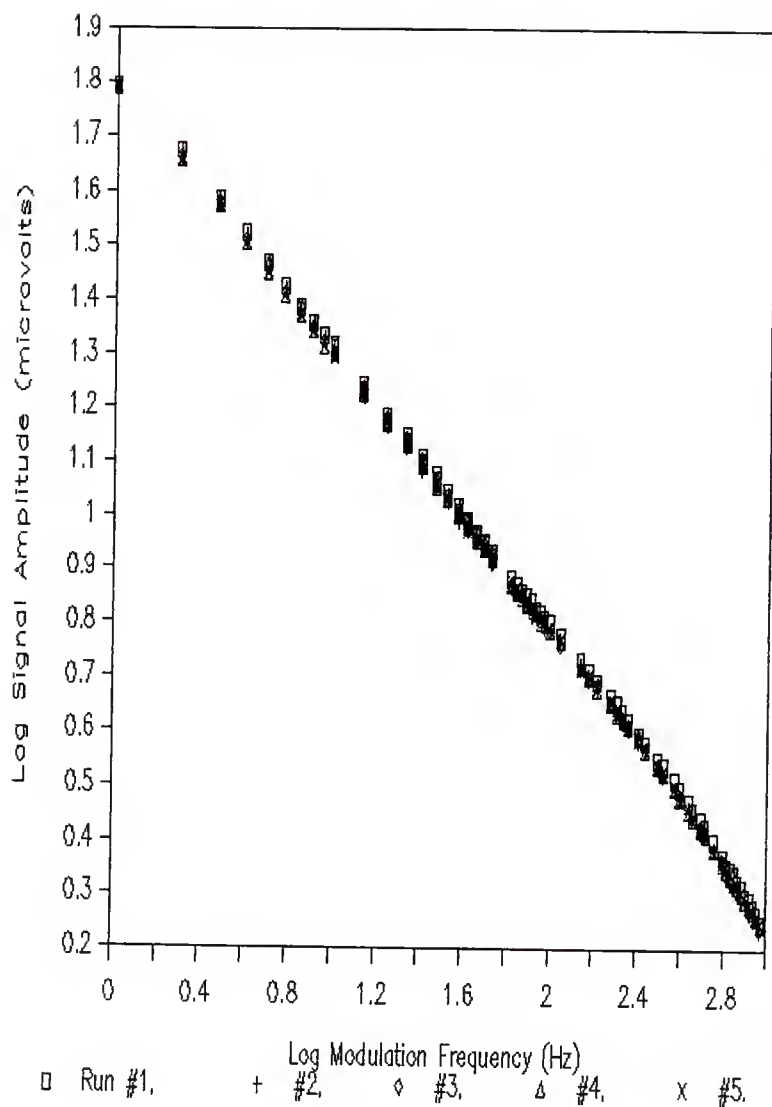
Figure 4.17. A plot of the phase of the photoacoustic
response vs log modulation frequency for a single
wheat kernel (variety: Scout-66). For each of the
five runs plotted, the kernel was removed and placed
in the sample chamber again, and the chamber was
reflushed with helium.

Legend:

square - run #1
plus - run #2
diamond - run #3
triangle - run #4
cross - run #5

118

Phase Angle (degrees) vs Log Modulation Frequency (Hz)

□ Run #1,   + #2,   ◇ #3,   △ #4,   X #5.

119
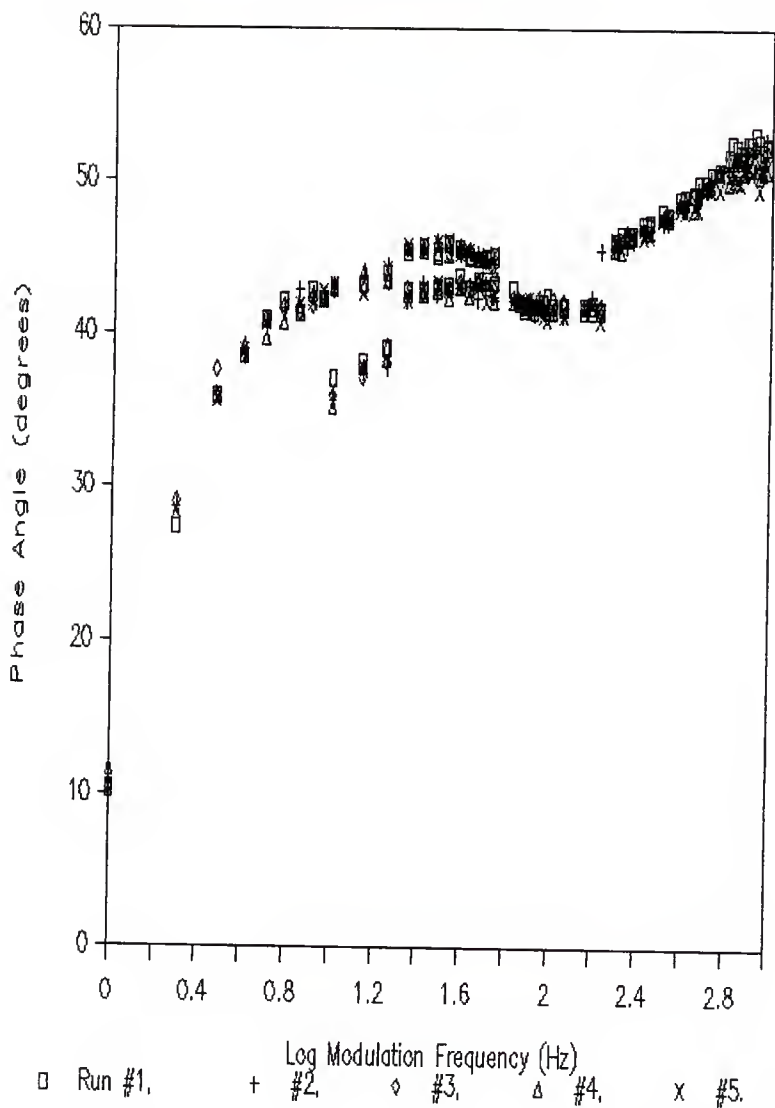
tory degree of reproducibility is obtainable with the apparatus
and procedures used in these studies.

4.3 Kernel Moisture Evaporation Studies

In earlier photoacoustic studies of wheat kernels (25), it
has been seen that moisture content has a very pronounced effect
on the amplitude of the photoacoustic response. Due to the high
specific heat of water, its presence in a kernel results in an
reduction in the amplitude of the photoacoustic response, as,
theoretically, the amplitude varies inversely as the specific
heat for an opaque, thermally thick solid with a thermal diffu-
sion length less than its optical absorption length. Further-
more, moisture content is a kernel property which has the poten-
tial to vary substantially between samples. Therefore, in order
to make valid comparisons of the inherent photoacoustic signals
from different kernels, it is first necessary to bring those
kernels to be compared to the same state, with respect to moist-
ure content. The purpose of this study is to see how the photoa-
coustic response varies as moisture is removed from a wheat
kernel by drying.

These studies were performed relatively early in the course
of our experimentation, prior to the earlier described O-ring and
aperture modifications made to the photoacoustic cell, and before
we had the capability to extend our studies to modulation fre-
quencies below 10 Hz (before we acquired the 1-100 Hz component
boards for the lock-in amplifier). Thus, the photoacoustic data

120

is not directly comparable to data later obtained, and the re-
sults may be somewhat inconclusive. Although a number of differ-
ent varieties of kernels were examined in this study, they all
demonstrated a similar variation in their photoacoustic response
with increased drying. Thus, only the results for two represent-
ative kernels with similar initial kernel mass are considered
here, these varieties being Arkan (hard red winter) and Pike
(soft red winter).

Since one of the purposes of this study was to determine the
length of drying time necessary for preparation of wheat samples
for our future experiments, no special sample preparation was
done prior to the study, and the kernels were studied with an
initial moisture content as received. Before the drying process
was begun, each kernel was weighed and its photoacoustic response
was obtained throughout the 10-1000 Hz frequency range. The
samples were then dried in a conventional air oven at a tempera-
ture of 103 degrees Centigrade (+/-2 degrees) for five hours, re-
moved, weighed, and the photoacoustic response was again mea-
sured. This process was continued, with increased drying times
being allotted between samplings as the mass and signal varia-
tions became more gradual, until a total drying time of 95 hours
was reached. Figures 4.18-4.21 display the results obtained for
the Pike and Arkan kernels analyzed, throughout the entire fre-
quency range scanned, for both the amplitude and phase of the
response. Figure 4.22 shows the variation in mass as a function
of drying time for the both kernels. Assuming that mass loss

121

represents moisture evaporation from the kernel, this plot should give a relative indication of the variation in total kernel moisture content. Figures 4.23 and 4.24 more clearly demonstrate the change in photoacoustic signal amplitude with drying time for modulation frequencies of 10 and 100 Hz respectively.

These results show that as the drying time is increased, and the total kernel moisture content is decreased, as indicated by the decreased kernel mass, the amplitude of the photoacoustic response increases. The change in the amplitude is rapid when the drying process begins, but becomes more gradual as the drying time increases, appearing to eventually level off, as does the kernel moisture content. The fact that the signal amplitude seems to vary inversely with moisture content is in compliance with theory, as the Rosencwaig-Gersho theory predicts that amplitude should vary as the inverse of specific heat for a solid with the thermal and optical properties of wheat, and the specific heat of water is much higher than any other substances of which the kernel is composed. Upon examining the amplitude of the photoacoustic response shown in Figures 4.18 and 4.20, it is seen that the amplitude does not increase uniformly over the entire frequency range. Due to the fact that the presence of moisture in a kernel has such a large effect on the photoacoustic response, and variation of the modulation frequency enables the profiling of a sample as a function of depth, it is reasonable to expect that this behavior reflects a non-uniform extraction of moisture from a given depth within the kernel. If the change in

Figure 4.18. A log-log plot showing the variation in
the amplitude of the photoacoustic response vs
modulation frequency for a single kernel sample of
Pike (soft red winter), as the kernel was dried
over a period of 75 hours. Oven temperature =
103 deg. C.

Legend:

square - before drying process begun

plus - after 5 hours drying time

diamond - after 10 hours drying time

cross - after 35 hours drying time

inverted triangle - after 75 hours drying time
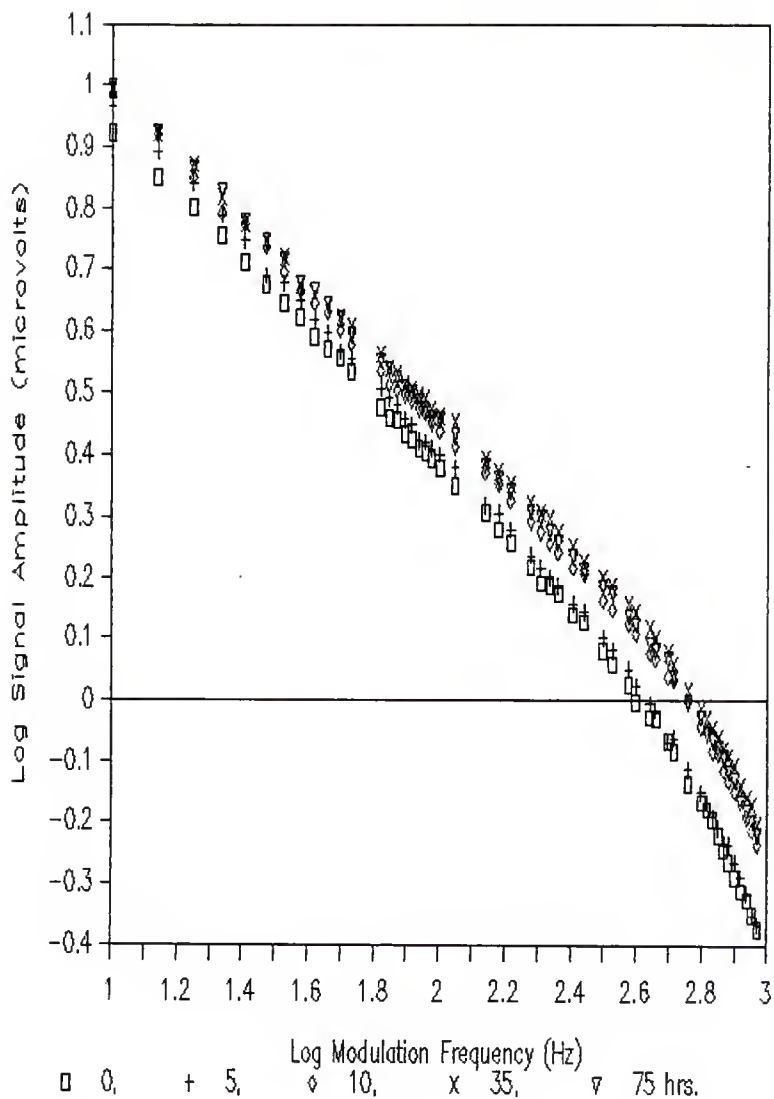
Figure 4.19. A plot showing the variation in the phase

of the photoacoustic response vs log modulation

frequency for a single kernel sample of Pike (soft

red winter), as the kernel was dried over a period

of 75 hours. Oven temperature = 103 deg. C.

Legend:

square - before drying process begun

plus - after 5 hours drying time

diamond - after 10 hours drying time

cross - after 35 hours drying time

inverted triangle - after 75 hours drying time

Figure showing Log Signal Amplitude (microvolts) versus Log Modulation Frequency (Hz).

X-axis: Log Modulation Frequency (Hz)

Y-axis: Log Signal Amplitude (microvolts)

Legend: □ 0, + 5, ◊ 10, X 35, ▽ 75 hrs.
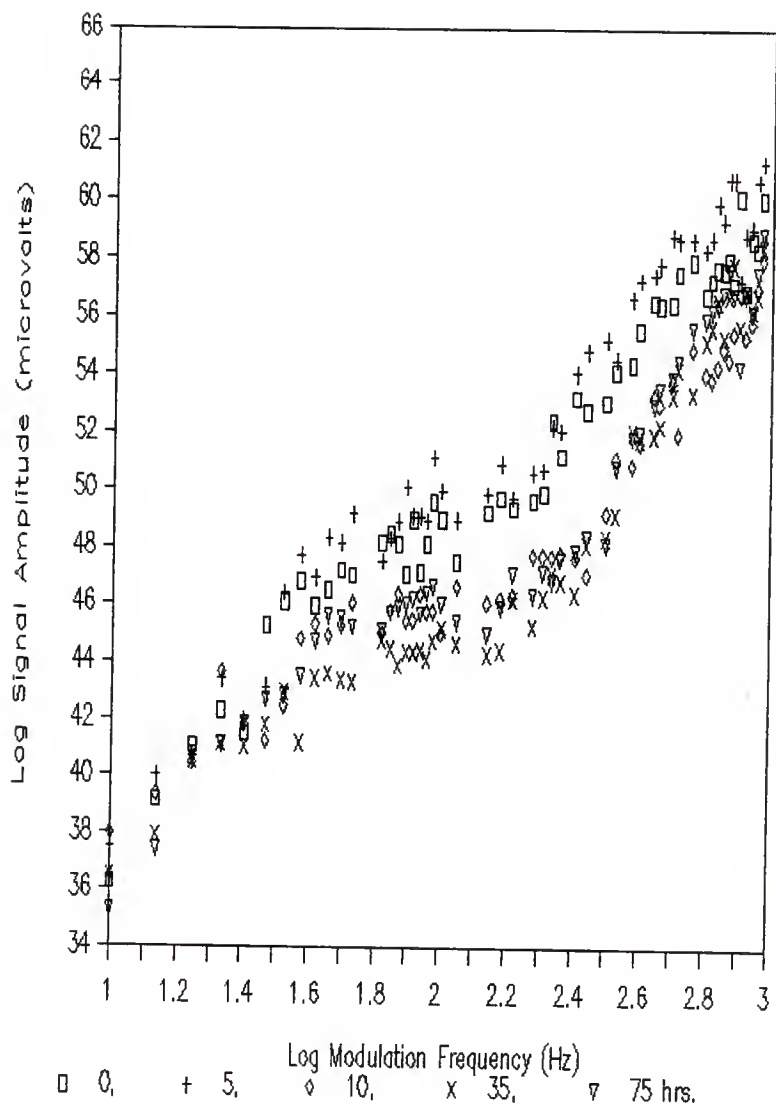
Figure 4.20. A log-log plot showing the variation in
    the amplitude of the photoacoustic response vs
    modulation frequency for a single kernel sample of
    Arkan (hard red winter), as the kernel was dried
    over a period of 75 hours. Oven temperature =
    103 deg. C.

    Legend:

        square - before drying process begun
        plus - after 5 hours drying time
        diamond - after 10 hours drying time
        cross - after 35 hours drying time
        inverted triangle - after 75 hours drying time

Log Signal Amplitude (microvolts) vs. Log Modulation Frequency (Hz)

□ 0,   + 5,   ◇ 10,   ✕ 35,   ▽ 75 hrs.
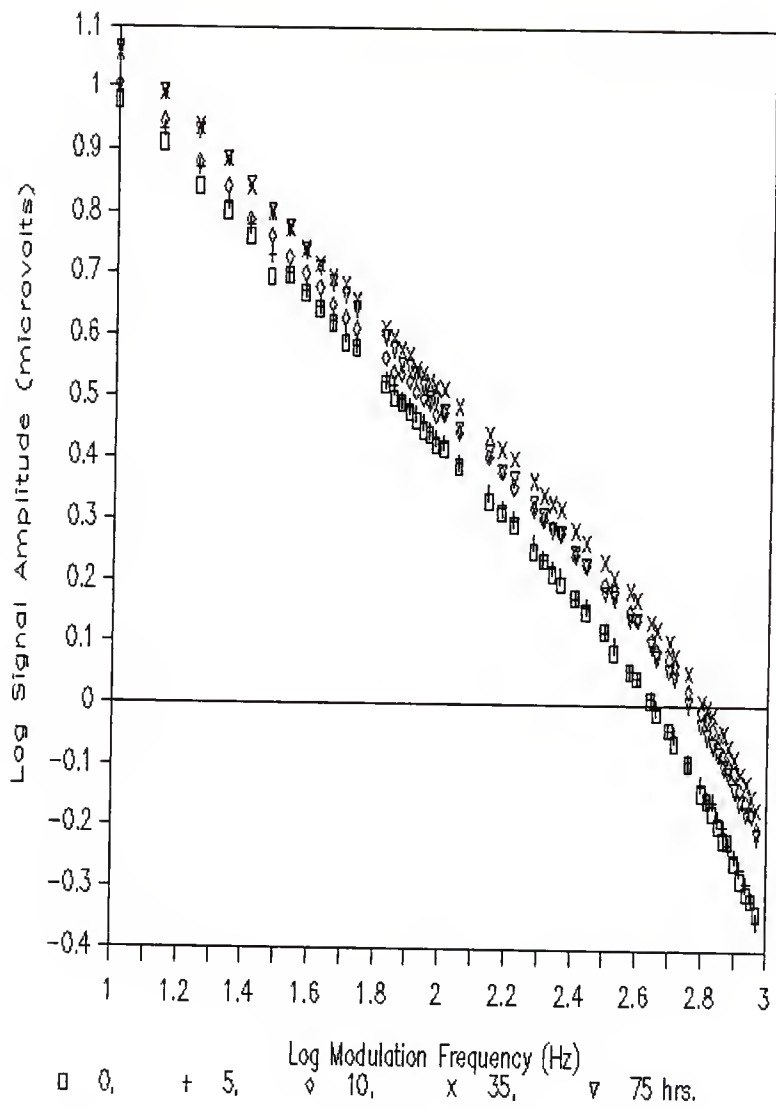
Figure 4.21. A plot showing the variation in the phase
of the photoacoustic response vs log modulation
frequency for a single kernel sample of Arkan (hard
red winter), as the kernel was dried over a period
of 75 hours. Oven temperature = 103 deg. C.

Legend:

square - before drying process begun

plus - after 5 hours drying time

diamond - after 10 hours drying time

cross - after 35 hours drying time

inverted triangle - after 75 hours drying time

Figure showing Phase Angle (degrees) vs Log Modulation Frequency (Hz), with data series: □ 0, + 5, ◇ 10, X 35, ▽ 75 hrs.
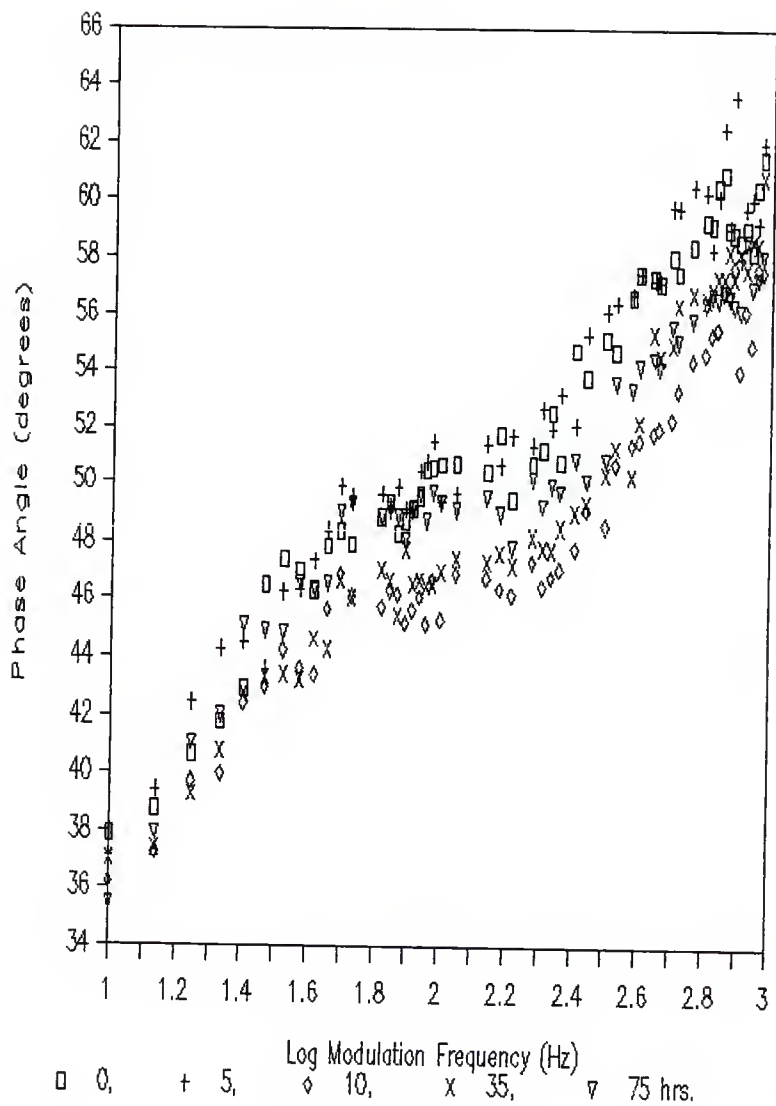
Figure 4.22. A plot showing the variation in the

    total kernel mass with increased drying time (at

    103 deg. C.) for the varieties Pike and Arkan.

    Legend:

        square - Pike (soft red winter)

        diamond - Arkan (hard red winter)
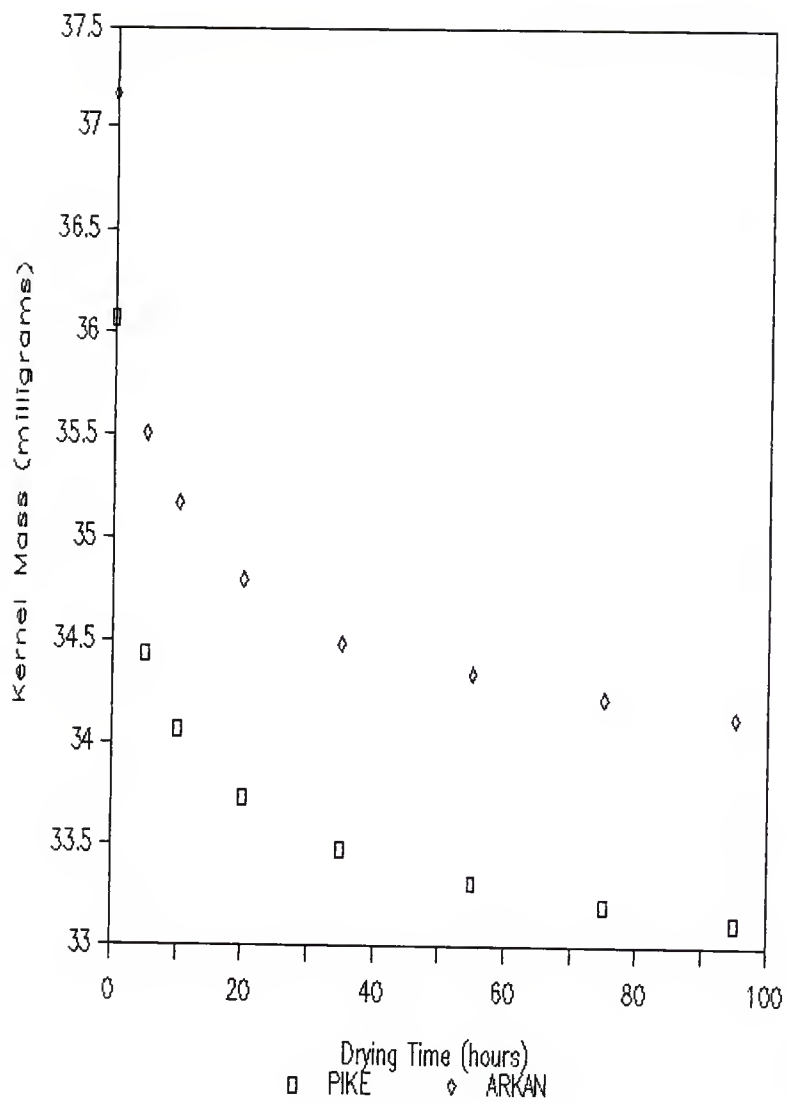
Figure 4.23. A plot showing the variation in the amp-
     litude of the photoacoustic response with increased
     drying time (at 103 deg. C.), at a modulation fre-
     quency of 10 Hz, for the varieties Pike and Arkan.

     Legend:

          square - Pike (soft red winter)
          diamond - Arkan (hard red winter)
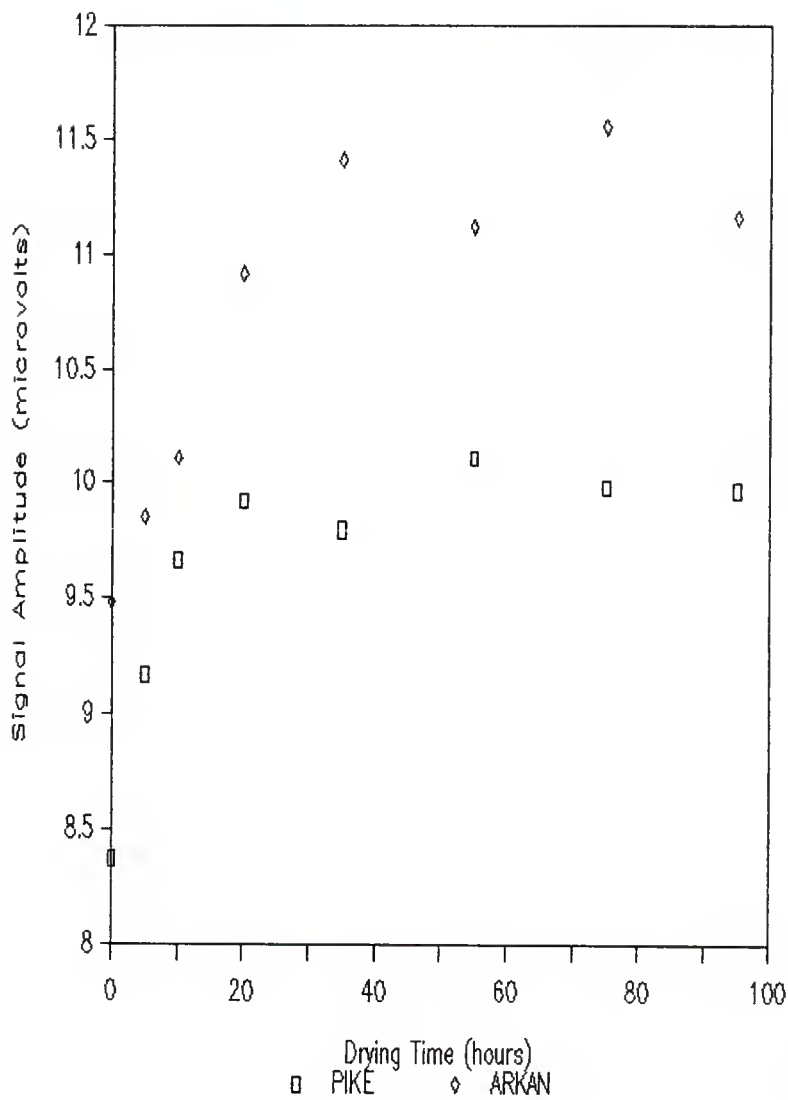
Figure 4.24. A plot showing the variation in the amp-
litude of the photoacoustic response with increased
drying time (at 103 deg. C.), at a modulation fre-
quency of 100 Hz, for the varieties Pike and Arkan.

Legend:

square - Pike (soft red winter)

diamond - Arkan (hard red winter)

Signal Amplitude (microvolts) vs Drying Time (hours)

□ PIKE   ◇ ARKAN

136
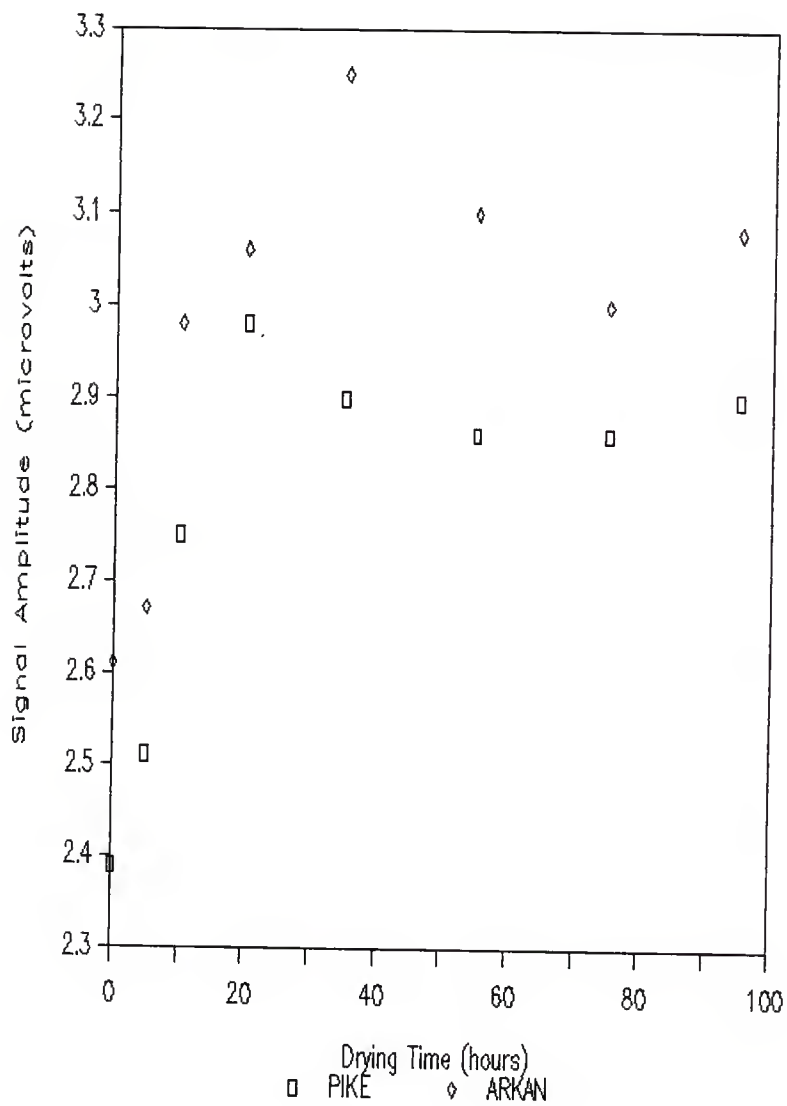
the shape of these curves are interpreted in this manner, it is seen that as the drying is begun, a larger change in kernel moisture occurs more deeply within the kernel (lower modulation frequencies) than at the kernel surface (higher modulation frequencies). After a period of drying time, however, the amount of moisture at the kernel surface greatly decreases, and afterward the variation seems to become relatively uniform throughout the entire range of depths from which information was obtained. This seems to parallel the manner by which moisture is presently understood to be driven from a wheat kernel upon drying. If a kernel has not been recently damped (bran drier than endosperm), moisture will first be drawn from the interior of the grain until a moisture distribution in which the bran is damper than the endosperm is established (26). It appears from our experiment that after much of the moisture has been drawn from the interior of the kernel, a rather extreme reduction in the kernel's surface moisture occurs. Although the phase of the signal did vary with drying time, as seen in Figures 4.19 and 4.21, the behavior was a great deal more complex than the amplitude variation. No consistent trend of either decrease or increase in phase angle with drying time was observed, and the manner with which it did change was not the same for each kernel tested. It is possible that the phase lag is more sensitive to the distribution of moisture throughout the portion of the kernel in which the thermal wave must propagate to reach the kernel surface. Thus, even though the phase of the signal seems to be dependent on the kernel

137

moisture content, the exact nature of its dependency is not clear.

The temperature, 103 degrees Centigrade, used in this study was chosen since a USDA standard wheat drying technique specifies heating at this temperature for fifty hours. Since our results indicate that very little change in the moisture content occurs after fifty hours drying time, we decided to use these standard temperature and drying time parameters in our initial preparation of samples tested in subsequent studies.

4.4 Kernel Variety Studies

The objectives of these experiments were to examine the photoacoustic response of a number of different wheat varieties, and attempt to pinpoint differences in the photoacoustic response characteristic of a given variety. Twelve different varieties of wheat were chosen to be used in this experiment, eight hard red winter and four soft red winter varieties. The specific varieties studied are listed below.

TABLE 4.2. Listing of Varieties Analyzed.

Hard Red Winter	Soft Red Winter
Arkan	Arthur
Bounty-310	Caldwell
Hawk	Coker-916
Mustang	Pike
Newton	
Scout-66	
Tam-105	
Vona	

To verify our observations, runs were made for five differ-
ent kernels of each variety. In order to bring all kernels
examined to the same state with respect to moisture content,
moisture was removed from each of the kernels prior to the study
by the procedure described in the previous section, with all
kernels studied being dried at the same time. After the drying
process, the kernels were stored in a desiccator up until and
after they were individually examined. The analysis was per-
formed for all kernels first at the low frequency range (1-50
Hz), after which the internal component boards of the lock-in
amplifier were exchanged and the high frequency range (10-1000
Hz) analysis was done, completing the experiment. As in previous
studies, the chamber was flushed for five minutes with helium
before each run. The chamber depth used for this experiment was
0.47 cm.

Although variations were observed in the photoacoustic re-
sponse for the different kernels tested, even kernels of the same
variety were found to vary somewhat from kernel to kernel. Fig-
ures 4.25-4.28 show the extent of the variation in the amplitude
and phase of the photoacoustic signal for the varieties that
seemed to exhibit the most and least variance between kernels.
Figures 4.29-4.34 show the photoacoustic responses for the twelve
varieties tested, as averaged over the five kernels tested within
each variety. The average of the amplitude and phase angle vs
modulation frequency curves for a given variety were seen to
differ somewhat between varieties. However, the kernel to kernel

139

Figure 4.25. A log-log plot of the amplitude of the

photoacoustic response vs modulation frequency

for five different kernels (variety: Hawk), each

analyzed separately. This plot represents the

least amount of kernel to kernel scatter in the

signal amplitude observed within a given variety

for the twelve varieties tested.

Legend:

    square — kernel #1

    plus — kernel #2

    diamond — kernel #3

    triangle — kernel #4

    cross — kernel #5
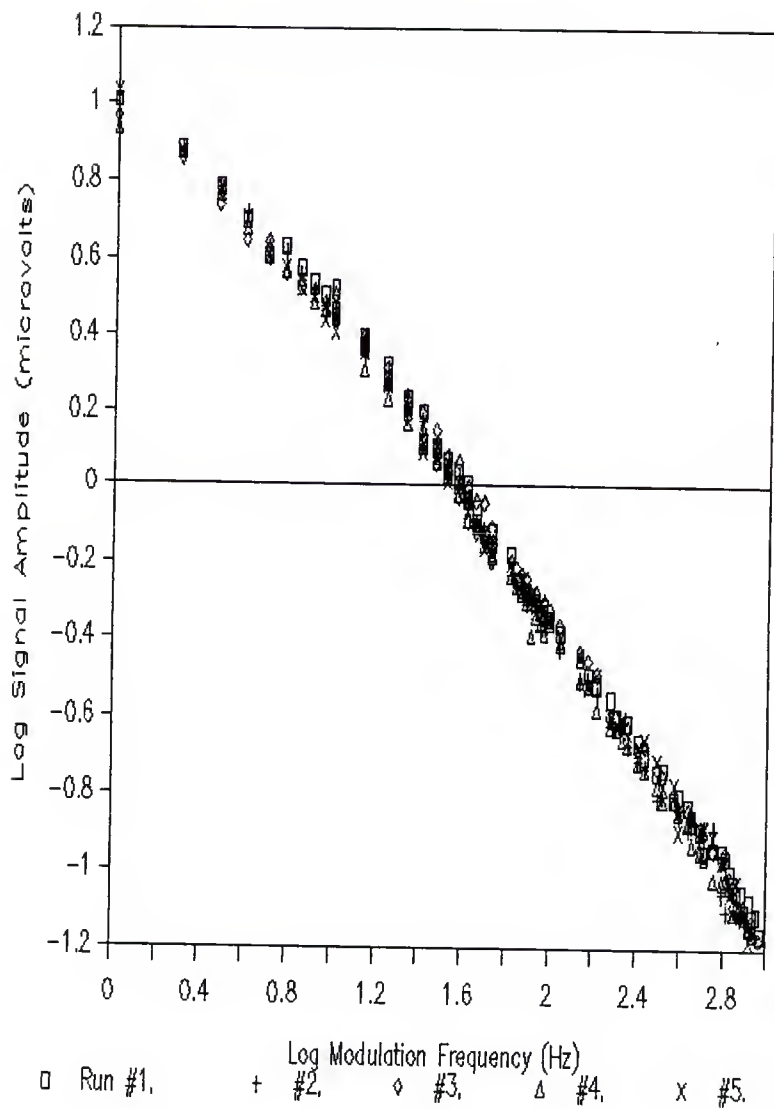
Figure 4.26. A log-log plot of the amplitude of the
photoacoustic response vs modulation frequency
for five different kernels (variety: Vona), each
analyzed separately. This plot represents the
most kernel to kernel scatter in signal amplitude
observed within a given variety for the twelve
varieties tested.

Legend:

    square - kernel #1

    plus - kernel #2

    diamond - kernel #3

    triangle - kernel #4

    cross - kernel #5

Log Signal Amplitude (microvolts) vs Log Modulation Frequency (Hz)

□ Run #1,   + #2,   ◊ #3,   △ #4,   x #5.
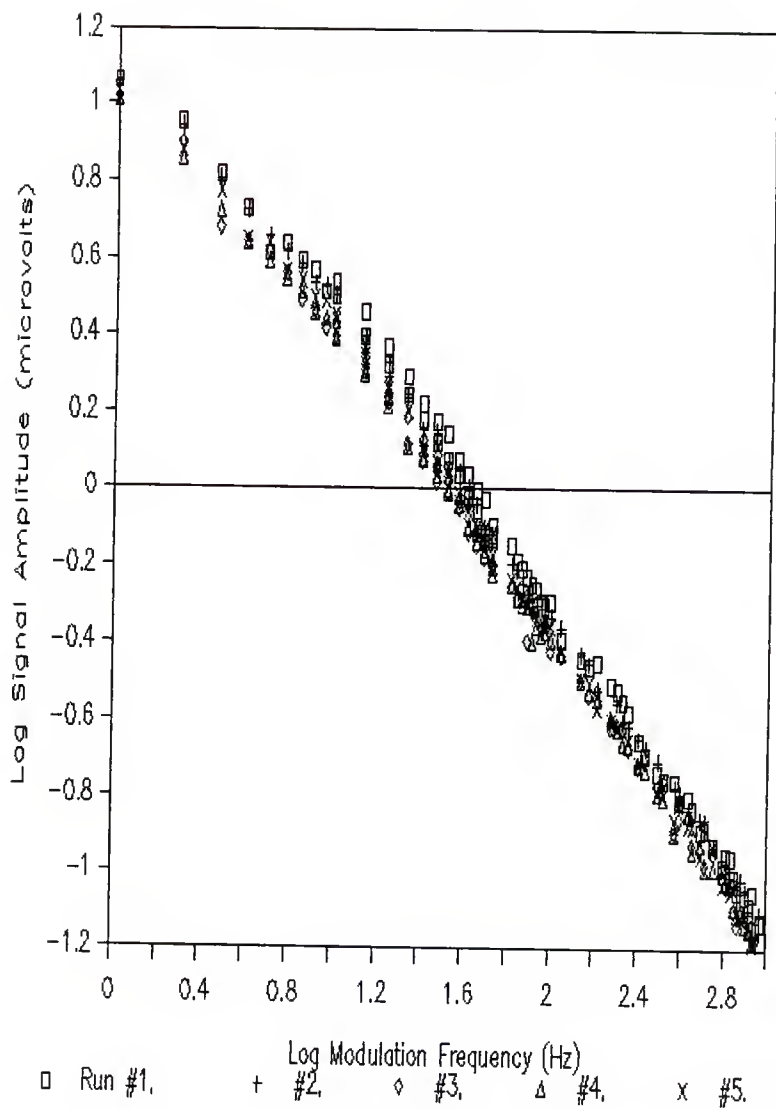
Figure 4.27. A plot of the phase of the photoacoustic response vs log modulation frequency for five different kernels (variety: Mustang), each analyzed separately. This plot represents the least amount of kernel to kernel scatter in the phase angle observed within a given variety for the twelve varieties tested.

Legend:

      square - kernel #1

      plus - kernel #2

      diamond - kernel #3

      triangle - kernel #4

      cross - kernel #5

Figure: Phase Angle (degrees) versus Log Modulation Frequency (Hz)

□ Run #1,　　+　#2,　◊　#3,　△　#4,　x　#5.
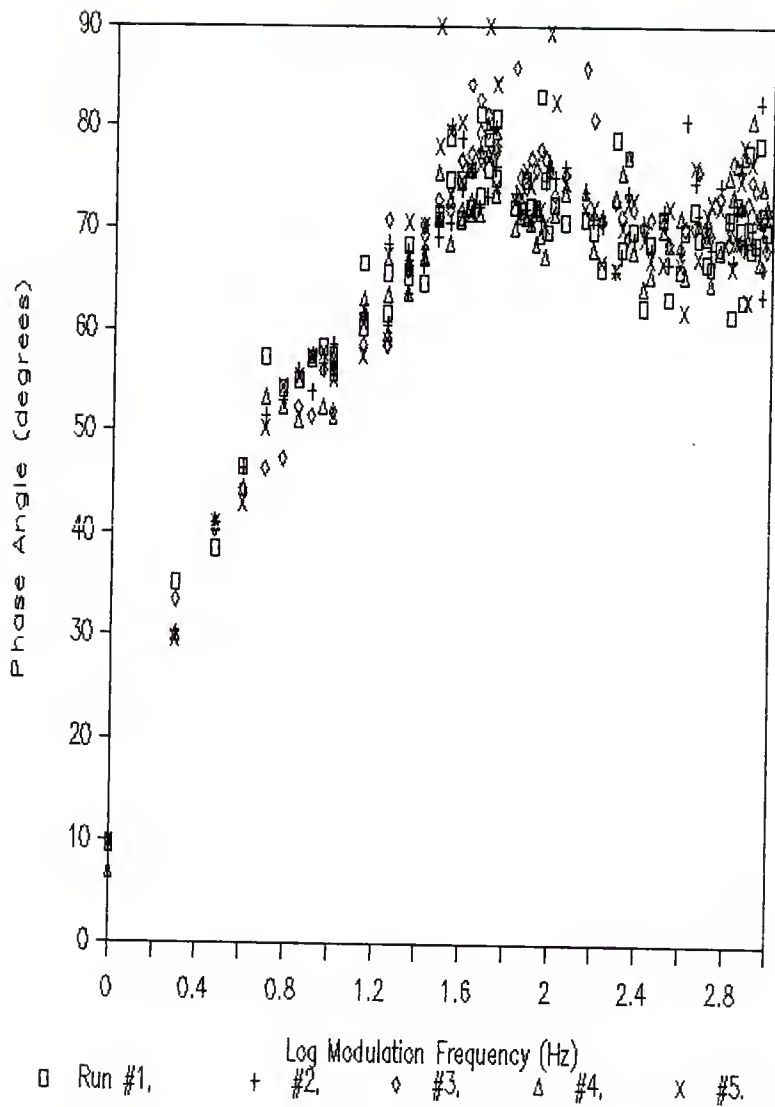
Figure 4.28. A plot of the phase of the photoacoustic
    response vs log modulation frequency for five dif-
    ferent kernels (variety: Scout-66), each analyzed
    separately. This plot represents the most kernel
    to kernel scatter in the phase angle observed within
    a given variety for the twelve varieties tested.

    Legend:

        square - kernel #1
        plus - kernel #2
        diamond - kernel #3
        triangle - kernel #4
        cross - kernel #5

Log Modulation Frequency (Hz)

□ Run #1,　　+　#2,　◇　#3,　△　#4,　x　#5.
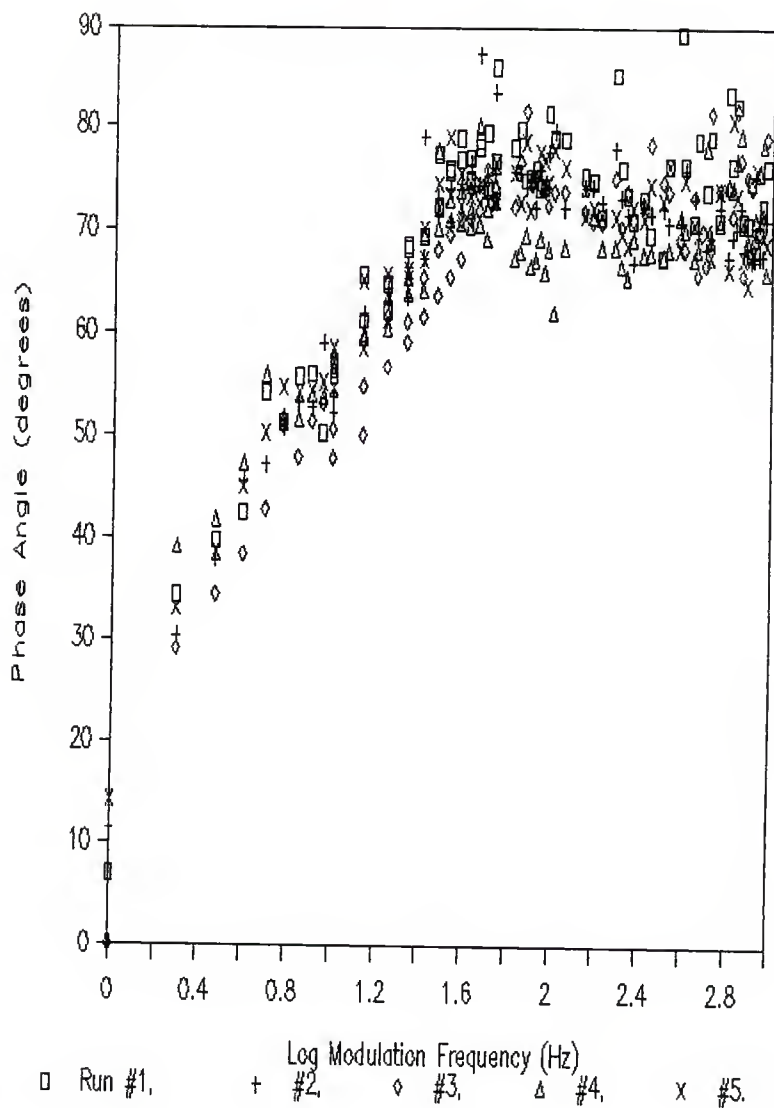
Figure 4.29. A log-log plot showing the average amp-
      litude of the photoacoustic response vs modulation
      frequency for each of the four soft red winter
      wheat varieties tested. The photoacoustic responses
      from a total of five separate kernels were used to
      obtain the average results for each variety.

      Legend:

            square - Arthur (AT)
            plus - Caldwell (CW)
            diamond - Coker-916 (CK)
            triangle - Pike (PK)
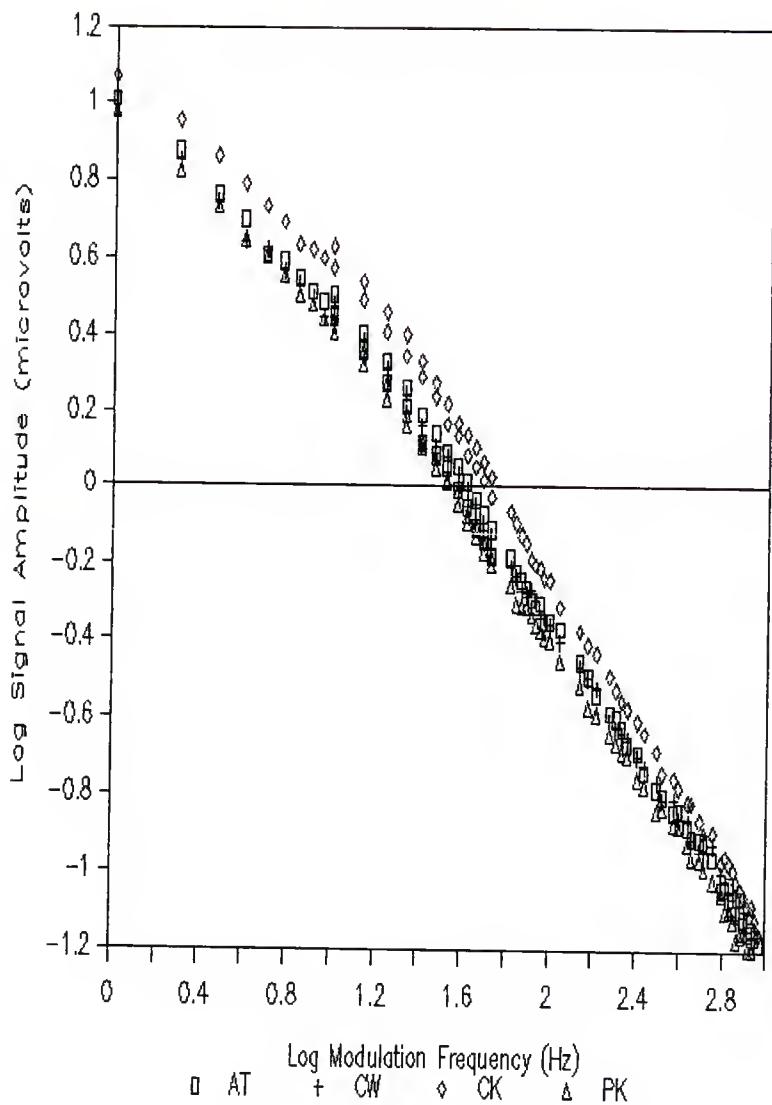
Figure 4.30. A log-log plot showing the average amp-
      litude of the photoacoustic response vs modulation
      frequency for four of the eight hard red winter
      wheat varieties tested. The photoacoustic responses
      from a total of five separate kernels were used to
      obtain the average results for each variety.

      Legend:

            square - Arkan (AK)
            plus - Bounty-310 (BY)
            diamond - Hawk (HK)
            triangle - Mustang (MG)

151
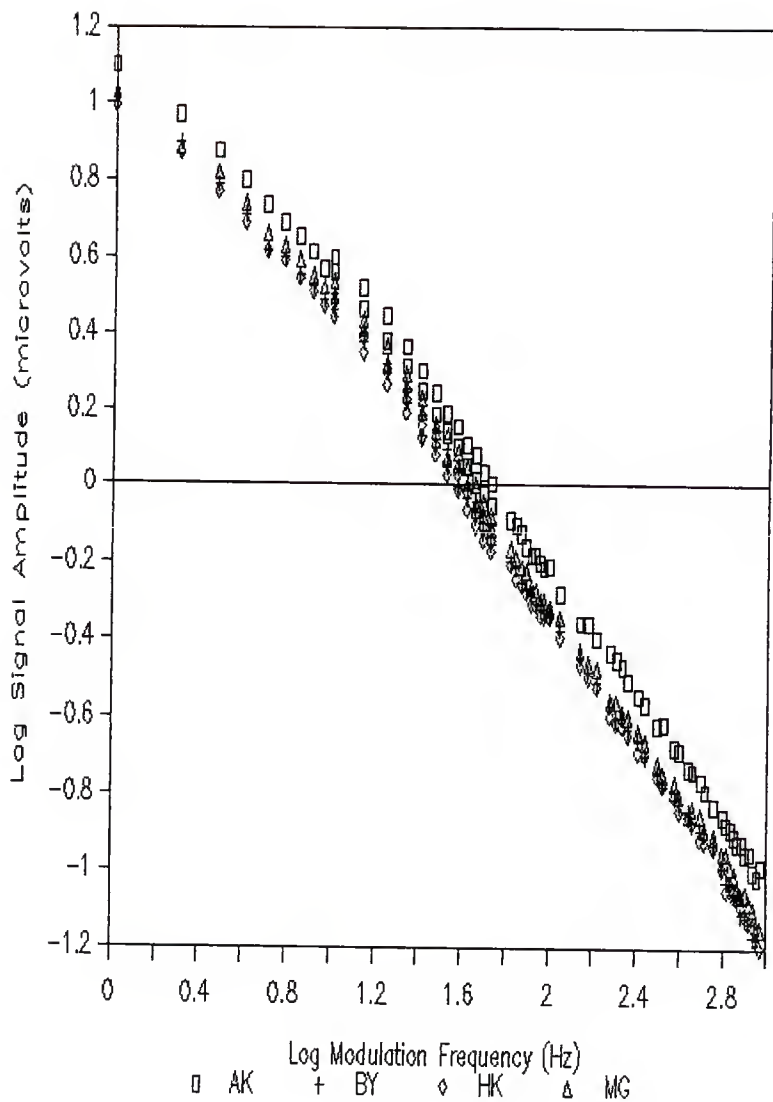
Figure 4.31. A log-log plot showing the average amp-
        litude of the photoacoustic response vs modulation
        frequency for the remaining four hard red winter
        wheat varieties tested. The photoacoustic responses
        from a total of five separate kernels were used to
        obtain the average results for each variety.

        Legend:

            square — Newton (NW)
            plus — Scout-66 (SC)
            diamond — Tam-105 (TM)
            triangle — Vona (VN)

Log Signal Amplitude (microvolts) vs Log Modulation Frequency (Hz)

□ NW   + SC   ◇ TM   △ VN
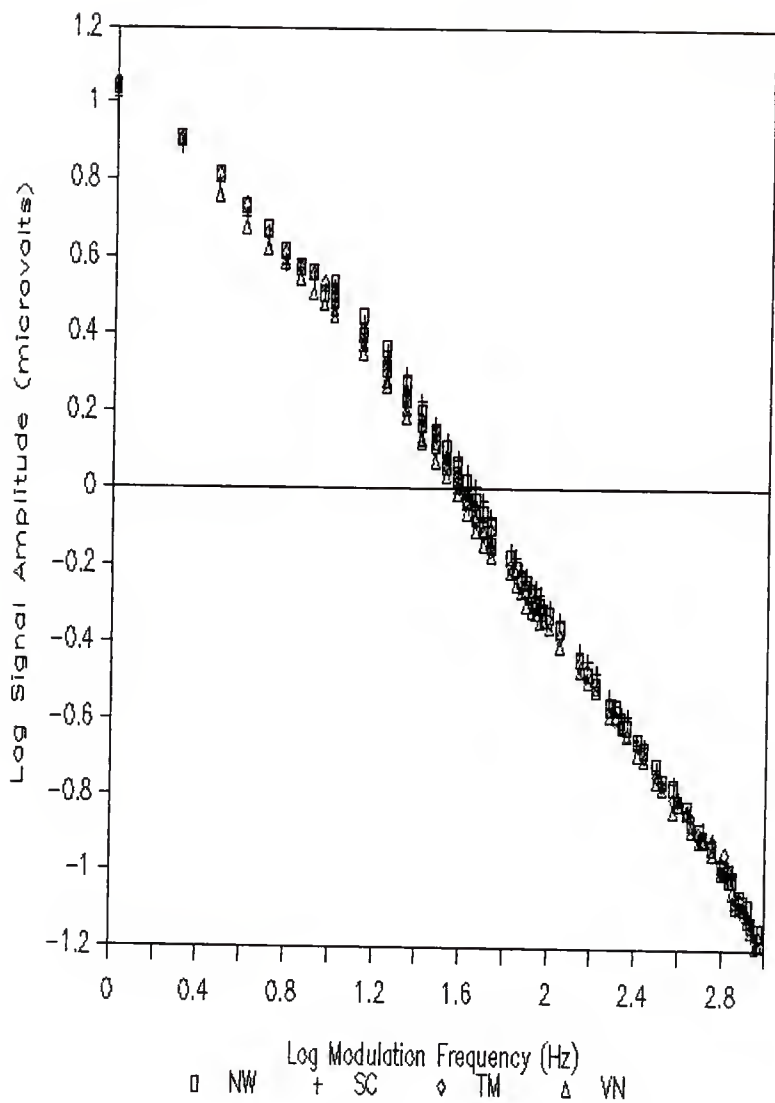
Figure 4.32. A plot showing the average phase of the
    photoacoustic response vs log modulation frequency
    for each of the four soft red winter wheat varie-
    ties tested. The photoacoustic responses from a
    total of five separate kernels were used to obtain
    the average results for each variety.

    Legend:

        square - Arthur (AT)
        plus - Caldwell (CW)
        diamond - Coker-916 (CK)
        triangle - Pike (PK)

154

155

Figure 4.33.   A plot showing the average phase of the
        photoacoustic response vs log modulation frequency
        for four of the eight hard red winter wheat varie-
        ties tested.   The photoacoustic responses from a
        total of five separate kernels were used to obtain
        the average results for each variety.

        Legend:

                square – Arkan (AK)
                plus – Bounty-310 (BY)
                diamond – Hawk (HK)
                triangle – Mustang (MG)

156

Figure 4.34. A plot showing the average phase of the
photoacoustic response vs log modulation frequency
for the remaining four hard red winter wheat varie-
ties tested. The photoacoustic responses from a
total of five separate kernels were used to obtain
the average results for each variety.

Legend:

      square - Newton (NW)

      plus - Scout-66 (SC)

      diamond - Tam-105 (TM)

      triangle - Vona (VN)
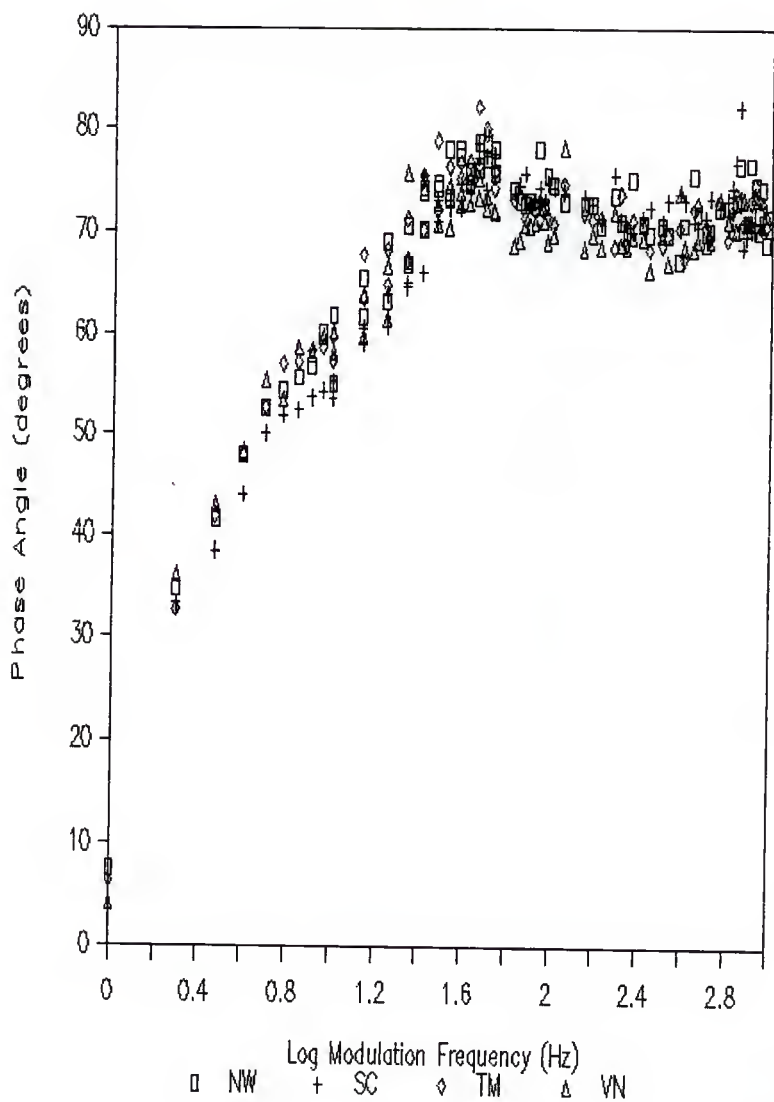
variation within a given variety was generally at least as great as this separation. Two varieties which seemed to consistently produce photoacoustic signals significantly stronger than the other varieties tested were Arkan and Coker-916. In addition, the phase of the response from Coker-916 seemed to vary with modulation frequency somewhat differently than typically observed with the other varieties. Based on these observations, the identification of a kernel from the twelve varieties tested as being either of these two varieties appears to be immediately feasible. More detailed analysis of data obtained by the above-described technique may permit further identification as well.

One obvious variability factor in individual wheat kernels is the kernel size. In an attempt to help reduce the variation that this might cause in the photoacoustic response, a normalization on the basis of kernel cross-sectional area was attempted. The normalization procedure tried assumed elipsoid-shaped kernels of constant density, using the functional dependence of cross-sectional area on the kernel mass to normalize the data on the basis of the area of the kernel being illuminated. The normalized data, however, did not appear to exhibit any less kernel to kernel variation within a given variety, and was often found to actually increase the scatter. Such a normalization procedure assumes that the spot size of the incident e-m radiation is larger than the kernel's cross sectional area. Since for these experiments the chamber depth was fairly shallow (0.47 cm), and the previously described aperture restricting the cone of radia-

tion entering the chamber was used, it is possible that the spot
size of significantly intense radiation at the kernel depth was
smaller than the size of the wheat kernels sampled. At the cham-
ber depth which was used, the 3 mm diameter aperture should
restrict the spot size to a diameter of approximately 2.8 mm at
the chamber floor, which is slightly larger than the width of a
typical wheat kernel. However, the radiation having intensity
greater than or equal to half the intensity occurring at the
center of the spot was confined to a diameter of only 1.1 mm,
assuming the manufacturer's specifications for the diode to be
accurate. Thus, it is probable that all significantly intense
direct irradiation impinged upon the kernel. Assuming this to be
the case, such a normalization procedure would be counterproduc-
tive, as we found it to be with our data.

Another possible factor increasing the observed variation in
the photoacoustic response among kernels of the same variety is
the presence of moisture remaining in the kernel after the drying
process which we used was completed. As previously stated,
standardization of the moisture content is very important, due to
its large effect on the photoacoustic signal. Although our
drying studies seemed to indicate that after fifty hours drying,
the majority of moisture is lost by the kernel, it is possible
that a sufficiently large amount of moisture is still present in
the kernel to influence the response. If this amount varies from
kernel to kernel, it should contribute to the variation seen in
the photoacoustic response. To reduce this problem, it might be

161

necessary to use a much longer drying time or higher temperature to drive any remaining moisture from the kernel. Alternatively, a standardization procedure bringing all kernels to the same moisture content by moisture saturation might be effective, although this would decrease the amplitude of the overall response.

Figures 4.35 and 4.36 show the average photoacoustic response for all hard wheat kernels and all soft wheat kernels tested. It is seen that the average amplitude of the response is slightly greater on the average for hard wheats, except for in the intermediate portion of the modulation frequency range. The greater amplitude for hard wheat is consistent with results obtained in an earlier study, comparing the photoacoustic response of a typical hard and a typical soft variety (27). The average phase of the photoacoustic response for hard wheat varieties tends to be slightly less than for soft varieties at modulation frequencies above approximately 40 Hz, although at frequencies below this value there seems to be little difference.

Figure 4.35. A log-log plot showing the average amp-
    litude of the photoacoustic response vs modulation
    frequency of all of the hard red winter wheat ker-
    nels and all of the soft red winter wheat kernels
    tested.

    Legend:

        square - average response, soft red winter
        plus - average response, hard red winter
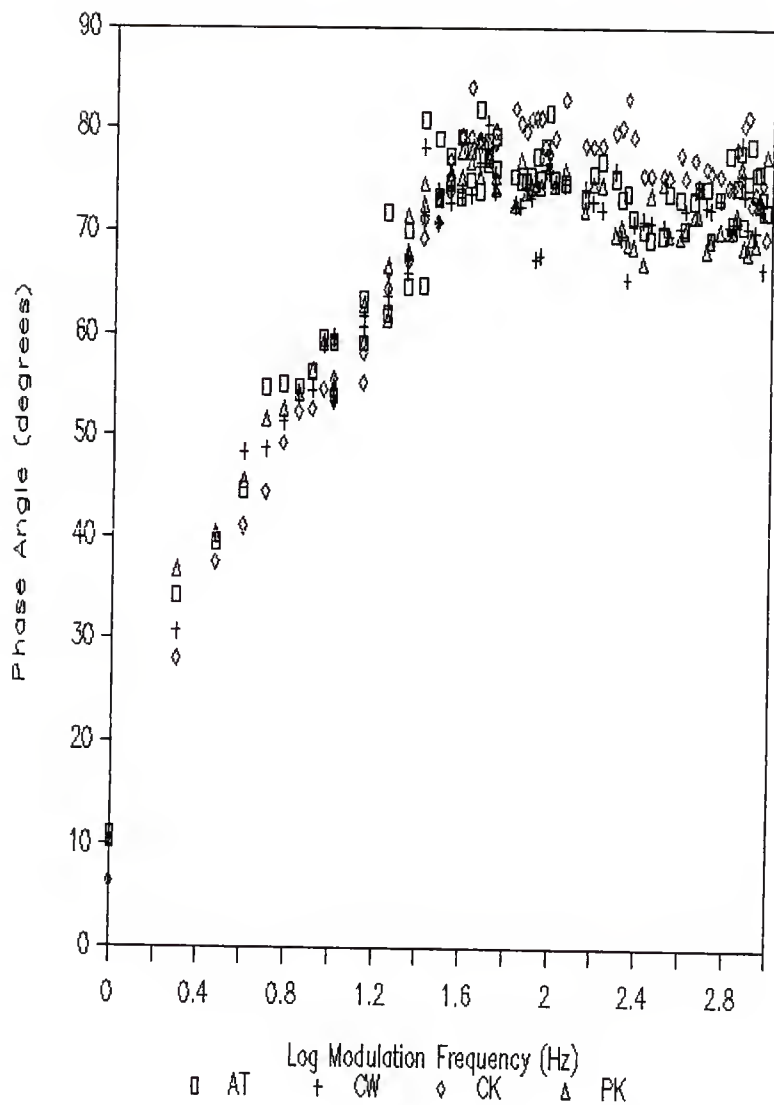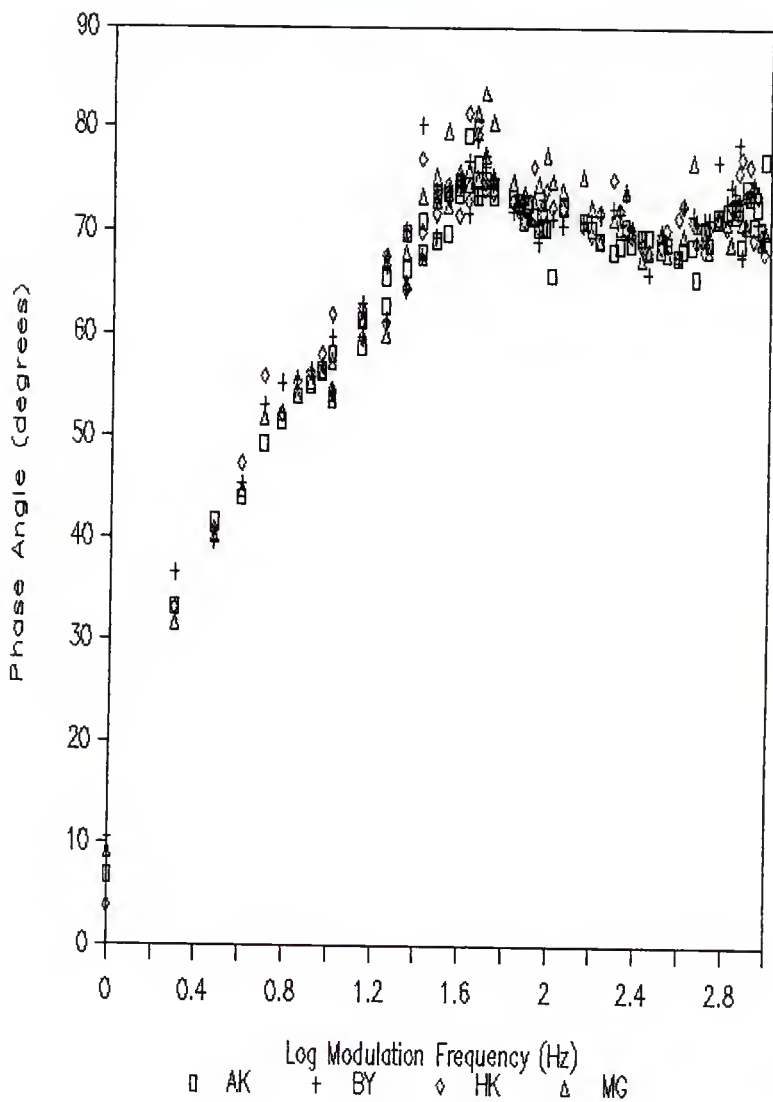
163

Log Modulation Frequency (Hz)
□ SOFT   + HARD
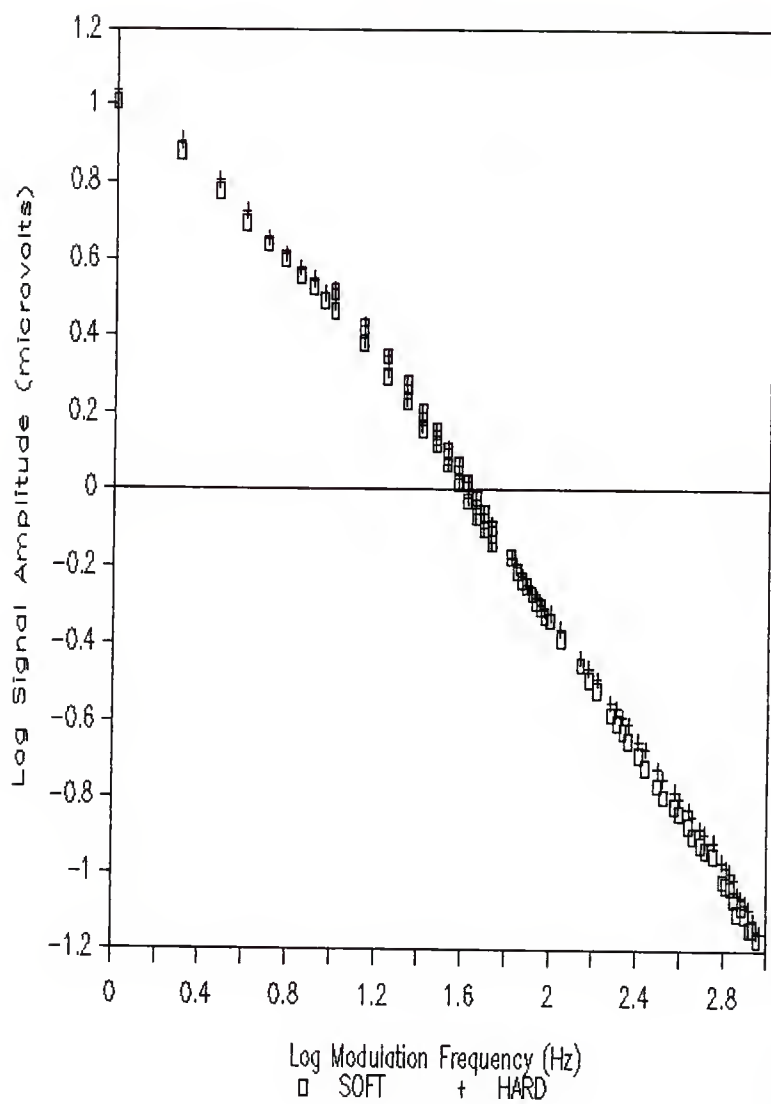
Figure 4.36. A plot showing the average phase of the photoacoustic response vs log modulation frequency of all of the hard red winter wheat kernels and all of the soft red winter wheat kernels tested.

Legend:

square - average response, soft red winter

plus - average response, hard red winter

Phase Angle (degrees) vs Log Modulation Frequency (Hz)

□ SOFT   + HARD
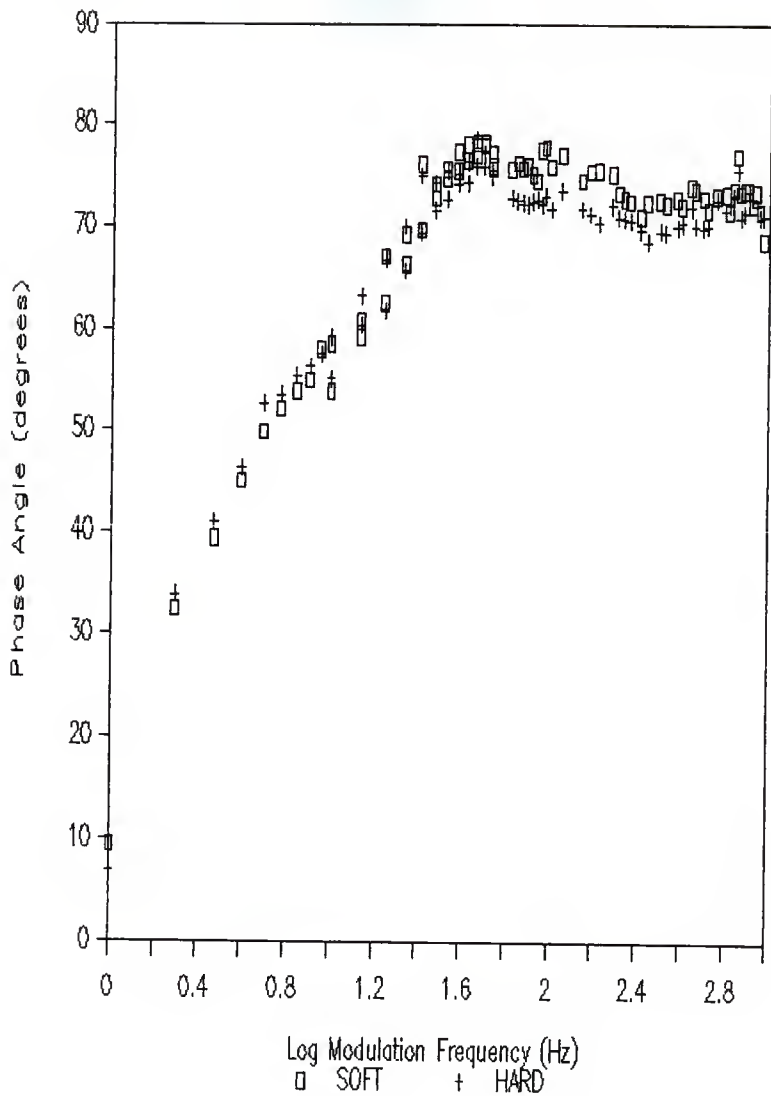
CHAPTER V

SUMMARY AND CONCLUSIONS

The results obtained from these studies clearly show that different kernels of the same variety may produce photoacoustic responses that are significantly different from one another, which implies that there is a certain amount of variation in thermal properties between individual kernels, even when the kernels are of the same variety. If moisture content is the main contributor to the observed variations, then more extensive sample preparation, either by increased drying or some other method, might sufficiently eliminate differences in moisture content, and allow the intrinsic thermal properties of the kernels themselves to dominate the photoacoustic response.

Despite the kernel to kernel variation which was found to occur in our results, we did find significant differences in the photoacoustic responses of Arkan and Coker-916, both of which provided signals relatively strong in comparison to the other varieties tested. This seems to suggest that positive identification on the basis of variety may be possible using photoacoustic analysis, if reduction in the variation between kernels of the same variety can be achieved. Although Coker-916 is a soft wheat variety, and it exhibited a relatively strong photoacoustic amplitude, the average amplitude of soft wheats was found to be slightly lower than for hard wheats, and the average phase seemed to be slightly greater in the higher modulation frequency range.

167

This implies that even with the kernel to kernel variations, there seem to be differences in the thermal properties of hard and soft varieties which can be detected using photoacoustic analysis techniques.

The kernel drying studies carried out in this project seemed to yield interesting results, even though they were performed prior to improvements made in both the extent of the modulation frequency range which was able to be monitored and the ratio of the sample chamber contribution to the photoacoustic signal. Since moisture has such a pronounced effect on the photoacoustic response, and since frequency modulation of the incident e-m radiation permits profiling of a sample as a function of depth, detection of the relative distribution of moisture in a kernel as it is either dried or allowed to absorb water seems to be feasible. This may prove valuable for more detailed studies of either moisture evaporation or absorption in grains. Alternatively, photoacoustic analysis may provide a rapid method for determining the relative moisture content of a single kernel.

With the addition of the aperture to the photoacoustic cell, the ratio of the empty chamber response to the response with a wheat kernel sample present was greatly improved. However, it is still possible that the chamber itself was interfering significantly with the sample response, especially at higher modulation frequencies, where the empty chamber and wheat kernel responses were comparable. A further reduction of the empty chamber response might decrease the similarity of the responses obtained

for kernels of different varieties, thus increasing the ability to make more clear-cut distinctions between them. Improvements to the apparatus which could be made include the use of a sharply focused, higher intensity e-m radiation source. This would serve to increase the amplitude of the photoacoustic response, thus improving the signal to noise ratio. If the spot size were focused so that it were smaller than the cross-sectional area of a typical wheat kernel, the chamber's contribution to the response should not increase nearly as much, as only an increase in indirect illumination caused by radiation scattered from the sample would occur. Use of a sufficiently intense near-infrared laser could be used to achieve this, although it would most likely require a redesign of the photoacoustic cell used in these experiments. Variation of the material used to construct the photoacoustic cell might be advantageous with regard to decreasing the unwanted contribution to the photoacoustic response from the chamber itself. Using stainless steel, for example, would provide a thermal diffusion length approximately five times lower than aluminum at a given modulation frequency (21), due primarily to its much larger density. Since the photoacoustic response typically increases with increasing thermal diffusion length, a much smaller empty chamber response should be expected. Use of a photoacoustic cell with transparent walls would essentially eliminate absorption of radiation by the sample chamber itself, and thus would greatly decrease the contribution to the photoacoustic response from the chamber. However, acoustic isolation and the

169

ability of heat to diffuse from the sample chamber may be compromised.

In photoacoustic sample analysis, it is the purpose of the gas-filled photoacoustic cell to allow for indirect detection of temperature variations at the surface of the sample being analyzed, by monitoring the resultant pressure fluctuations occurring in the cell. If these temperature fluctuations could be measured more directly, it might be possible to eliminate many of the interfering effects, restrictions, and variables associated with the gas-microphone configuration, while the same information could be obtained. Using an infrared radiation detection device, thermal radiation emitted from the sample surface could be monitored as a function of the modulation frequency, instead of monitoring the acoustic signal, allowing for direct detection of temperature fluctuations at the sample surface. Such an analysis technique would offer several advantageous features. Since the sample would not have to be confined to a gas-filled cell, the need for maintaining a helium gas atmosphere would be eliminated. Also, the sample could be easily positioned for illumination, and high-intensity and well-focused light sources such as lasers could thus more easily used. The problem with contributions to the signal from the sample chamber in our gas-microphone photoacoustic measurements would be eliminated, as well as would be problems with background noise. Again, since the temperature fluctuations at the sample surface provides the essential information about the thermal properties of the sample, more precise

170

results might be obtainable from experiments similar to those carried out in this project, utilizing a method which incorporates some of these improvements.

REFERENCES

1. J. A. Shellenberger, Wheat: Chemistry and Technology (American Association of Cereal Chemists, Inc., St. Paul, Minnesota, 1971), p. 4.

2. Ibid., p. 2.

3. J. W. Schmidt, Wheat: Production and Utilization (The AVI Publishing Company, Inc., Westport, Connecticut, 1974), p. 11.

4. W. Bushuk, Proceedings of the National Conference of Wheat Utilization Research, (USDA Agricultural Reviews and Manuals ARM-W-4, 1977).

5. J. A. Shellenberger, CRC Handbook of Processing and Utilization in Agriculture (CRC Press, Inc., Boca Raton, Florida, 1982), p. 92.

6. M. M. MacMasters, J. J. C. Hinton, and D. Bradbury, Wheat: Chemistry and Technology (American Association of Cereal Chemists, Inc., St. Paul, Minnesota, 1971), p. 52.

7. The Wheat Flour Institute, Washington, D.C.

8. MacMasters, op. cit., p. 53.

9. D. W. Kent-Jones and A. J. Amos, Modern Cereal Chemistry (Food Trade Press, London, 1967).

10. N. L. Kent, Technology of Cereals (Pergamon Press, Oxford, 1983), p. 30.

11. MacMasters, op. cit., pp. 51-113.

12. Kent, op. cit., p. 52.

13. R. C. Hoseney and P. A. Seib, Structural differences in hard and soft wheat. The Bakers Digest (1973).

14. S. O. Berg, Is the degree of grittiness of wheat flour mainly a varietal character? Cereal Chem. 24, 274 (1947).

15. L. Zeleny, Wheat: Chemistry and Technology (American Association of Cereal Chemists, Inc., St. Paul, Minnesota, 1971), p. 24.

16. Ibid., p. 24.

17. W. Obuchowski and W. Bushuk, Wheat hardness: Comparison of methods of its evaluation. Cereal Chem. 57, 421 (1980).

18. A. Rosencwaig, Photoacoustics and Photoacoustic Spectroscopy (John Wiley & Sons, New York, 1980), pp. 7-9.

19. A. Rosencwaig and A. Gersho, Theory of the photoacoustic effect with solids. J. Appl. Phys. 47, 64 (1976).

20. A. Rosencwaig, Photoacoustic spectroscopy: A new tool for investigation of solids. Anal. Chem. 47, 592 (1975).

21. A. Rosencwaig, Photoacoustics and Photoacoustic Spectroscopy (John Wiley & Sons, New York, 1980), p. 96.

22. L. C. Aamodt, J. C. Murphy, and J. G. Parker, Size considerations in the design of cells for photoacoustic spectroscopy. J. Appl. Phys. 48, 927 (1977).

23. Lotus Development Corporation, Cambridge, Massachusetts (1983).

24. ASAE Data: ASAE D241.2 and ASAE D243.2. Agricultural Engineers Yearbook of Standards, 1983 edition, pp. 294, 296.

25. V. Venkataraman, M.Sc. Thesis, Kansas State University, pp. 55-106.

26. Kent, op. cit., p. 81.

27. Venkataraman, op. cit.

APPENDIX I

A general flowchart of the data acquisition routine incor-
porated into the programs used by the microcomputer operated data
acquisition system. Complete listings of the actual programs
used are provided in Appendices II and III.

.

174

START
data acquisition
routine

Compute voltage being
sent to function gener-
ator VCO input

8

Compute function generator
modulation frequency as a
function of VCO input

Has
portion #2
of acquisition
process
begun

No

Yes

Correct computed modulation
frequency value for high
function generator range

Correct computed modulation
frequency value for high
function generator range

Is
modula-
tion frequency a
harmonic of
60 Hz

Yes

1

No

2

175

```
        ┌───┐
        │ 2 │
        └─┬─┘
          ▼
┌─────────────────────────┐
│ Increase data point counter │
│ by 1                        │
└─────────────┬───────────┘
              ▼
┌─────────────────────────┐
│ Save modulation frequency   │
│ in data matrix              │
└─────────────┬───────────┘
              ▼
      ┌──────────────────┐
      │   Send new voltage   │
      │   to function gen-   │
      │   erator VCO input  │
      └─────────┬────────┘
                ▼
┌─────────────────────────┐
│ Execute delay loop to       │
│ allow lock-in amplifier     │
│ to stabilize                │
└─────────────┬───────────┘
              ▼
      ┌──────────────────┐
      │   Obtain 50 separ-   │
      │   ate readings of   │
      │   PIN diode output  │
      └─────────┬────────┘
                ▼
┌─────────────────────────┐
│ Compute average of PIN di-  │
│ ode output signal readings  │
└─────────────┬───────────┘
              ▼
┌─────────────────────────┐
│ Convert average value into  │
│ microvolts and save in data │
│ matrix                      │
└─────────────┬───────────┘
              ▼
          ┌───────┐
          │   3   │
          └───────┘
```

176

```
                          ┌─────┐
                          │  3  │
                          └──┬──┘
                             │
                             ▼
              ┌──────────────────────────┐
             /  Obtain numerous amp-      │
            /   litude and in-phase       │
            │   comp. readings of         │
            │   microphone signal         │
            └──────────────┬──────────────┘
                           │
                           ▼
            ┌──────────────────────────────┐
            │  Compute average amplitude    │
            │  and in-phase component of    │
            │  microphone signal            │
            └───────────────┬──────────────┘
                            │
                            ▼
            ┌──────────────────────────────┐
            │  Convert average values into  │
            │  microvolts and save in data  │
            │  matrix                       │
            └───────────────┬──────────────┘
                            │
                            ▼
            ┌──────────────────────────────┐
            │  Calculate phase angle from   │
            │  amplitude and in-phase com-  │
            │  ponent values                │
            └───────────────┬──────────────┘
                            │
                            ▼
            ┌──────────────────────────────┐
            │  Save phase angle in data     │
            │  matrix                       │
            └───────────────┬──────────────┘
                            │
                            ▼
              ┌──────────────────────────┐
             /  Print data matrix         /
            /   values for current       /
            /   iteration               /
            └──────────────┬─────────────┘
                           │
                           ▼
                        ┌─────┐
                        │  4  │
                        └─────┘
```

```
                    ┌───┐
                    │ 6 │
                    └─┬─┘
                      │
                      ▼
        ┌─────────────────────────┐
        │ Increase output value to│
        │ be sent to function gen- │
        │ erator by appropriate    │
        │ increment                │
        └────────────┬─────────────┘
                     │
                     ▼
         ╱───────────────────────╲
        │ Send new voltage         │
        │ function generator       │
        │ VCO input                │
         ╲───────────────────────╱
                     │
                     ▼
        ╱─────────────────────────╲
        │ Increase sensitiv-       │
        │ ity setting of lock-     │
        │ in amplifier             │
        ╲─────────────────────────╱
                     │
                     ▼
        ┌─────────────────────────┐
        │ Accept acknowledgement   │
        │ to proceed with acqui-   │
        │ sition process at new    │
        │ sensitivity setting      │
        └────────────┬─────────────┘
                     │
                     ▼
        ┌─────────────────────────┐
        │ Redefine sensitivity of  │
        │ lock-in amplifier to     │
        │ accommodate setting      │
        │ change                   │
        └────────────┬─────────────┘
                     │
   ┌───┐             │
   │ 5 │─────────────┤
   └───┘             │
                     ▼
              ╱─────────────╲
             ╱   Should       ╲
            ╱  range setting    ╲        No        ┌───┐
           ╱  of function gen-   ╲───────────────▶│ 8 │
            ╲ erator be in-      ╱                 └───┘
             ╲   creased        ╱
              ╲───────────────╱
                     │ Yes
                     ▼
                   ┌───┐
                   │ 7 │
                   └───┘
```

APPENDIX II

The acquisition program used in acquiring data for the 1-50
Hz modulation frequency range. The program was written to be
used with the Microsoft BASICA interpreter. A discussion of the
program is provided in Section 3.4, and Appendix I gives a gen-
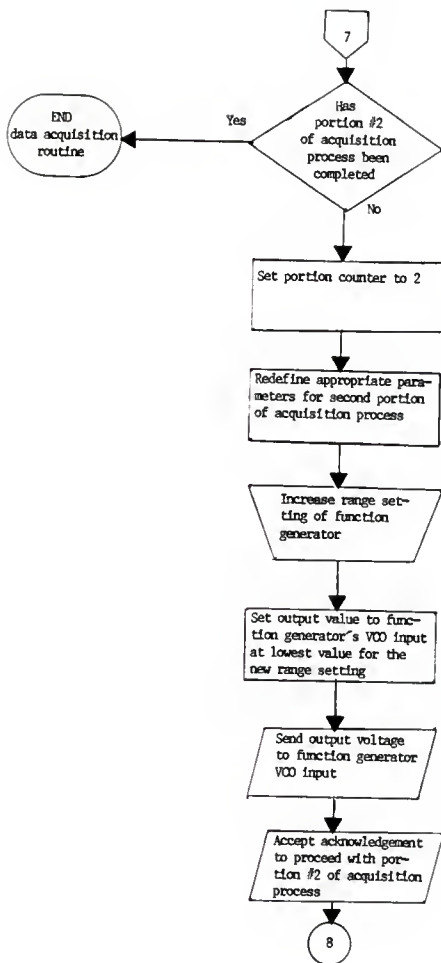eral flowchart of the portion of the program in which the data is
actually acquired.

181

```
10 ADC.SETUP=&H8B4:ALTOUT12.B=&H72E:ALTOUT12.BT=&H78A:ALTOUT12.R=&H7E9
15 ALTOUT12.RT=&H847:ALTOUT12.S=&H6E5:ALTOUT12.ST=&H708:ALTOUT8.B=&H2CF
20 ALTOUT8.BT=&H359:ALTOUT8.R=&H3E9:ALTOUT8.RT=479:ALTOUT8.S=&H24A
25 ALTOUT8.ST=&H28A:DAC.SETUP=&H1A:INADC12.B=&HCDF:INADC12.BT=&HD4B
30 INADC12.EXTCLOCK=&HDC7:INADC12.S=&HC70:INADC12.ST=&HC9C:INADC8.B=&H97B
35 INADC8.BT=&H9E2:INADC8.EXTCLOCK=&HA4C:INADC8.S=&H904:INADC8.ST=&H933
40 OUTDAC12.B=&H564:OUTDAC12.BT=&H5C4:OUTDAC12.R=&H627:OUTDAC12.RT=&H67B
45 OUTDAC12.S=&H50F:OUTDAC12.ST=&H538:OUTDAC8.B=&HBC:OUTDAC8.BT=&H11D
50 OUTDAC8.R=&H181:OUTDAC8.RT=&H1E4:OUTDAC8.S=&H6D:OUTDAC8.ST=&H93
55 SCAN12.B=&HEE5:SCAN12.BT=&HF7A:SCAN12.S=&HE36:SCAN12.ST=&HE82
60 SCAN8.B=&HB4B:SCAN8.BT=&HBDA:SCAN8.S=&HA9E:SCAN8.ST=&HAE9
65 DEF SEG=0
70 CSEG=(256*PEEK(&H3CB))+PEEK(&H3CA)
75 DEF SEG=CSEG
91 ´
92 ´
93 ´THE FIRST 100 LINES ARE RESERVED FOR LABSTAR SOFTWARE
94 ´THE APPLICATION PROGRAM STARTS AT LINE 100
95 ´
96 ´
97 ´
98 ´
99 ´
100 CLS:PRINT:PRINT:PRINT
110 PRINT"THE FOLLOWING DATA ACQUISITION PROGRAM IS DESIGNED TO OBTAIN AND"
120 PRINT"PROCESS THE PHOTOACOUSTIC SIGNAL FROM A LOCK IN AMPLIFIER AS A"
130 PRINT"FUNCTION OF THE MODULATION FREQUENCY OF THE LIGHT SOURCE AS"
140 PRINT"DRIVEN BY A VARIABLE FREQUENCY WAVEFORM GENERATOR."
150 :
160 REM —THE FOLLOWING SEVERAL LINES DEFINE CONSTANTS NECESSARY FOR IMPLEMENTAT
ION OF PROG.
170 :
175 ZERO$="0000000000"
180 C0=100:C1=163.654:C2=3.627054:C3=-.4178307
190 OVER=256:INCR=15:PORTION=1
210 CORRECT=10^.5:LG=LOG(10)
215 TMG%=3994:LNG%=50:ADJ=2
220 DIM DATMAT(1000,5):DIM ARRAY%(200):DIM AAY%(50)
230 ADDRESS%=&H304
240 CALL DAC.SETUP(ADDRESS%)
250 CHANNEL%=0
260 VALUE%=128 ´ENABLES INITIAL MODULATION FREQUENCY OF 10.0 HERTZ.
270 CALL OUTDAC8.S(CHANNEL%,VALUE%) ´SENDS INITIAL VOLTAGE TO WFG.
280 PRINT:PRINT:PRINT:PRINT"TURN ON POWER TO PHOTOACOUSTIC SAMPLING EQUIPTMENT."
290 PRINT:PRINT:PRINT
300 PRINT"SET WAVEFORM GENERATOR RANGE AT 100 HZ. AND ADJUST UNTIL COUNTER CONSI
STANTLY"
310 PRINT"REGISTERS A 100 HZ. READING."
```

```
320 PRINT:INPUT"WHEN ADJUSTMENT IS COMPLETE, SET WFG RANGE TO 10 HZ. AND THEN PR
ESS RETURN.";RTN
330 CLS:PRINT:PRINT:PRINT:PRINT"FROM THE METERS ON POWER SUPPLY DRIVING LED:";PR
INT:PRINT
340 INPUT"ENTER DC VOLTAGE TO LED (IN VOLTS)";LEDVLT
350 PRINT:INPUT"ENTER CURRENT TO LED (IN AMPS)";CURRENT
360 PRINT:PRINT:INPUT"ENTER RANGE SETTING OF MICROVOLTMETER (IN MICROVOLTS)";MIC
RO
362 CLS:PRINT:PRINT:PRINT:PRINT:PRINT:PRINT:PRINT"SET WAVEFORM GENERATOR TO 1 HZ
. RANGE AND MAKE NECESSARY ADJUSTMENTS ON LIA."
365 PRINT:PRINT:INPUT"ONCE FINISHED, PRESS RETURN";RRN$
370 CLS:PRINT:PRINT:PRINT
380 PRINT"ENTER THE FOLLOWING LOCK IN AMPLIFIER SETTINGS:":PRINT:PRINT
390 INPUT"TIME CONSTANT (IN SECONDS)";TICON
400 INPUT"SENSITIVITY (IN MICROVOLTS)";SENSI
410 SENSI$=STR$(SENSI)
420 IF LEFT$(SENSI$,2)=" 3" THEN SENSI=(SENSI/3)*CORRECT
430 INPUT"PHASE SETTING (IN DEGREES)";PHSET$
440 CLS:PRINT:PRINT:PRINT"IS A DELAY TIME OF "TICON*4" SECONDS ADEQUATE TO ALLOW
 LOCK IN AMPLIFIER"
450 INPUT"TO STABILIZE";SEY$
460 IF LEFT$(SEY$,1)="Y" OR LEFT$(SEY$,1)="y" THEN DELAY=TICON*4:GOTO 510
470 CLS:PRINT:PRINT:PRINT
480 PRINT"ENTER DESIRED DELAY TIME (IN SECONDS) BETWEEN MODULATION FREQUENCY"
490 PRINT"INCREMENT AND SUBSEQUENT ACQUISITION OF SIGNAL FROM LOCK IN AMP."
500 PRINT:INPUT DELAY
510 DELAY=DELAY*840 'CONVERTS LOOP DELAY PARAMETER TO SECONDS.
520 CLS:PRINT:PRINT:PRINT
530 PRINT"IS 50 DATA POINTS TAKEN PER MODULATION FREQ. INCREMENT SUFFICIENT, YES
 OR NO";:INPUT ESY$
540 IF LEFT$(ESY$,1)="Y" OR LEFT$(ESY$,1)="y" THEN POINTNO=50:GOTO 570
550 PRINT:PRINT"HOW MANY DATA POINTS ARE TO BE TAKEN AT EACH MODULATION FREQUENC
Y"
560 INPUT POINTNO:IF INT(POINTNO)<>POINTNO OR POINTNO<1 THEN GOTO 550
570 LENGTH%=POINTNO
580 RATE=TICON/POINTNO
590 PRINT:PRINT:PRINT:PRINT"IS A SAMPLING RATE OF ";INT(RATE*10000)/10000;" SECO
NDS BETWEEN ACQUISITION OF DATA"
600 PRINT"POINTS AT A GIVEN MODULATION FREQUENCY SUFFICIENT";:INPUT AN$
610 IF LEFT$(AN$,1)="Y" OR LEFT$(AN$,1)="y" THEN GOTO 630
620 PRINT:INPUT"ENTER DESIRED SAMPLING RATE (IN SECONDS)";RATE
630 BETWEEN=RATE/.000005
640 IF BETWEEN>65536! THEN PRINT:PRINT"DESIRED SAMPLING RATE IS TOO LARGE, IT CA
NNOT EXCEED 0.327 SECONDS":PRINT:PRINT:GOTO 620
650 IF BETWEEN>32767 THEN BETWEEN=BETWEEN-65536!
660 TIMING%=INT(BETWEEN)
670 CLS:PRINT:PRINT:PRINT
680 INPUT"ENTER SAMPLE IDENTIFICATION NAME";SAMPLE$
```

```
690 PRINT:PRINT:PRINT"ENTER PRESENT DATE: MONTH/DAY/YEAR.";:INPUT TODAY$
700 CLS:PRINT:PRINT:PRINT"SAMPLE IDENTIFICATION NAME IS: ";SAMPLE$
710 PRINT:PRINT"TODAY IS ";TODAY$:PRINT:PRINT"YES OR NO";:INPUT YYY$
720 IF LEFT$(YYY$,1)<>"Y" AND LEFT$(YYY$,1)<>"y" THEN GOTO 670
730 CLS:PRINT:PRINT:PRINT:INPUT"WHEN READY TO BEGIN, PRESS RETURN.";START$
740 IF START$="STOP" THEN GOTO 1910 'SENDS TO END OF PROGRAM.
750 LPRINT:LPRINT:LPRINT"DATA FOR ";SAMPLE$
760 LPRINT:LPRINT"DATE DATA ACQUIRED: ";TODAY$
770 CLS:PRINT:PRINT"DATA FOR ";SAMPLE$
780 PRINT:PRINT"CHOP. FREQ.";TAB(15);"SIG. AMP.";TAB(30);"A SIN(p.a.)";TAB(45);"
PHASE ANGLE";TAB(60);"PIN DIODE VLT.":PRINT
790 LPRINT:LPRINT:LPRINT"CHOP. FREQ.";TAB(15);"SIG. AMP.";TAB(30);"A SIN(p.a.)";
TAB(45);"PHASE ANGLE";TAB(60);"PIN DIODE VLT.":LPRINT
800 :
810 REM --DATA ACQUISITION PORTION OF PROGRAM BEGINS HERE.
820 :
830 WFGINP=INT(((VALUE%-128)*.03906)*100)/100 'COMPUTES VOLTAGE SENT TO WFG.
840 CHFREQ=INT((C0+C1*WFGINP+C2*WFGINP^2+C3*WFGINP^3)*10)/10
850 IF PORTION=1 THEN CHFREQ=INT(CHFREQ)/100:GOTO 890
855 IF PORTION=2 THEN CHFREQ=INT(CHFREQ)/10
860 XYZ=INT(CHFREQ/HICUT)
870 IF CHFREQ<XYZ*60+LOCUT OR CHFREQ>XYZ*60+HICUT THEN GOTO 890
880 GOTO 1440 'SENDS TO POINT WHERE FREQ. IS ALLOWED TO INCREASE.
890 COUNT=COUNT+1
900 DATMAT(COUNT,1)=CHFREQ
910 CHANNEL%=0
920 ADDRESS%=&H304
930 CALL DAC.SETUP(ADDRESS%)
940 CALL OUTDAC8.S(CHANNEL%,VALUE%) 'SENDS DESIRED VOLTAGE TO WFG.
950 FOR I=1 TO DELAY:NEXT I 'DELAY LOOP TO ALLOW LOCK IN AMP. TO STABILIZE.
960 ADDRESS%=&H300
970 CALL ADC.SETUP(ADDRESS%)
971 CHANNEL%=1
973 CALL INADC8.B(CHANNEL%,TMG%,LNG%,AAY%(1))
974 PNVLT=0
975 FOR I=1 TO LNG%
976 PNVLT=PNVLT+AAY%(I)
977 NEXT I
978 PNVLT=PNVLT/LNG%
979 DATMAT(COUNT,5)=PNVLT*ADJ*.0019608*MICRO
980 BCHANNEL%=4:ECHANNEL%=5
1000 CALL SCAN8.B(BCHANNEL%,ECHANNEL%,TIMING%,LENGTH%,ARRAY%(1))
1010 FOR I=1 TO POINTNO*2 STEP 2
1020 ASUM=ASUM+ARRAY%(I)
1030 SSUM=SSUM+ARRAY%(I+1)
1035 NEXT I
1040 AV=(ASUM/POINTNO)*.0019608 'CONVERTS BINARY SIGNAL TO LIA OUTPUT VOLTAGE.
1050 SV=(SSUM/POINTNO)*.0019608
```

```
1060 DATMAT(COUNT,2)=AV*SENSI 'CONVERTS VOLT. TO LIA METER READING (IN MICROV.).
1070 DATMAT(COUNT,3)=SV*SENSI
1080 X=DATMAT(COUNT,3)/DATMAT(COUNT,2) 'FINDS SINE OF PHASE ANGLE
1085 IF X>1 THEN DATMAT(COUNT,4)=90.99999:GOTO 1100
1090 DATMAT(COUNT,4)=ATN(X/SQR(-X*X+1))*57.29578 'FINDS PHASE ANGLE (IN DEG.)
1100 ASUM=0:SSUM=0
1110 FOR I=1 TO 5
1120 PRINT DATMAT(COUNT,I);TAB(15*I);
1130 NEXT I
1140 PRINT
1150 FOR I=1 TO 5
1160 LPRINT DATMAT(COUNT,I);TAB(15*I);
1170 NEXT I
1180 LPRINT
1230 IF AV/.0019608>80 OR ABC$="C" THEN GOTO 1440 'CHECKS IF SENSITIVITY SHOULD
BE INCREASED.
1240 FOR I=1 TO 4:BEEP:FOR J=1 TO 90:NEXT J:NEXT I
1250 IF MES=1 THEN GOTO 1310
1260 PRINT:PRINT:PRINT:PRINT"SIGNAL AMP. HAS DECREASED TO A POINT WHERE THE SENS
ITIVITY CAN BE INCREASED.":MES=1
1270 PRINT"IF YOU WISH TO MAINTAIN THE SAME SENSITIVITY THROUGHOUT THE EXPERIMEN
T, ENTER"
1280 PRINT"C FOR CONTINUE.   OTHERWISE SIMPLY ENTER A BLANK LINE.":INPUT ABC$
1290 IF ABC$="C" THEN GOTO 1440
1300 IF VALUE%+INCR>=OVER AND PORTION=2 THEN GOTO 1650
1310 VALUE%=VALUE%+INCR
1320 ADDRESS%=&H304
1330 CALL DAC.SETUP(ADDRESS%)
1340 CHANNEL%=0
1350 CALL OUTDAC8.S(CHANNEL%,VALUE%)
1360 PRINT:PRINT:PRINT"SENSITIVITY MAY NOW BE INCREASED.":PRINT:PRINT
1370 SENSI=SENSI/CORRECT
1380 PRINT"AFTER SENSITIVITY SETTING IS INCREASED, AND LOCK IN AMP. HAS STABILIZ
ED,"
1390 INPUT"PRESS RETURN.";RTN$
1400 JKL$=STR$(INT(SENSI+.5))
1405 IF LEFT$(JKL$,2)=" 3" THEN JKL$=LEFT$(JKL$,2)+LEFT$(ZERO$,LEN(JKL$)-2)
1410 PRINT:PRINT"NEW SENSITIVITY IS";JKL$;" MICROVOLTS.":PRINT:PRINT
1420 LPRINT:LPRINT;"NEW SENSITIVITY IS";JKL$;" MICROVOLTS.":LPRINT
1430 IF VALUE%<OVER THEN GOTO 830
1440 VALUE%=VALUE%+INCR 'ALLOWS INCREMENT IN VOLTAGE SENT TO WFG.
1450 IF VALUE%<OVER THEN GOTO 830
1460 IF PORTION=2 THEN GOTO 1650
1470 FOR I=1 TO 5:BEEP:FOR J=1 TO 130:NEXT J:NEXT I
1480 PORTION=2
1490 INCR=6:OVER=200
1500 LOCUT=57.5:HICUT=62.5
1510 PRINT:PRINT:PRINT"PORTION #1 OF DATA ACQUISITION IS COMPLETE."
```

```
1520 PRINT:PRINT"CHANGE APPROPRIATE SETTINGS ON WFG AND LIA."
1530 PRINT:PRINT"WHEN READY TO CONTINUE SAMPLING, HIT RETURN:"
1540 PRINT"OR, IF YOU WISH TO DISCONTINUE SAMPLING, ENTER STOP.";
1550 CHANNEL%=0
1560 VALUE%=128 ´ENABLES MODULATION FREQUENCY OF 10 HZ.
1570 CALL OUTDAC8.S(CHANNEL%,VALUE%) ´SENDS NEW VOLT. SIG. TO WFG FOR PORTION 2.
1580 INPUT GO$
1590 IF GO$="" THEN GOTO 830
1600 IF GO$="STOP" THEN GOTO 1650
1610 GOTO 1580
1620 :
1630 REM —DATA ACQUISITION PORTION OF PROGRAM ENDS HERE.
1640 :
1650 LPRINT:LPRINT:LPRINT
1660 LPRINT"NUMBER OF DATA POINTS TAKEN: ";COUNT
1670 LPRINT"INITIAL LIA SENSITIVITY SETTING: ";SENSI$;" MICROVOLTS."
1680 LPRINT"LIA TIME CONSTANT SETTING: ";TICON;"SECONDS."
1690 LPRINT"DELAY TIME USED: ";DELAY/840;"SECONDS."
1695 LPRINT"NUMBER OF SAMPLINGS PER DATA POINT: ";POINTNO
1700 LPRINT"SAMPLING RATE: ";RATE+.000033;"SECONDS."
1710 LPRINT"VOLTAGE TO LED (AT 10 HZ.): ";LEDVLT;" VOLTS."
1720 LPRINT"CURRENT TO LED (AT 10 HZ.): ";CURRENT;" AMPS."
1730 LPRINT"RANGE SETTING OF MICROVOLTMETER: ";MICRO;" MICROVOLTS."
1740 LPRINT:LPRINT:LPRINT
1750 PRINT:PRINT:PRINT"SAMPLING IS COMPLETED."
1760 :
1770 REM —THE FOLLOWING LINES ALLOW FOR FILING OF ACQUIRED DATA.
1780 :
1790 PRINT:PRINT:PRINT:INPUT"DO YOU WISH TO FILE ACQUIRED DATA";Y$
1800 IF LEFT$(Y$,1)="N" OR LEFT$(Y$,1)="n" THEN GOTO 1910
1810 CLS:PRINT:PRINT:PRINT"DO YOU WISH TO FILE ACQUIRED DATA UNDER FILENAME ";SA
MPLE$;:INPUT YE$:PRINT:PRINT
1820 IF LEFT$(YE$,1)="Y" OR LEFT$(YE$,1)="y" THEN NME$=SAMPLE$:GOTO 1850
1830 PRINT:PRINT:PRINT"INPUT DESIRED FILENAME FOR ";SAMPLE$
1840 PRINT:INPUT NME$
1850 OPEN "O",#1,NME$+".PRN"
1860 FOR I=1 TO COUNT
1870 PRINT#1,DATMAT(I,1);LOG(DATMAT(I,1))/LG;DATMAT(I,2);LOG(DATMAT(I,2))/LG;DAT
MAT(I,4);DATMAT(I,5)
1880 NEXT I
1890 CLOSE
1900 CLS:PRINT:PRINT:PRINT:PRINT"FILING IS COMPLETE."
1910 END
```

APPENDIX III

The acquisition program used in acquiring data for the 10-
1000 Hz modulation frequency range. The program was written to
be used with the Microsoft BASICA interpreter. A discussion of
the program is provided in Section 3.4, and Appendix I gives a
general flowchart of the portion of the program in which the data
is actually acquired.

```
10 ADC.SETUP=&H8B4:ALTOUT12.B=&H72E:ALTOUT12.BT=&H78A:ALTOUT12.R=&H7E9
15 ALTOUT12.RT=&H847:ALTOUT12.S=&H6E5:ALTOUT12.ST=&H708:ALTOUT8.B=&H2CF
20 ALTOUT8.BT=&H359:ALTOUT8.R=&H3E9:ALTOUT8.RT=479:ALTOUT8.S=&H24A
25 ALTOUT8.ST=&H28A:DAC.SETUP=&H1A:INADC12.B=&HCDF:INADC12.BT=&HD4B
30 INADC12.EXTCLOCK=&HDC7:INADC12.S=&HC70:INADC12.ST=&HC9C:INADC8.B=&H97B
35 INADC8.BT=&H9E2:INADC8.EXTCLOCK=&HA4C:INADC8.S=&H904:INADC8.ST=&H933
40 OUTDAC12.B=&H564:OUTDAC12.BT=&H5C4:OUTDAC12.R=&H627:OUTDAC12.RT=&H67B
45 OUTDAC12.S=&H50F:OUTDAC12.ST=&H538:OUTDAC8.B=&HBC:OUTDAC8.BT=&H11D
50 OUTDAC8.R=&H181:OUTDAC8.RT=&H1E4:OUTDAC8.S=&H6D:OUTDAC8.ST=&H93
55 SCAN12.B=&HEE5:SCAN12.BT=&HF7A:SCAN12.S=&HE36:SCAN12.ST=&HE82
60 SCAN8.B=&HB4B:SCAN8.BT=&HBDA:SCAN8.S=&HA9E:SCAN8.ST=&HAE9
65 DEF SEG=0
70 CSEG=(256*PEEK(&H3CB))+PEEK(&H3CA)
75 DEF SEG=CSEG
91 ´
92 ´
93 ´THE FIRST 100 LINES ARE RESERVED FOR LABSTAR SOFTWARE
94 ´THE APPLICATION PROGRAM STARTS AT LINE 100
95 ´
96 ´
97 ´
98 ´
99 ´
100 CLS:PRINT:PRINT:PRINT
110 PRINT"THE FOLLOWING DATA ACQUISITION PROGRAM IS DESIGNED TO OBTAIN AND"
120 PRINT"PROCESS THE PHOTOACCOUSTIC SIGNAL FROM A LOCK IN AMPLIFIER AS A"
130 PRINT"FUNCTION OF THE MODULATION FREQUENCY OF THE LIGHT SOURCE AS"
140 PRINT"DRIVEN BY A VARIABLE FREQUENCY WAVEFORM GENERATOR."
150 :
160 REM —THE FOLLOWING SEVERAL LINES DEFINE CONSTANTS NECESSARY FOR IMPLEMENTAT
ION OF PROG.
170 :
175 ZERO$="0000000000"
180 CO=100:C1=163.654:C2=3.627054:C3=-.4178307
190 OVER=256:INCR=6:PORTION=1
195 FINC=1:IFREQ=250:STFREQ=250
200 LOCUT=57.5:HICUT=62.5
210 CORRECT=10^.5:LG=LOG(10)
215 TMG%=3994:LNG%=50:ADJ=2
220 DIM DATMAT(1000,5):DIM ARRAY%(200):DIM AAY%(50)
230 ADDRESS%=&H304
240 CALL DAC.SETUP(ADDRESS%)
250 CHANNEL%=0
260 VALUE%=128 ´ENABLES INITIAL MODULATION FREQUENCY OF 10.0 HERTZ.
270 CALL OUTDAC8.S(CHANNEL%,VALUE%) ´SENDS INITIAL VOLTAGE TO WFG.
280 PRINT:PRINT:PRINT:PRINT"TURN ON POWER TO PHOTOACOUSTIC SAMPLING EQUIPTMENT."
290 PRINT:PRINT:PRINT
300 PRINT"SET WAVEFORM GENERATOR RANGE AT 100 HZ. AND ADJUST UNTIL COUNTER CONSI
```

STANTLY"
310 PRINT"REGISTERS A 100 HZ. READING."
320 PRINT:INPUT"WHEN ADJUSTMENT IS COMPLETE, SET WFG RANGE TO 10 HZ. AND THEN PR
ESS RETURN.";RTN
330 CLS:PRINT:PRINT:PRINT:PRINT"FROM THE METERS ON POWER SUPPLY DRIVING LED:":PR
INT:PRINT
340 INPUT"ENTER DC VOLTAGE TO LED (IN VOLTS)";LEDVLT
350 PRINT:INPUT"ENTER CURRENT TO LED (IN AMPS)";CURRENT
360 PRINT:PRINT:INPUT"ENTER RANGE SETTING OF MICROVOLTMETER (IN MICROVOLTS)";MIC
RO
370 CLS:PRINT:PRINT:PRINT
380 PRINT"ENTER THE FOLLOWING LOCK IN AMPLIFIER SETTINGS:":PRINT:PRINT
390 INPUT"TIME CONSTANT (IN SECONDS)";TICON
400 INPUT"SENSITIVITY (IN MICROVOLTS)";SENSI
410 SENSI$=STR$(SENSI)
420 IF LEFT$(SENSI$,2)=" 3" THEN SENSI=(SENSI/3)*CORRECT
430 INPUT"PHASE SETTING (IN DEGREES)";PHSET$
440 CLS:PRINT:PRINT:PRINT"IS A DELAY TIME OF "TICON*4" SECONDS ADEQUATE TO ALLOW
 LOCK IN AMPLIFIER"
450 INPUT"TO STABILIZE";SEY$
460 IF LEFT$(SEY$,1)="Y" OR LEFT$(SEY$,1)="y" THEN DELAY=TICON*4:GOTO 510
470 CLS:PRINT:PRINT:PRINT
480 PRINT"ENTER DESIRED DELAY TIME (IN SECONDS) BETWEEN MODULATION FREQUENCY"
490 PRINT"INCREMENT AND SUBSEQUENT ACQUISITION OF SIGNAL FROM LOCK IN AMP."
500 PRINT:INPUT DELAY
510 DELAY=DELAY*840 'CONVERTS LOOP DELAY PARAMETER TO SECONDS.
520 CLS:PRINT:PRINT:PRINT
530 PRINT"IS 50 DATA POINTS TAKEN PER MODULATION FREQ. INCREMENT SUFFICIENT, YES
 OR NO";:INPUT ESY$
540 IF LEFT$(ESY$,1)="Y" OR LEFT$(ESY$,1)="y" THEN POINTNO=50:GOTO 570
550 PRINT:PRINT"HOW MANY DATA POINTS ARE TO BE TAKEN AT EACH MODULATION FREQUENC
Y"
560 INPUT POINTNO:IF INT(POINTNO)<>POINTNO OR POINTNO<1 THEN GOTO 550
570 LENGTH%=POINTNO
580 RATE=TICON/POINTNO
590 PRINT:PRINT:PRINT:PRINT"IS A SAMPLING RATE OF ";INT(RATE*10000)/10000;" SECO
NDS BETWEEN ACQUISITION OF DATA"
600 PRINT"POINTS AT A GIVEN MODULATION FREQUENCY SUFFICIENT";:INPUT AN$
610 IF LEFT$(AN$,1)="Y" OR LEFT$(AN$,1)="y" THEN GOTO 630
620 PRINT:INPUT"ENTER DESIRED SAMPLING RATE (IN SECONDS)";RATE
630 BETWEEN=RATE/.000005
640 IF BETWEEN>65536! THEN PRINT:PRINT"DESIRED SAMPLING RATE IS TOO LARGE, IT CA
NNOT EXCEED 0.327 SECONDS":PRINT:PRINT:GOTO 620
650 IF BETWEEN>32767 THEN BETWEEN=BETWEEN-65536!
660 TIMING%=INT(BETWEEN)
670 CLS:PRINT:PRINT:PRINT
680 INPUT"ENTER SAMPLE IDENTIFICATION NAME";SAMPLE$
690 PRINT:PRINT:PRINT"ENTER PRESENT DATE: MONTH/DAY/YEAR.";:INPUT TODAY$

```
700 CLS:PRINT:PRINT:PRINT"SAMPLE IDENTIFICATION NAME IS: ";SAMPLE$
710 PRINT:PRINT"TODAY IS ";TODAY$:PRINT:PRINT"YES OR NO";:INPUT YYY$
720 IF LEFT$(YYY$,1)<>"Y" AND LEFT$(YYY$,1)<>"y" THEN GOTO 670
730 CLS:PRINT:PRINT:PRINT:INPUT"WHEN READY TO BEGIN, PRESS RETURN.";START$
740 IF START$="STOP" THEN GOTO 1910 'SENDS TO END OF PROGRAM.
750 LPRINT:LPRINT:LPRINT"DATA FOR ";SAMPLE$
760 LPRINT:LPRINT"DATE DATA ACQUIRED: ";TODAY$
770 CLS:PRINT:PRINT"DATA FOR ";SAMPLE$
780 PRINT:PRINT"CHOP. FREQ.";TAB(15);"SIG. AMP.";TAB(30);"A SIN(p.a.)";TAB(45);"
PHASE ANGLE";TAB(60);"PIN DIODE VLT.":PRINT
790 LPRINT:LPRINT:LPRINT"CHOP. FREQ.";TAB(15);"SIG. AMP.";TAB(30);"A SIN(p.a.)";
TAB(45);"PHASE ANGLE";TAB(60);"PIN DIODE VLT.":LPRINT
800 :
810 REM —DATA ACQUISITION PORTION OF PROGRAM BEGINS HERE.
820 :
830 WFGINP=INT((((VALUE%-128)*.03906)*100)/100 'COMPUTES VOLTAGE SENT TO WFG.
840 CHFREQ=INT((C0+C1*WFGINP+C2*WFGINP^2+C3*WFGINP^3)*10)/10
850 IF PORTION=1 THEN CHFREQ=INT(CHFREQ)/10
860 XYZ=INT(CHFREQ/HICUT)
870 IF CHFREQ<XYZ*60+LOCUT OR CHFREQ>XYZ*60+HICUT THEN GOTO 890
880 GOTO 1440 'SENDS TO POINT WHERE FREQ IS ALLOWED TO INCREASE.
890 COUNT=COUNT+1
900 DATMAT(COUNT,1)=CHFREQ
910 CHANNEL%=0
920 ADDRESS%=&H304
930 CALL DAC.SETUP(ADDRESS%)
940 CALL OUTDAC8.S(CHANNEL%,VALUE%) 'SENDS DESIRED VOLTAGE TO WFG.
950 FOR I=1 TO DELAY:NEXT I 'DELAY LOOP TO ALLOW LOCK IN AMP. TO STABILIZE.
960 ADDRESS%=&H300
970 CALL ADC.SETUP(ADDRESS%)
971 CHANNEL%=1
973 CALL INADC8.B(CHANNEL%,TMG%,LNG%,AAY%(1))
974 PNVLT=0
975 FOR I=1 TO LNG%
976 PNVLT=PNVLT+AAY%(I)
977 NEXT I
978 PNVLT=PNVLT/LNG%
979 DATMAT(COUNT,5)=PNVLT*ADJ*.0019608*MICRO
980 BCHANNEL%=4:ECHANNEL%=5
990 CALL SCAN8.B(BCHANNEL%,ECHANNEL%,TIMING%,LENGTH%,ARRAY%(1))
1000 FOR I=1 TO POINTNO*2 STEP 2
1010 ASUM=ASUM+ARRAY%(I)
1020 SSUM=SSUM+ARRAY%(I+1)
1030 NEXT I
1040 AV=(ASUM/POINTNO)*.0019608 'CONVERTS BINARY SIGNAL TO LIA OUTPUT VOLTAGE.
1050 SV=(SSUM/POINTNO)*.0019608
1060 DATMAT(COUNT,2)=AV*SENSI 'CONVERTS VOLT. TO LIA METER READING (IN MICROV.).
1070 DATMAT(COUNT,3)=SV*SENSI
```

190

```
1080 X=DATMAT(COUNT,3)/DATMAT(COUNT,2) 'FINDS SINE OF PHASE ANGLE
1085 IF X>1 THEN DATMAT(COUNT,4)=90.99999:GOTO 1100
1090 DATMAT(COUNT,4)=ATN(X/SQR(-X*X+1))*57.29578 'FINDS PHASE ANGLE (IN DEG.)
1100 ASUM=0:SSUM=0
1110 FOR I=1 TO 5
1120 PRINT DATMAT(COUNT,I);TAB(15*I);
1130 NEXT I
1140 PRINT
1150 FOR I=1 TO 5
1160 LPRINT DATMAT(COUNT,I);TAB(15*I);
1170 NEXT I
1180 LPRINT
1190 IF CHFREQ<STFREQ THEN GOTO 1220 'THESE 3 LINES ALLOW FOR INCR. IN FREQ. INC
REMENT IN INTERVALS OF IFREQ.
1200 STFREQ=STFREQ+IFREQ
1210 INCR=INCR+FINC
1220 IF VALUE%+INCR>=OVER AND PORTION=2 THEN GOTO 1650
1230 IF AV/.0019608>80 OR ABC$="C" THEN GOTO 1440 'CHECKS IF SENSITIVITY SHOULD
 BE INCREASED.
1240 FOR I=1 TO 4:BEEP:FOR J=1 TO 90:NEXT J:NEXT I
1250 IF MES=1 THEN GOTO 1310
1260 PRINT:PRINT:PRINT:PRINT"SIGNAL AMP. HAS DECREASED TO A POINT WHERE THE SENS
ITIVITY CAN BE INCREASED.":MES=1
1270 PRINT"IF YOU WISH TO MAINTAIN THE SAME SENSITIVITY THROUGHOUT THE EXPERIMEN
T, ENTER"
1280 PRINT"C FOR CONTINUE.  OTHERWISE SIMPLY ENTER A BLANK LINE.":INPUT ABC$
1290 IF ABC$="C" THEN GOTO 1440
1300 IF VALUE%+INCR>=OVER AND PORTION=2 THEN GOTO 1650
1310 VALUE%=VALUE%+INCR
1320 ADDRESS%=&H304
1330 CALL DAC.SETUP(ADDRESS%)
1340 CHANNEL%=0
1350 CALL OUTDAC8.S(CHANNEL%,VALUE%)
1360 PRINT:PRINT:PRINT"SENSITIVITY MAY NOW BE INCREASED.":PRINT:PRINT
1370 SENSI=SENSI/CORRECT
1380 PRINT"AFTER SENSITIVITY SETTING IS INCREASED, AND LOCK IN AMP. HAS STABILIZ
ED,"
1390 INPUT"PRESS RETURN.";RTN$
1400 JKL$=STR$(INT(SENSI+.5))
1405 IF LEFT$(JKL$,2)=" 3" THEN JKL$=LEFT$(JKL$,2)+LEFT$(ZERO$,LEN(JKL$)-2)
1410 PRINT:PRINT"NEW SENSITIVITY IS";JKL$;" MICROVOLTS.":PRINT:PRINT
1420 LPRINT:LPRINT;"NEW SENSITIVITY IS";JKL$;" MICROVOLTS.":LPRINT
1430 IF VALUE%<OVER THEN GOTO 830
1440 VALUE%=VALUE%+INCR 'ALLOWS INCREMENT IN VOLTAGE SENT TO WFG.
1450 IF VALUE%<OVER THEN GOTO 830
1460 IF PORTION=2 THEN GOTO 1650
1470 FOR I=1 TO 5:BEEP:FOR J=1 TO 130:NEXT J:NEXT I
1480 PORTION=2
```

```
1490 INCR=2:OVER=256
1500 LOCUT=55:HICUT=65
1510 PRINT:PRINT:PRINT"PORTION #1 OF DATA ACQUISITION IS COMPLETE."
1520 PRINT:PRINT"CHANGE APPROPRIATE SETTINGS ON WFG AND LIA."
1530 PRINT:PRINT"WHEN READY TO CONTINUE SAMPLING, HIT RETURN:"
1540 PRINT"OR, IF YOU WISH TO DISCONTINUE SAMPLING, ENTER STOP.";
1550 CHANNEL%=0
1560 VALUE%=128 'ENABLES MODULATION FREQUENCY OF 100 HZ.
1570 CALL OUTDAC8.S(CHANNEL%,VALUE%) 'SENDS NEW VOLT. SIG. TO WFG FOR PORTION 2.
1580 INPUT GO$
1590 IF GO$="" THEN GOTO 830
1600 IF GO$="STOP" THEN GOTO 1650
1610 GOTO 1580
1620 :
1630 REM --DATA ACQUISITION PORTION OF PROGRAM ENDS HERE.
1640 :
1650 LPRINT:LPRINT:LPRINT
1660 LPRINT"NUMBER OF DATA POINTS TAKEN: ";COUNT
1670 LPRINT"INITIAL LIA SENSITIVITY SETTING: ";SENSI$;" MICROVOLTS."
1680 LPRINT"LIA TIME CONSTANT SETTING: ";TICON;"SECONDS."
1690 LPRINT"DELAY TIME USED: ";DELAY/840;"SECONDS."
1695 LPRINT"NUMBER OF SAMPLINGS PER DATA POINT: ";POINTNO
1700 LPRINT"SAMPLING RATE: ";RATE+.000033;"SECONDS."
1710 LPRINT"VOLTAGE TO LED (AT 10 HZ.): ";LEDVLT;" VOLTS."
1720 LPRINT"CURRENT TO LED (AT 10 HZ.): ";CURRENT;" AMPS."
1730 LPRINT"RANGE SETTING OF MICROVOLTMETER: ";MICRO;" MICROVOLTS."
1740 LPRINT:LPRINT:LPRINT
1750 PRINT:PRINT:PRINT"SAMPLING IS COMPLETED."
1760 :
1770 REM --THE FOLLOWING LINES ALLOW FOR FILING OF ACQUIRED DATA.
1780 :
1790 PRINT:PRINT:PRINT:INPUT"DO YOU WISH TO FILE ACQUIRED DATA";Y$
1800 IF LEFT$(Y$,1)="N" OR LEFT$(Y$,1)="n" THEN GOTO 1910
1810 CLS:PRINT:PRINT:PRINT"DO YOU WISH TO FILE ACQUIRED DATA UNDER FILENAME ";SA
MPLE$;:INPUT YE$:PRINT:PRINT
1820 IF LEFT$(YE$,1)="Y" OR LEFT$(YE$,1)="y" THEN NME$=SAMPLE$:GOTO 1850
1830 PRINT:PRINT:PRINT"INPUT DESIRED FILENAME FOR ";SAMPLE$
1840 PRINT:INPUT NME$
1850 OPEN "O",#1,NME$+".PRN"
1860 FOR I=1 TO COUNT
1870 PRINT#1,DATMAT(I,1);LOG(DATMAT(I,1))/LG;DATMAT(I,2);LOG(DATMAT(I,2))/LG;DAT
MAT(I,4);DATMAT(I,5)
1880 NEXT I
1890 CLOSE
1900 CLS:PRINT:PRINT:PRINT:PRINT"FILING IS COMPLETE."
1910 END
```

PHOTOACOUSTIC ANALYSIS OF WHEAT KERNELS

by

Arnold J. Eilert

B.Sc., Benedictine College,
Atchison, Kansas, 1984

————————————

AN ABSTRACT OF A MASTER'S THESIS

submitted in partial fulfillment of the

requirements for the degree

MASTER OF SCIENCE

Department of Physics

KANSAS STATE UNIVERSITY
Manhattan, Kansas

1986

ABSTRACT

A phenomenon commonly referred to as the photoacoustic ef-
fect is known to occur when an intensity modulated source of
electromagnetic radiation impinges on a solid sample enclosed in
a gas-filled chamber. Upon absorption of the incident radiation,
an acoustic signal is produced in the gas with a frequency equal
to the modulation frequency. The amplitude and phase of the
signal depends on the thermal, and in many cases, the optical
properties of the sample, thus allowing the effect to be used as
a sample analysis technique.

A series of experiments was performed in this research
project to study the photoacoustic responses of individual wheat
kernels. The technique used involved varying the modulation fre-
quency of the incident radiation over a 1-1000 Hz frequency
range, and monitoring the photoacoustic response. The acoustic
signal was detected with a sensitive microphone and amplified
using a lock-in amplifier. A microcomputer-driven data acquisi-
tion system was used to step the modulation frequency and to
record the data. By systematically varying the modulation fre-
quency of the e-m radiation illuminating the sample, it is possi-
ble to obtain a profile of the sample's thermal properties as a
function of depth beneath its surface. The purpose of the inves-
tigation was to determine whether the photoacoustic response of
wheat kernels can be related to other kernel properties, such as
hardness and moisture content.

In this project, we studied a number of different wheat varieties, including both hard and soft red winter wheats. Our studies indicate that some varieties of wheat exhibit photoacoustic responses measurably different from others, although substantial scatter amongst individual kernels of a given variety is often present. Improvements in the standardization procedure for the individual kernels and/or modifications in the apparatus which increase the magnitude of the kernel's contribution to the photoacoustic response may help to improve the separation between varieties, and decrease the kernel to kernel scatter found in our results.